ABSTRACT

Title of Document: STIFFNESS AND STRENGTH OF K-COR SANDWICH STRUCTURES UNDER COMPRESSION AND SHEAR LOADING CONDITIONS

Ananth Kumar Musurapakam Virakthi, M.S., 2011

Directed By: Dr. Sung. W. Lee, Dept. of Aerospace Engineering

Pin reinforced sandwich cores, with composite facesheets, offer a great means of structural construction owing to their low weight and high stiffness and strength. In this research, FE models have been developed to obtain their stiffness and strengths under compressive and shear loading conditions. Computationally obtained values have been compared with experimental results for various sandwich specimens. Since the pins have a high modulus, and the facesheets have a low modulus, the pins penetrate into the facesheets. The pin-facesheet interaction then becomes important in determining the stiffness of the sandwich structures. The effect of adhesive layer yielding on the stiffness of the structure is analyzed. Geometrically non-linear models for the reinforcing pins have been developed to study their behavior at critical loads. Different parameters affecting the compressive and shear stiffness and strengths have been investigated.

STIFFNESS AND STRENGTH OF K-COR SANDWICH STRUCTURES UNDER COMPRESSION AND SHEAR LOADING CONDITIONS

by
Ananth Kumar Musurapakam Virakthi

Thesis submitted to the Faculty of the Graduate School of the
University of Maryland in partial fulfillment
of the requirements for the degree of
Master of Science
2011

Advisory Committee:
Prof. Sung W. Lee, Chair
Prof. Hugh Bruck
Prof. Norman M. Wereley

Acknowledgements

I am grateful to my advisor, Dr. Sung Lee, for giving me an opportunity to work on this project and for his support, guidance and encouragement. I would like to thank Dr. Hugh Bruck and Dr. Norman Wereley for agreeing to serve on my committee and reviewing this thesis.

I am also thankful to my co-worker Soon Kwon for providing prior information and to Sandip Haldar for the much needed experimental data required for this research. I gratefully acknowledge the financial support that I have received as a Graduate Research Assistant. I am thankful to University of Maryland for providing access to required journals and papers that have been useful in my research work.

I would like to thank my friends who I have had some best times with and who have encouraged me throughout. And finally, I would like to thank my parents and my sister for their love and unwavering support all these years of my life.

Table of Contents

List of Figures

List of Tables

Chapter 1

Introduction

1.1 Sandwich Constructions

Sandwich structures are composite structures constructed using two thin and stiff face sheets, usually composite laminates, attached to a thick soft core. The stiff face sheets separated by the thick core allows for a high bending stiffness and an overall low density for the structure. The facesheets are the major load bearing components while the lightweight core supports the facesheets. Sandwich structures have many applications including aerospace, marine, automotive, windmills, building and consumer industries owing to their light-weights and high strengths.

The core of the sandwich structures is usually composed of a foam material or a honeycomb structure. The geometry of honeycomb structures can vary largely but the common characteristic of such structures is that they are composed of an array of hollow cells, columnar or hexagonal in shape, separated by thin vertical walls. A honeycomb shaped structure allows for a core with lower density and yet provides for relatively high out-of-plane compression properties and out-of-plane shear properties. It also allows for minimization of the amount of material used to achieve minimal weight and minimal material cost. Much of the earlier work involved in the study on sandwich composites focused on the honeycomb core sandwich constructions. Usually honeycomb cores are made out of aluminum or out of composite materials like Nomex, glass thermoplastic or glass-phenolic. Although honeycomb structures have some merits, some of their problems include the low surface area of core for bonding, higher cost of manufacture and maintenance and sensitivity to hot and humid environment. Also, honeycomb

structures are susceptible to ingress by water, which can be a problem in situations where water-absorption and free-thaw cycles are not desired.

The closed-cell polymer foam is an alternate kind of core used in sandwich structures. The most commonly used foam materials are closed-cell rigid polyurethane foams (RPUF), which are often thermoset to achieve reasonably high thermal tolerance. The foam core is water-resistant and much more weight efficient compared with honeycomb core. The advantages of foam cores are that they are anti-hot and humid with excellent performance, have adjustable density and provide increased support surface for bonding with the facesheets. In addition, the foam can be used as energy absorber and thermal insulating material. Such a core also has favorable acoustical behavior. But the stiffness and strength of polymer foam are much lower than that of honeycomb-core, and foam cored sandwich panels are prone to damage when subject to local loading. There is an additional problem of relative low bonding strength and stiffness in the core-facesheet interfaces for the traditional foam core sandwich structures, which restrain the application of foam cores.

For stiffer reinforcement materials, a hybrid variety of sandwich structures may be constructed, made with facesheets and square honeycomb or folded plate metal cores filled with polymer foam [13]. Such hybrid constructions can be designed to combine most of the advantages of metallic and polymeric materials while avoiding some of their main disadvantages. Usually facesheets are used at the outer surfaces to maximize rigidity while introducing in between lightweight cores adhesively bonded to keep the whole structure together. In addition, composite layers may be used as intermediate

layers to improve impact resistance. Hybrid sandwich structures are especially beneficial if multifunctional advantages such as acoustic and thermal insulation are considered.

The main functionality for hybrid sandwich constructions is that they stiffen the foam core which has weak out-of-plane stiffness and strengths. Among other strategies to improve the core performance is to reinforce the foam core with reinforcement pins. Pin reinforced sandwich structures are constructed by inserting pins through the foam and bonding the pin ends to the face sheets. Many papers [1-12] in literature have addressed the need for pin reinforcement in sandwich structures and the properties thus obtained from them. Usually metallic or carbon fiber pins are used for reinforcement. The reinforcing pins can be bonded to the facesheet in different ways and prominent methods include Z-pinning and C-pinning [8]. In C-pin reinforcement, the protrusions of the pins are folded in the same direction giving the pins a C-shape across the thickness of the sandwich structure as shown in Figure 1.1.

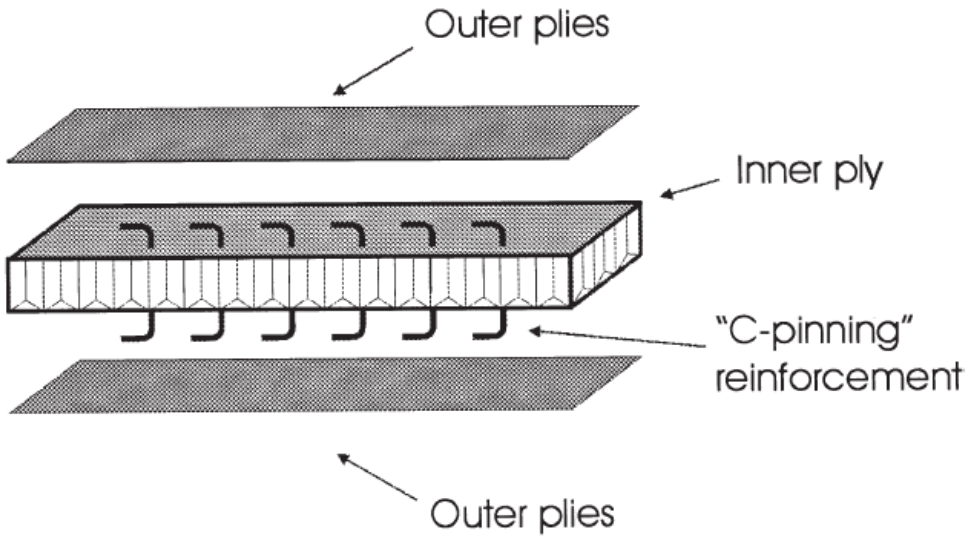

Figure 1.1: Insertion of reinforcement for "C-pinning" technique [8]

Z-pinning is a more common type of reinforcement than C-pinning. Z-pin reinforcement can have either K-cor or X-cor kind of pin bonding with the facesheets [1, 4, 6, 7, 9]. When the protrusions of the pins outside the core are folded on either sides of the pin and bonded to the facesheet using an adhesive layer as shown in Figure 1.3b, it is known as K-Cor. In an X-cor type of construction, the protrusions of the pin are made to penetrate into the facesheets before curing requiring no additional adhesive film or bonding. The combination of the Z-pin configuration and the soft core provides a means for high structural efficiency by improving the bending, compressive and out of plane shear moduli and strength of the sandwich structure. The pins also provide a superior core-facesheet bond, improving the structure's tolerance to local loading. In addition, the reinforced core supports transverse shear and impact loads through the thickness and also provides for high fracture toughness and resistance to fatigue crack propagation. The high stiffness, strength and resistance to failure makes pin-reinforced sandwich structures ideal for aerospace applications, such as in fuselage wing and tail skins of the aircraft. Besides they are useful in naval and automotive applications too.

1.2 K-Cor sandwich structures and Literature Review

In study of Z-pin sandwich structures in this research, we mainly focus on K-Cor sandwich structures. In a K-Cor type of construction, the reinforcing pins are made to extend beyond the foam surface, giving rise to excess lengths of the pins called reveal lengths. The length of the pins that extends out of the foam is pressed flat on the surface of the foam. The reveal lengths are then adhesively bonded to the face sheets. A sketch of the K-Cor construction is shown in Figure 1.2. The reveal lengths of the pins are flattened

out on the foam surface away from the direction of the penetration, forming an obtuse angle between the pin directions at the foam surface as shown in Figure 1.3.

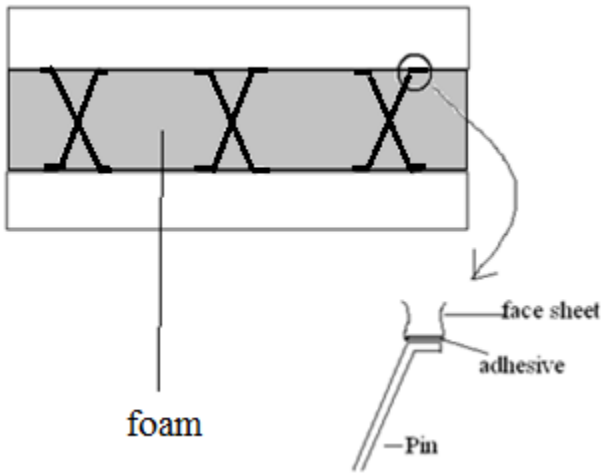

Figure 1.2: K-Cor arrangement for sandwich panels.

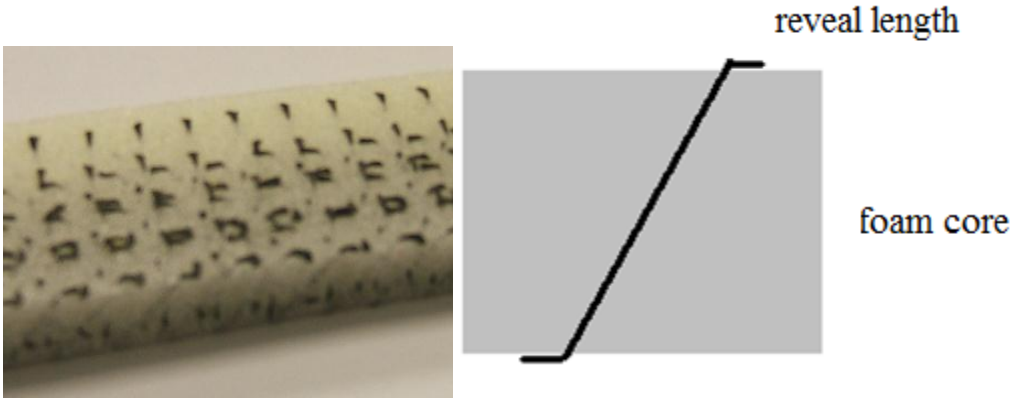

Figure 1.3(a): A K-cor sandwich panel **(b)** Sketch of a single pin showing the orientation of the reveal lengths

The pin truss geometry of a sandwich structure is an important part of design and different kinds of pin geometries have been studied in literature. The pyramidal pin

arrangement is used in the sandwich structures analyzed in this research. In this type of arrangement, the pins in the sandwich structures are aligned in a pyramid kind of geometry as shown in Figure 1.4 below. The figure shows a part of the sandwich structure containing a section of the face sheets bonded to four oblique pins inclined at a constant angle to the vertical. Oblique pins 1 and 3 lie in the x-z plane pointing in the positive and negative x-directions. Oblique pins 2 and 4 are in the y-z plane pointing in the positive and negative y-directions. These pins repeat themselves at a fixed distance in both x and y directions until the boundaries of the structure. Essentially, one may define a unit cell of the specimen as a square section of side length equal to the pin spacing. The unit cell pattern repeats on either side until the boundaries. In Figure 1.4(a) below, only 4 pins (of all possible orientations) and none others are shown for the sake of brevity. The top view of the four pins is shown in Figure 1.4(b). Some sandwich specimens have a vertical pin at the center of the unit cell which as shown in Figure 1.5.

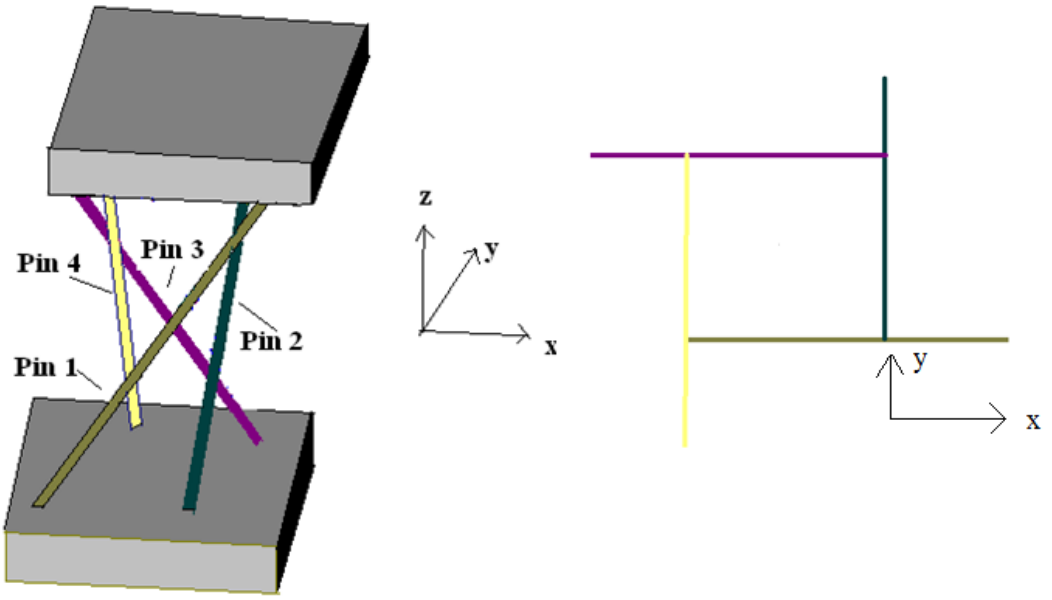

Figure 1.4: An isometric view of the pyramid geometry of a unit cell of the Z-pin reinforced sandwich structure with no vertical pins (b) Top view of the same arrangement

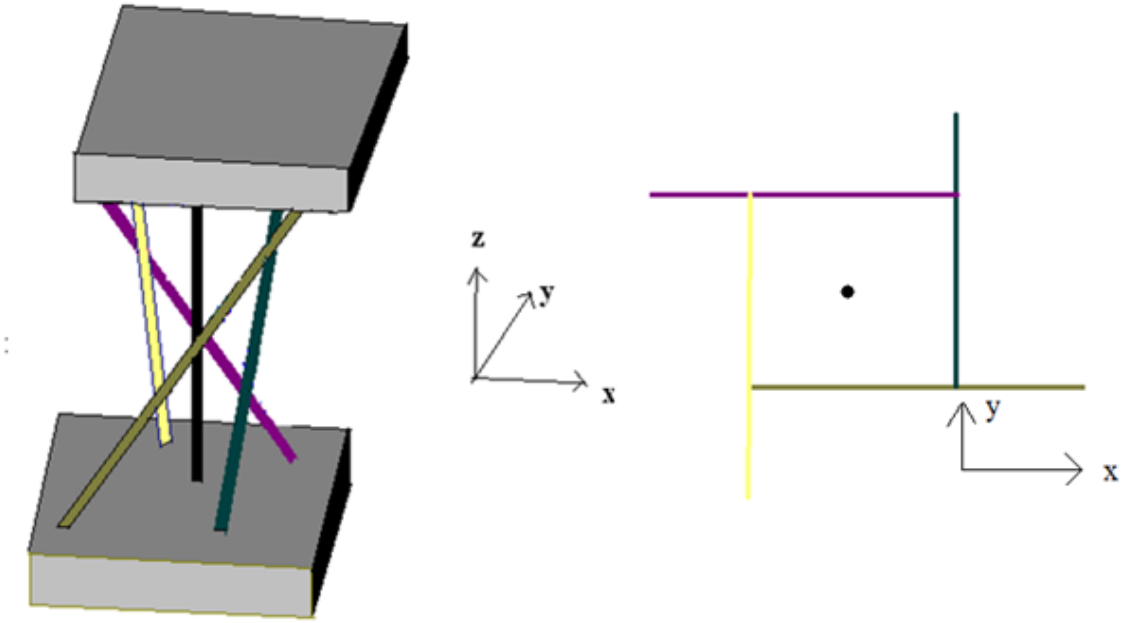

Figure 1.5: An isometric view of the pyramid geometry of a unit cell of the Z-pin reinforced sandwich structure with vertical pins (b) Top view of the same arrangement

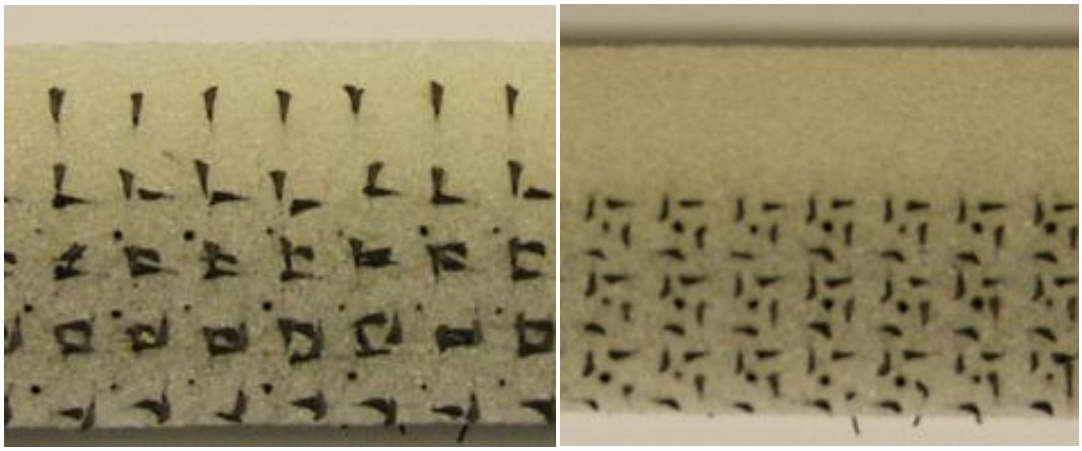

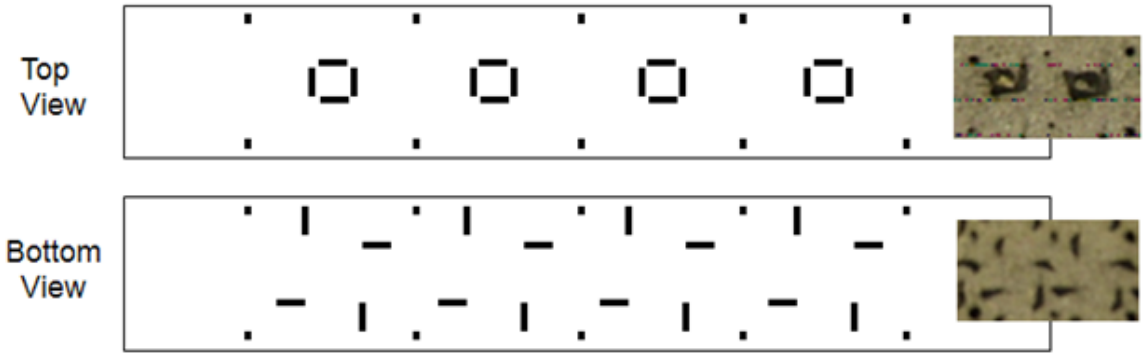

Figure 1.6 (a), (b): Top and Bottom views of a section of sandwich panel **(c)** Geometric representation of the top view and bottom view of the sandwich structure containing vertical pins.

Figure 1.6 shows the top and the bottom views of a section of the sandwich panel containing four oblique pins and one vertical pin in a unit cell depicting the direction of the reveal lengths of the pins.

The pin truss configuration of a sandwich structure is described by two specific geometric parameters namely the pin insertion angle and the cell interval. The pin insertion angle is the angle that the oblique pins of the sandwich panel make with the

vertical. Cell interval is the distance between adjacent pins of same kind in a sandwich panel, which is also the side length of a unit cell. The magnitude of the cell interval also decides the pin density, which is the weight of the pins contained in a unit volume of the sandwich structure. Closely packed pin configurations naturally have higher pin densities. Pin density of a sandwich structure depends only on the pin spacing and the material properties of the pin, but not on the core thickness or the actual length of the pins. Figure 1.7 depicts these parameters on a section of the sandwich panel.

The sensitivity of stiffness and strengths of the sandwich structures to various parameters such as pin density, foam thickness, pin incident angles, number of pins, pin truss configuration, facesheet configuration is analyzed in various studies in literature [1, 3, 5, 6, 7, 10, 11] allowing for design capabilities.

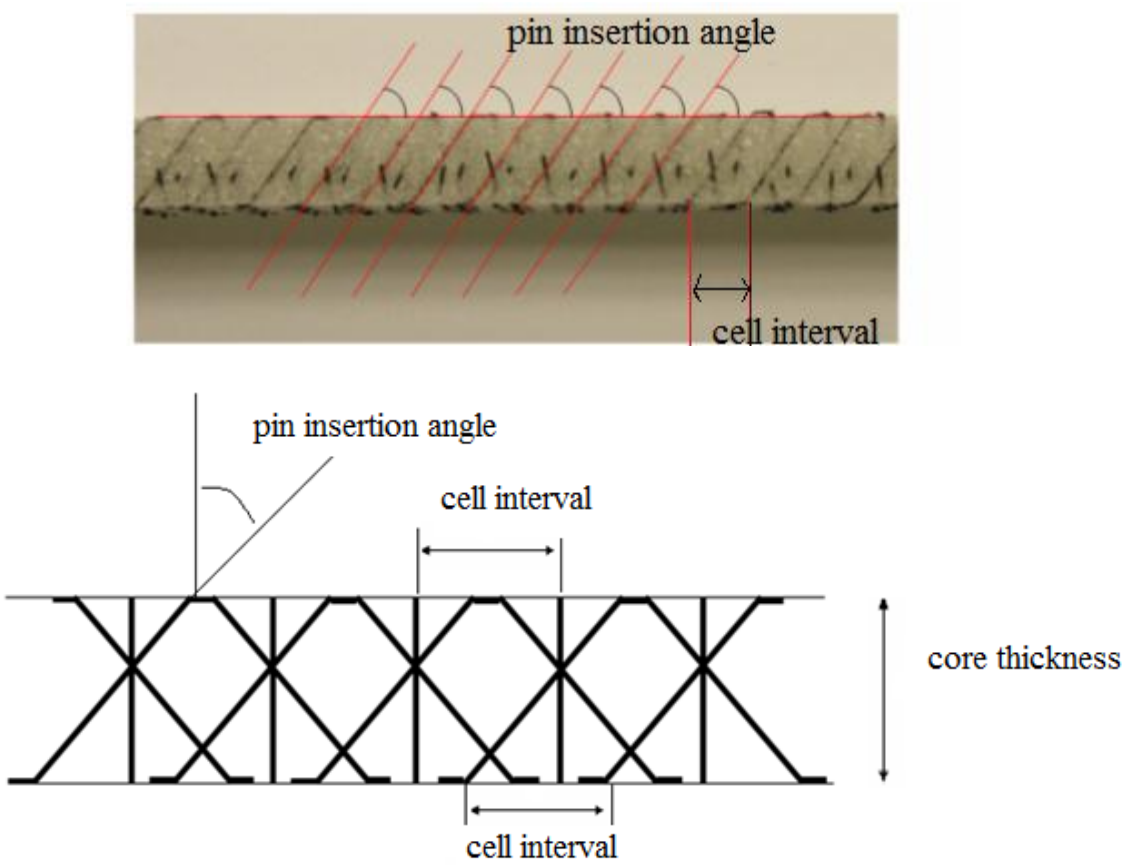

Figure 1.7 (a) Side view of a sandwich panel showing the pin insertion angle and the cell interval. **(b)** A geometric sketch showing the same parameters

In addition to the pyramidal pin arrangement described above, other pin geometries have been considered in literature. Some of the common ones include using only vertical pins in the structure or using only cross pins (a pair of oblique pins in a unit cell running in the length direction). A tetrahedral configuration consists of three different oblique pins in a unit cell, two in the length direction and one in the width direction. A different kind of pyramidal arrangement for the pins is also possible that allows four pins of a pyramidal set to meet at a single point on the top facesheet [10].

The primary objective in the study of sandwich structures is to characterize them by determining their stiffness and strengths. Several papers [1, 6, 7, 9, 11, 12] studied compressive stiffness and strengths of Z-pin reinforced sandwich structures. A.P. Mouritz [11] experimentally compared the reinforcement properties for pins with different materials such as carbon nanotubes, composite, Steel, Aluminum and Titanium pins under compressive loads. The sandwich structures with carbon nanotubes was observed to perform the best in terms of compressive modulus and strength per unit volume content of the Z-pins, while aluminum pinned sandwich structures was seen to have the least performance. Du Long, Jiao Guiqiong [5] compared perpendicular, cross and pyramidal pin arrangements for indentation study on pin reinforced sandwich structures. Tao Liu et al. [9] compared tetrahedral and pyramidal pin arrangements for the pin truss structure for compressive strength of the sandwich structure.

Most of the studies in obtaining the stiffness of the sandwich structure are experimental. Analytical models have been proposed by some studies in which the effect of foam has been included by modeling the foam as a spring foundation (Winkler foundation) on the pins [7, 9, 12]. Empirical relations were provided for spring constant of the foundation in both horizontal and vertical directions, and verified by experiments involving pulling of the pin through a foam material. In these studies, it was observed that the foam had little effect on the stiffness of the structure but it stabilizes the structure by increasing its strength by delaying pin buckling. A modified buckling load is then estimated for a pin on a spring foundation [7,9]. D.D. Cartie et al. [7] used X-ray CAT scans of deformed structure including the pins to obtain the buckling mode of the pins and compared the modified buckling strength of the pins on spring foundation with experimental results.

In estimating the strength of a sandwich structure, the main modes of failure were established in each study. Different failure modes have been predicted by different research groups. Marasco et al [6] observed two modes of failure depending on the type of loading. For an out-of-plane tensile loading, the core-skin interface bond seemed to be the determining parameter resulting in pulling out of pins and debonding of the pins from the facesheets. For an out-of-plane shear loading and compressive loading, the core behavior formed the basis for the strength of the structure. Strengthening from foam was observed to delay pin buckling in these cases. Nanayakkara et al [1] found that the z-pins failed close to their elastic stress limit via a complex process of kinking and fragmentation caused by voids in the carbon fibres resulting from incomplete wetting with the resin during the pultrusion process. After the buckling of the z-pins, the fractured ligaments of the z-pins pressed into the foam core under increasing compressive strain which strengthened the sandwich material. The pins were observed to carry some load on them until the foam core experienced crushing.

There are research studies on z-pin reinforced sandwich structures focused on obtaining the strength in other types of loading. Chang et al. [3] deal with flexural properties of the sandwich structures. Failure was observed due to damage in microstructure at the interface of the nearest z-pin near the site of loading and the facesheet that lead to breakage of fibres. Liu et al [9] studied the sandwich structure under bending loads as well. The effective properties like the stiffness of the sandwich structure were estimated using an analytical micromechanics based model verified by FE models. Failure was observed in four collapse modes based on the geometry of the sandwich structures-

composite facesheet yielding or microbuckling, facesheet wrinkling, plastic shear of the core and facesheet indentation beneath the rollers.

Fan et al. [4] and Long et al. [5] studied indentation or impact loads on the sandwich structures. The load-displacement curve of the sandwich structure was observed to be broken down into three regimes- the elastic response, the collapse of the core due to buckling of nearest pin and propagation of failure. Both analytical and FE models were studied with focus on non-linear analysis within the elastic regime [5].

Certain studies [8] included post-buckling analysis of the pins to estimate the strength of the structure. Wallace et al. [8] showed that besides providing reinforcement in the form of compressive stiffness, the oblique pins also suppressed delamination of the facesheets improving the damage tolerance of the structure.

Some studies [6] compared the performance of sandwich structures with a honeycomb core versus Z-pin reinforced core. There are differences in the absolute values of strength accompanied by differences in the mechanisms of failure. In the case of sandwich structures using a honeycomb core, Nomex, failure was observed in the core as the cell walls of the honeycomb failed in tension or experience shear buckling. For the pinned cores, the skin–core interface was observed to be the critical part where the specimen fails. Nomex honeycomb sandwich panels outperformed the pinned-core sandwich panels in terms of ultimate strength. However, when the sandwich panel stiffness was compared, the pinned core appeared to have superior properties than the honeycomb structures.

Although the manufacture and usage of sandwich structures is a very old procedure, pin reinforced sandwich structures have only recently been constructed. Several papers [1, 6, 7, 9, 11, 12] studied compressive stiffness and strengths of Z-pin reinforced sandwich

structures but most of the studies of sandwich panels/beams having pin-reinforced foam cores existing in literature are mainly based on experimental measurements. The theoretical and computational modeling on the performance of Z-pin sandwich structures is limited and a necessity for a clearer understanding of the structural performance and their design. Tao Liu et al [9] developed a micromechanics based model to calculate the effective properties of pin-reinforced foam cores and derived analytical formulae for the effective elastic–plastic properties of pin-reinforced foam cores with either a pyramidal or tetrahedral arrangement of pin reinforcements, calibrating the predictions to existing experimental data. In comparison with FE calculated results, they observed that the analytical models provided good estimates of the stiffness of a sandwich with pin-reinforced foam core, but however they underestimated its strength.

Among other few analytical studies on sandwich structures include the research of David W. Sleight et al [12], which focusses on traditional non-reinforced sandwich structures only. The Rayleigh-Ritz and finite-difference methods are used to predict the critical buckling load of the sandwich foam and the accuracy of the methods is assessed with a finite-element analysis.

1.3 Research objective and Scope

Lack of a comprehensive analytical and computational model to predict the performance (stiffness and strength) of a K-cor sandwich structure with particular focus on individual components of the structure and the interaction between them has prompted for this research. This research program is focused on developing appropriate macro-mechanical models that account for the meso-structural details unique to K-Cor composite sandwich

panels. Currently, there is no simulation capability for predicting the mechanical behavior of structures that are fabricated using these novel composite materials. Therefore, a new modeling approach is proposed utilizing multiscale Finite Element models in which the contribution of individual component of the sandwich structures will be studied in conjunction with the interaction potential between them. In particular, the interaction effects between the reinforcing pins and the flexible composite facesheet will be the focus of the study under compressive loads. The dependence of the pin-facesheet interaction effect on geometrical and material parameters of the sandwich structure will be analyzed. In addition, the adhesive layer bonding the pins to the facesheet will be modeled including its interaction effects with the pins. The adhesive layer being compliant is susceptible to yielding and the pin-adhesive interaction before and after yielding will be investigated. The effect of pin buckling in the context of estimating the strength and the load carrying capacity of the sandwich structures will be studied. In this research we will also develop different finite element models for estimating the size effect and comparing the performance of sandwich structures with different cutting edges. The finite element models constructed will be compared with different experimental data for validation.

The computational models developed in this research do not account for the interaction of the foam with the reinforcing pins. Also, the reveal lengths of the pins are not incorporated in the FE models constructed in this research. In addition to the above enhancements, detailed investigations regarding the pin-facesheet interaction by analysing local deformation pattern on the facesheets using a non-linear model is left for future studies.

The rest of the thesis is organized as follows. Chapter 2 deals with obtaining the analytical properties of the core due to the pin truss structure. The theoretical core stiffness and strengths are derived in this chapter. In chapter 3, we develop models of sandwich structures predicting the specimen response to compressive and shear loads. We correlate the theoretical models described in chapter 3 with experimental results obtained on different sandwich specimens in chapter 4. We conduct parametric studies in chapter 5, by investigating the influence of different parameters on the properties of sandwich structures. Conclusions and recommendations for future work are given in chapter 6.

Chapter 2

Core Properties due to pins

The pin truss forms the basis for the structural reinforcement of the sandwich structure. Since the pins have moduli much greater than that of the foam core, most of the stiffness and the strength of the core is contributed by the pins. In this chapter we carry out an analytical study on the stiffness and strength of the core with particular attention to their dependence on pin geometry. Effect of foam is not considered in the study. The study begins with analysis of individual pins and then studying a general pin truss structure.

2.1 Pin Spring Constants

In this section we proceed to compute the spring constant of a single pin under compression and shear loading conditions.

2.1.1 Compression

Consider a pin in the x-z plane inclined to the vertical by an angle, θ, as shown in Figure 2.1. One end of the pin is fixed and the other end has a guided boundary condition, allowing only vertical displacements. The compressive spring constant of the pin is defined as the reaction force on the pin in the z direction, F_z, for unit vertical tip displacement. We first obtain the expression for the spring constant assuming clamped conditions on both ends of the pin. The reaction force at the pin end can be split into an axial force, F_a, a perpendicular force in the plane, F_p, and a moment M. Let u and v denote the displacements of the tip in the axial and perpendicular directions respectively,

and Φ denote the angular displacement at the tip, in the x-y plane. Let E denote the stiffness of the pin and A_{pin} be the cross-sectional area of the pin. Let $\bar{x}$ and $\bar{y}$ denote axes directions along the axial and the transverse directions. We apply a unit tip displacement at the pin end, and compute the corresponding reaction force.

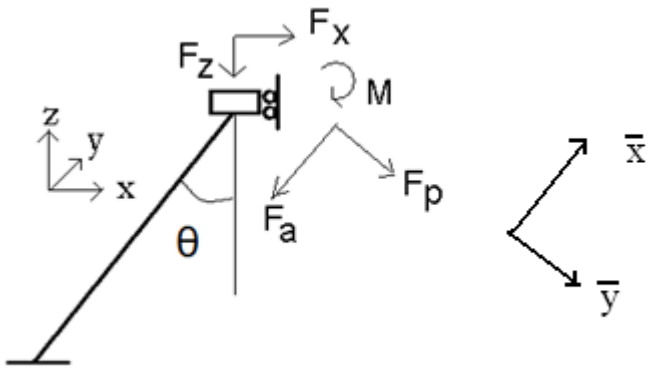

Figure 2.1: An oblique pin the x-z plane, showing the reaction forces and moment

For a unit vertical displacement at the tip, we must have,

$$u\cos(\theta) + v\sin(\theta) = 1 \tag{2.1}$$

$$u\sin(\theta) - v\cos(\theta) = 0 \tag{2.2}$$

$$\Phi = 0 \tag{2.3}$$

An approximate solution for the compressive spring constant can be obtained by assuming there is no coupling between the bending and axial directions. This, in effect, means that the axial loads do not affect the bending displacements of the beam and vice-versa. The validity of the solution is checked below by comparing with a non-linear computational model that includes coupling between the two directions. Consider the effect of the individual forces on the tip displacements of the beam. We must imagine

that these force act individually in no conjunction with other forces and calculate the corresponding pin displacements.

Effect of axial force, F_a :

Axial displacement = $u_1 = F_aL/ (A_{pin} E)$

Perpendicular displacement = $v_1 = 0$

Angular displacement = $\Phi_1 = 0$

Effect of transverse force F_p :

Axial displacement = $u_2 = 0$

Perpendicular displacement = $v_2 = F_pL^3/3EI$

Angular displacement = $\Phi_2 = F_pL^2/2EI$

Effect of M :

Axial displacement = $u_3 = 0$

Perpendicular displacement = $v_3 = ML^2/2EI$

Angular displacement = $\Phi_3 = ML/EI$

In the absence of coupling, the combination of these forces will result in displacements,

$$u = u_1 + u_2 + u_3 \tag{2.4}$$

$$v = v_1 + v_2 + v_3 \tag{2.5}$$

$$\Phi = \Phi_1 + \Phi_2 + \Phi_3 \tag{2.6}$$

Solving the above equations in conjunction with Equations (2.1)-(2.3) for F_a, F_p and M, we obtain the compressive spring constant of the pin as

$$K_c = F_a \cos\theta + F_p \sin\theta = \frac{E A_{pin}}{h}(1 + 3\xi^2 \sin^2\theta)\cos^3\theta \tag{2.7}$$

where ξ is equal to r/h, the ratio of the radius r of the pin to the core thickness h. The pins used in the sandwich structures studied in this research have a radius of 0.235 mm and the core thickness is nominally about 15 mm. Thus the value of ξ is of the order of 0.02, much less than 1. The second term in the parenthesis of the above expression, $3\xi^2\sin^2\theta$, corresponds to the bending stiffness of the pins under compression, which is much smaller compared to the axial stiffening. Neglecting the second term, the spring constant of the pin under compression can be seen to vary with the pin insertion angle as $\cos^3\theta$. Using the moduli values of the pin material T650-35/8606, E = 156.5 GPa, we plot the spring constant of the pin versus insertion angle for various core thicknesses, in Figure 2.2. It can be seen that the spring constant decreases monotonically as the insertion angle increases.

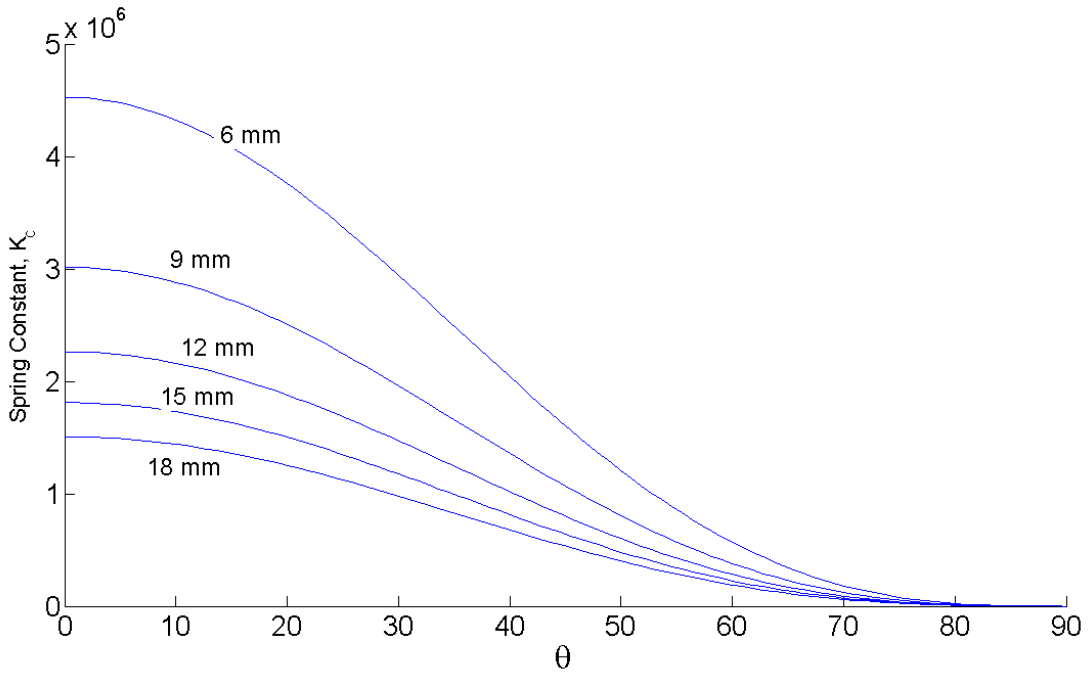

Figure 2.2. Spring constant under compression vs. the pin insertion angle for different core thicknesses.

The non-dimensional spring constant, $K_c/(EA_{pin}/h)$ is plotted in Figure 2.3. It shows that $K_c/(EA_{pin}/h)$ is nearly independent of core thicknesses. This is because most of the contribution to the spring constant comes from the axial stiffening of the pins, which varies linearly with pin lengths.

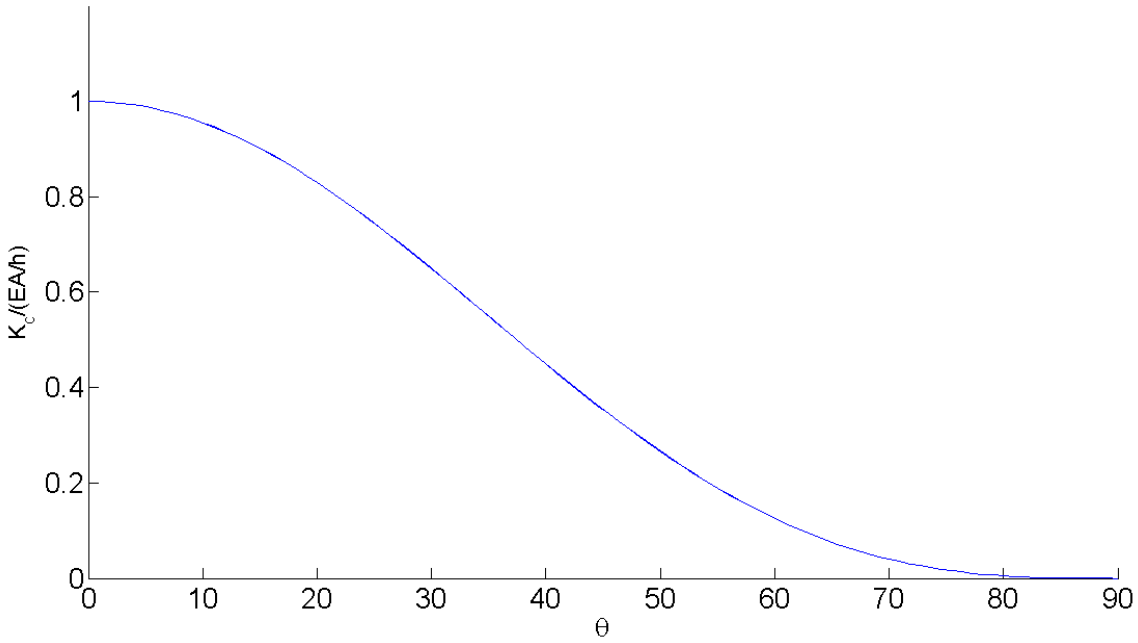

Figure 2.3. Non-dimensional spring constant for a compressive loading for different core thicknesses.

The pins in the sandwich structures are attached to the facesheets with the help of an adhesive. For the K-Cor type of sandwich structures, the pins extend beyond the point of contact with the facesheets into reveal lengths, which are flattened out on the foam and attached using an adhesive. The classical boundary conditions of simply supported and clamped may not apply for this kind of attachment, and the real boundary condition

might lie somewhere between the two. Thus we also consider the effect of simply supported boundary conditions on the pin ends as well.

There cannot exist moment reactions at the simply supported ends because of free rotations. In addition, there cannot exist transverse reaction forces at the supports as well because they will cause unbalanced moments on the beam. Hence in the deformed static state, the only reaction forces acting on the beam are axial forces. These axial forces act to compensate for the change in length of the beam in the new position from the original undeformed configuration.

For a unit z displacement, the change in length of the beam is $\cos(\theta)$, for small vertical displacements. The axial compressive force that acts as a result of change in beam length by this amount equals $F_z = E\ A_{pin} \cos(\theta)/L = E\ A_{pin} \cos^2(\theta)/h$. The vertical component of this force equals the spring constant of the pin in the vertical direction (under compression). The compressive spring constant thus equals $K_c = F_z \cos(\theta) = E\ A_{pin} \cos^3(\theta)/h$. Note that this equals the axial component of the spring constant of the pin with clamped supports. For clamped supports, the contribution of the bending component to the spring constant is negligible. Hence the spring constants are almost equal for either clamped supports of simple supports.

2.1.2 Shear

The spring constant of a single pin for shear loading is dependent on the direction of the shear displacement. If the shear displacement is in the x direction, then we have to consider a pin in the x-z plane and one in the y-z plane separately. Figure 2.4 shows the two pins.

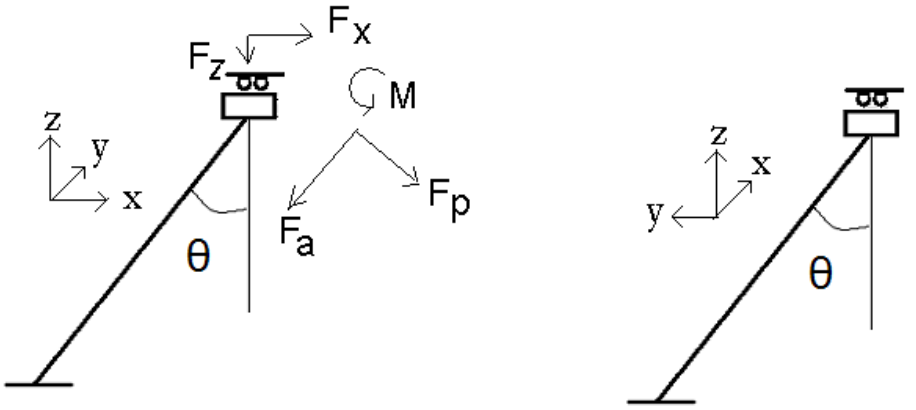

Figure 2.4: Two sets of oblique pins in x-z and y-z planes respectively that have different spring constants under shear loading

For the pin in x-z plane with a unit displacement in the x direction, we must have

$$u\cos\theta + v\sin\theta = 0 \tag{2.8}$$

$$u\sin\theta - v\cos\theta = 1 \tag{2.9}$$

$$\Phi = 0 \tag{2.10}$$

The three equations above are solved in adjunction with Equations (2.4)-(2.6), for F_a, F_p and M. The spring constant for a pin with clamped support ends is then given by

$$K_s = F_a \sin\theta - F_p \cos\theta = E A_{pin}/h\,(\sin^2\theta + 3\xi^2\cos^4\theta)\cos\theta \tag{2.11}$$

The shear spring constant for a T650-35/8606 pin is plotted versus the pin insertion angle for various core thicknesses, in Figure 2.5. Neglecting the quantity containing ξ^2, the spring constant is seen to vary approximately as $\sin^2\theta\cos\theta$. The spring constant attains a maximum at angle $\theta \sim 55^0$ independent of the core thickness. Figure 2.6 shows the plot of non-dimensional spring constant, $K_s/(EA_{pin}/h)$ vs. insertion angles.

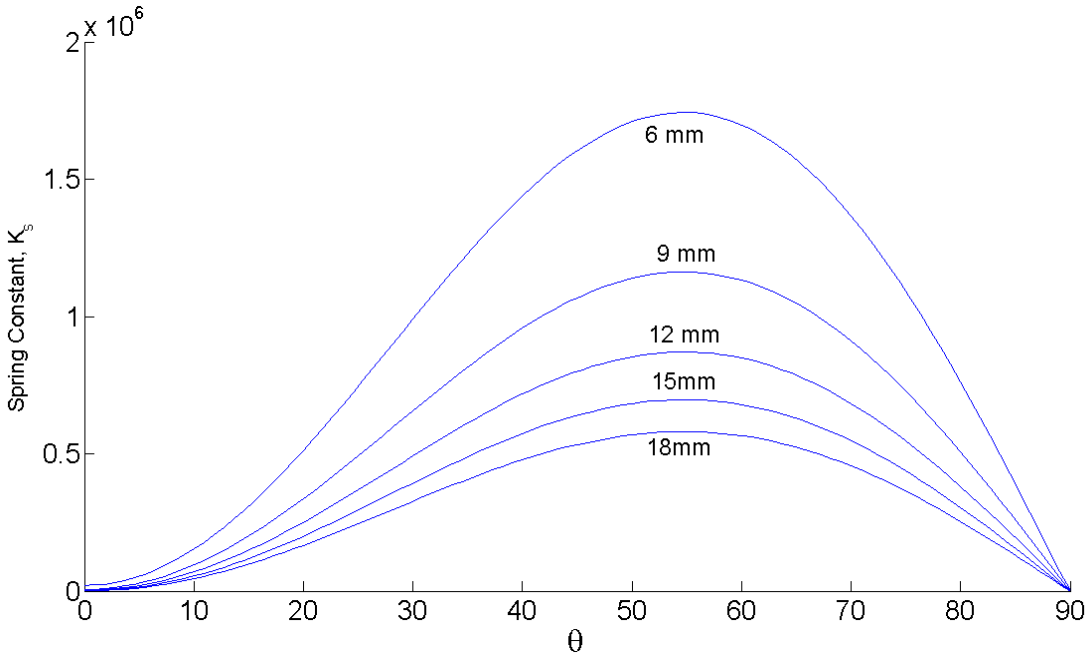

Figure 2.5. Spring constant under shear versus pin angle for different core thicknesses.

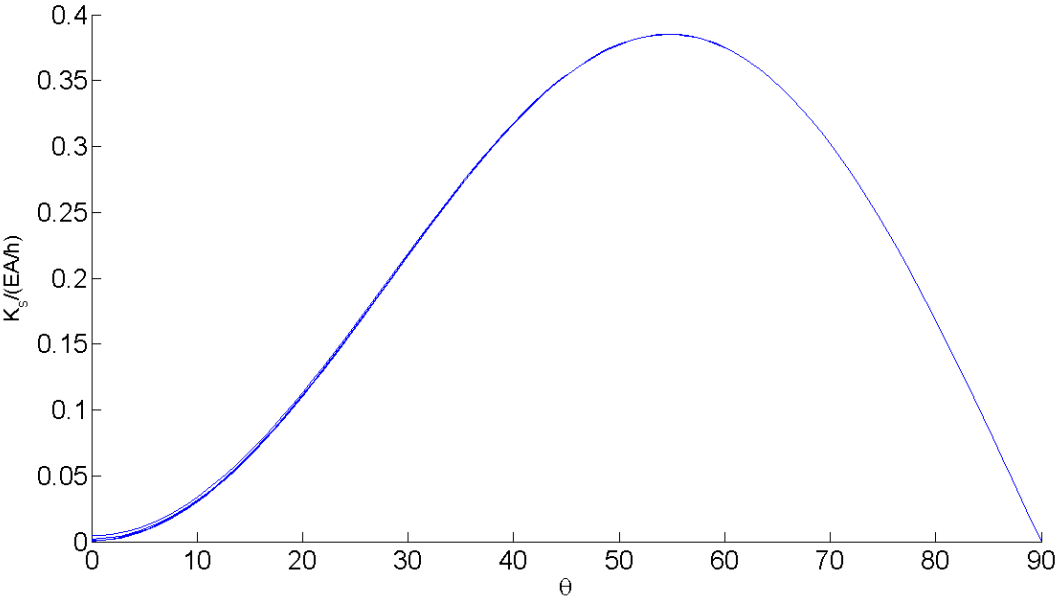

Figure 2.6: Non-dimensional spring constant of the x-z oblique pin under shear for different core thicknesses.

The non-dimensional spring constant is again nearly independent of the core thickness as the bending contribution to the shear spring constant is negligible.

For simply supported ends, only the axial component of the spring constant is relevant. The spring constant in this case is $K_s = EA_{pin}/h \sin^2\theta \cos\theta$, which is almost equal to the spring constant of the pin with clamped supports.

For the pin in the y-z plane, since the displacement is along the x direction, perpendicular to the pin, the spring constant is given by $12EI/L^3 = 12EI\cos^3\theta/h^3$, for clamped support ends. Simply supported boundary conditions do not offer any resistance to the shear displacement in the bending direction. The spring constant for clamped supports is plotted for a T650-35/8606 pin in Figure 2.7 as a function of the insertion angle. The spring constant monotonically decreases with respect to the insertion angle. Also, it is to be noted that this spring constant is very small and negligible compared with the spring constant of the pin oblique in the x-z plane.

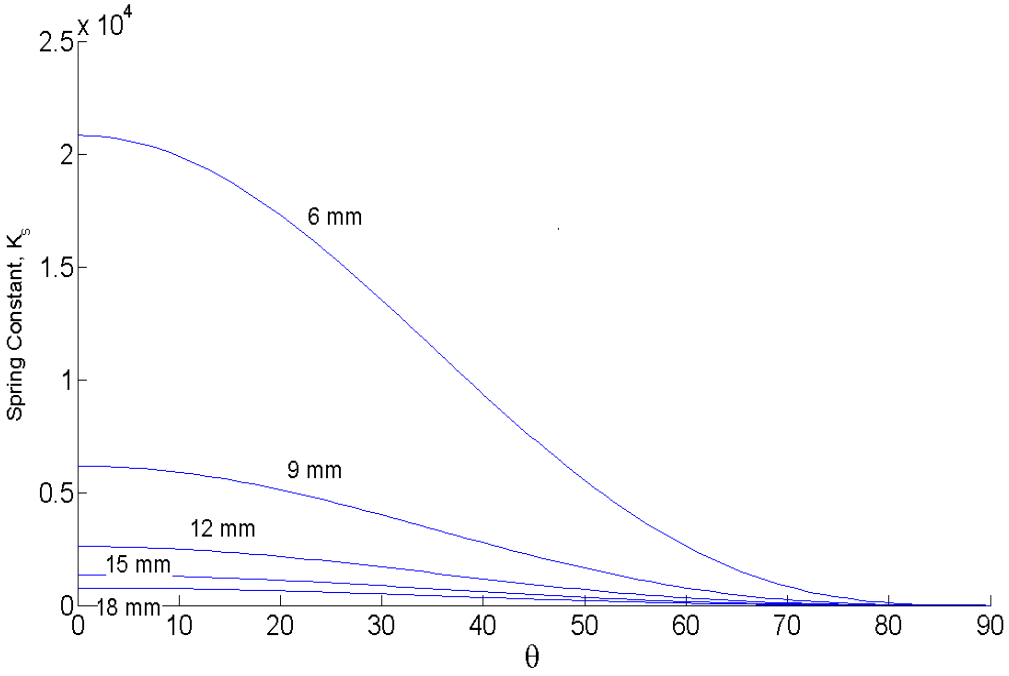

Figure 2.7 Spring constant of the y-z pin under shear with pin insertion angle for different core thicknesses.

2.2 Core Stiffness

Using the pin spring constants determined in the previous section, we can determine the core stiffness under compression and shear. In this section, we compute the core stiffness of an infinite panel, including only the pin truss structure in the core and not the foam, to focus the effect of the pins. The stiffness under compressive (or shear) loading conditions is obtained by applying a uniform unit displacement to top surface of the foam in the compressive (or shear) direction while fixing the bottom surface, and calculating the corresponding stress (force per unit area) at the top surface of the foam. In addition to the above parameters for the pin, the cell interval is an important parameter in determining the core stiffness. The stiffness is large for closely packed pin structure with smaller cell intervals. Let 'a' be the cell spacing of the sandwich panel, and β denote the non-dimensional quantity β=r/a, the ratio of the pin radius and the cell spacing. The formulae for stiffness in the next sections are derived assuming clamped boundary conditions only at the pin ends, as the boundary conditions (clamped or hinged) do not have a significant effect on the stiffness.

2.2.1 Compression

A sandwich panel with an infinite length and infinite width has the same stiffness as a unit cell. The stiffness of the unit cell is given by

$$E_c = K_u \frac{h}{A_u} \tag{2.12}$$

where A_u is the area of a unit cell, K_u is compressive spring constant from all the pins in the unit cell. The stiffness of the core then depends on whether the sandwich panel

contains vertical pins or not. For a sandwich panel with no vertical pins and a unit cell as shown in Figure 1.5, the core stiffness for a compressive loading is given by

$$Ec = 4\pi \beta^2 E_{pin}(1 + 3\xi^2 \sin^2 \theta) \cos^3 \theta \quad (2.13)$$

for clamped support ends, and

$$Ec = 4\pi \beta^2 E_{pin} \cos^3 \theta \quad (2.14)$$

for simply supported ends.

For a sandwich panel with vertical pins and a unit cell as shown in Figure 1.6, the core stiffness is given by

$$E_c = 4\pi \beta^2 E_{pin} (1 + 3\xi^2 \sin^2 \theta) \cos^3 \theta + \pi \beta^2 E_{pin} \quad (2.15)$$

for clamped support ends, and

$$E_c = 4\pi \beta^2 E_{pin} \cos^3 \theta + \pi \beta^2 E_{pin} \quad (2.16)$$

for simply support ends.

There is not much dependence of the compressive stiffness on the core thickness, but the cell interval is an important factor. This can be seen in Figure 2.8, where the compressive core stiffness is plotted for a T650-35/8606 pin, a 0.5 inch (12.7 mm) thick core and two different cell intervals, for both kinds of panels.

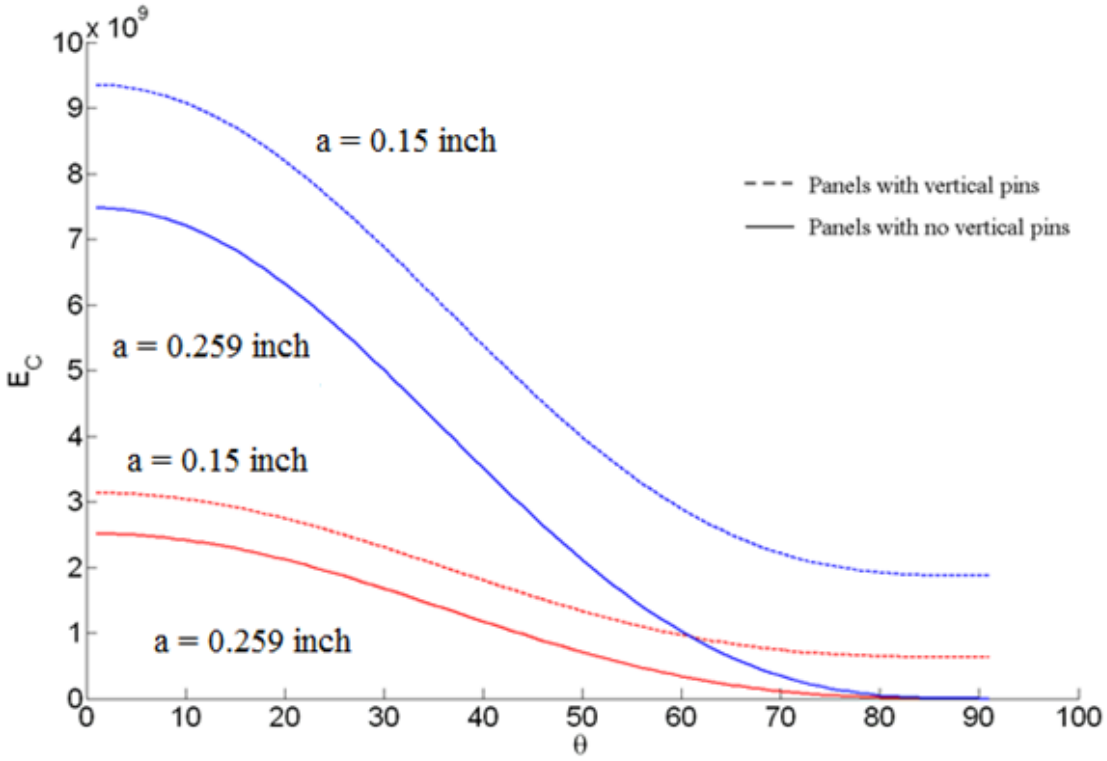

Figure 2.8: Compressive stiffness of the core vs. insertion angle for different cell spacing and different types of panels.

2.2.2 Shear

For an infinite sandwich panel with no vertical pins, the core stiffness under shear loading is given by

$$G_c = 2\pi \beta^2 E_{pin} [(\sin^2\theta + 3\xi^2 \cos^4\theta)\cos\theta + 3\xi^2 \cos^3\theta] \quad (2.17)$$

for clamped supports and

$$G_c = 2\pi \beta^2 E_{pin} \sin^2\theta \cos\theta \quad (2.18)$$

for simple supports.

For an infinite sandwich panel with vertical pins, the core stiffness under shear loading is given by

$$G_c = 2\pi\,\beta^2 E_{pin}\,[(\sin^2\theta + 3\xi^2\cos^4\theta)\cos\theta + 3\xi^2\cos^3\theta] + 6\pi\,E_{pin}\,\beta^2\xi^2 \quad (2.19)$$

for clamped supports and

$$G_c = 2\pi\,\beta^2 E_{pin}\,\sin^2\theta\cos\theta \quad (2.20)$$

for simple supports.

This core stiffness is plotted in Figure 2.9, for a T650-35/8606 pin, a 0.5 inch (12.7 mm) thick core and two different cell intervals, for both kinds of panels (for only clamped support ends, because there is not much dependence on tip boundary conditions). Since the vertical pins have very small spring constant (Figure 2.7), their contribution to the stiffness is also negligible. Hence, both kinds of panels have almost the same stiffness.

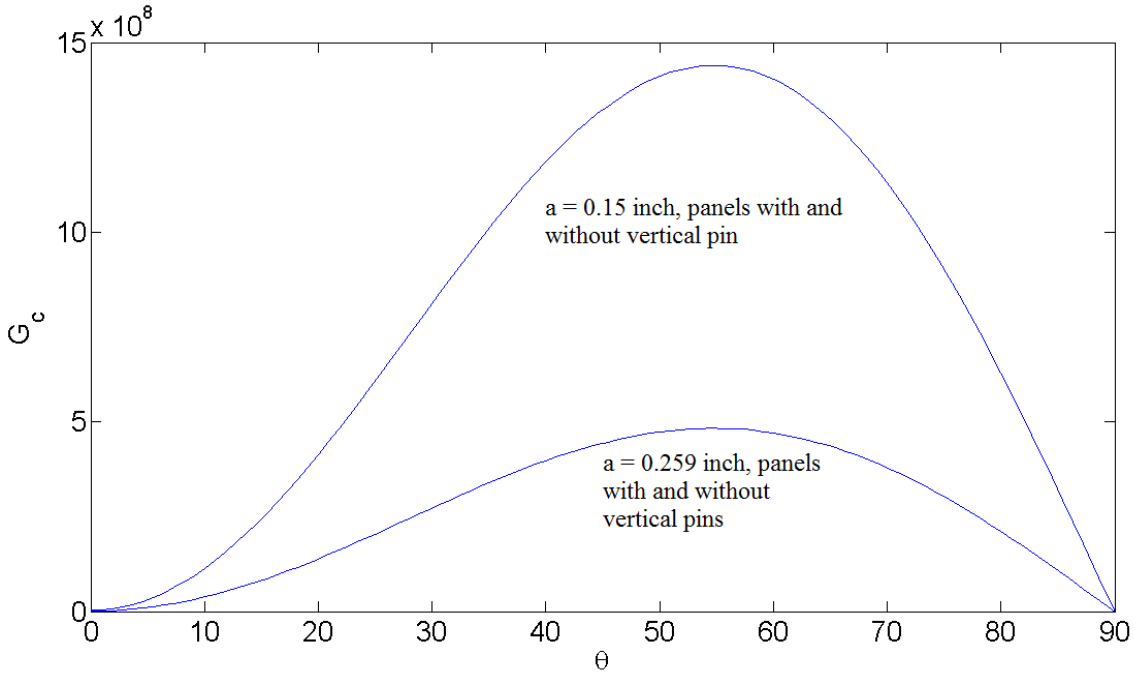

Figure 2.9: Shear stiffness of the core vs. insertion angle for different cell spacing and different types of panels.

2.2.3 Core Stiffness of finite panels

The formulas (2.13)-(2.20) for compressive and shear stiffness of the core were derived for infinite panels. Real sandwich structures are finite sized and the stiffness of the finite panels differ from those of the infinite panels. The stiffness of a finite panel depends on the number of pins. For instance, consider sandwich panels with only oblique pins in the model. Let N_x and N_y be the number of oblique pins running in the x and y directions of the sandwich panel respectively and the cross-sectional area of the facesheets, A_{fs}. The core stiffness for a compressive loading is given by

$$E_c = E\frac{(N_x + N_y)A_{pin}}{A_{fs}}(1 + 3\xi^2 \sin^2\theta)\cos^3\theta \tag{2.21}$$

for clamped support ends, and

$$E_c = E\,(N_x + N_y)\cos^3\theta \tag{2.22}$$

for sim ply supported ends.

The core stiffness for a shear loading (in the x-direction) is given by

$$E_s = E\,N_x\,\frac{A_{pin}}{A_{fs}}\,(\sin^2\theta + 3\xi^2\cos^4\theta)\cos\theta + 12E\,N_y\frac{I}{A_{fs}}\frac{\cos^3\theta}{h^2} \tag{2.23}$$

for clamped support ends, and

$$G_c = E\,N_x\,\frac{A_{pin}}{A_{fs}}\sin^2\theta\,\cos\theta + 12E\,N_y\frac{I}{A_{fs}}\frac{\cos^3\theta}{h^2} \tag{2.24}$$

for simply supported ends.

In section 5.1, we study the effect of cutting edges and specimen sizes on the compressive and shear stiffness of finite sandwich panels.

2.3 Core Strength

Determining the failure characteristics of the sandwich structures is an important part of their study. The maximum load that the sandwich structures can take before failure is called the strength of the material. In this section, we compute the core strength of a sandwich panel by considering only the pin truss structure. Failure can occur due to buckling of the pins or their pullout due to breakage of adhesive bonds between the pin and the face-sheet.

2.3.1 Compression

The strength of the core panel under compressive loading is largely governed by the buckling properties of the pins, as all pins are under compression. Consider an oblique pin the x-z plane under a compressive load (Figure 2.2). At buckling the following equations hold:

$$u \sin\theta - v \cos\theta = 0 \tag{2.25}$$

$$\Phi = 0 \tag{2.26}$$

$$F_a = \frac{4EI\pi^2}{L^2} \tag{2.27}$$

Assuming clamped boundary conditions, we solve the above equations in conjunction with equations (2.1)-(2.3) to obtain the z displacement, δ_{comp} at buckling as

$$\delta_{comp} = \frac{\pi^2 r^2}{h} \tag{2.28}$$

which is independent of the insertion angle. The oblique pins in the y-z plane also have the same buckling displacement due to symmetry. Hence all the pins in the core panel buckle at the same z displacement regardless of insertion angles.

For an infinite panel with no vertical pins, the compressive buckling strength in terms of force per unit area (stress) is given by

$$\sigma_c = 4E\pi^3\beta^2\xi^2 \ (1 + 3\xi^2 \sin^2\theta)\cos^3\theta \tag{2.29}$$

The compressive buckling strength for an infinite panel with vertical pins is given by

$$\sigma_c = 4E\pi^3\beta^2\xi^2 \ (1 + (1 + 3\xi^2 \sin^2\theta)\cos^3\theta) \tag{2.30}$$

The compressive strengths are plotted in Figure 2.10, versus insertion angles for different cell spacing and kinds of panels.

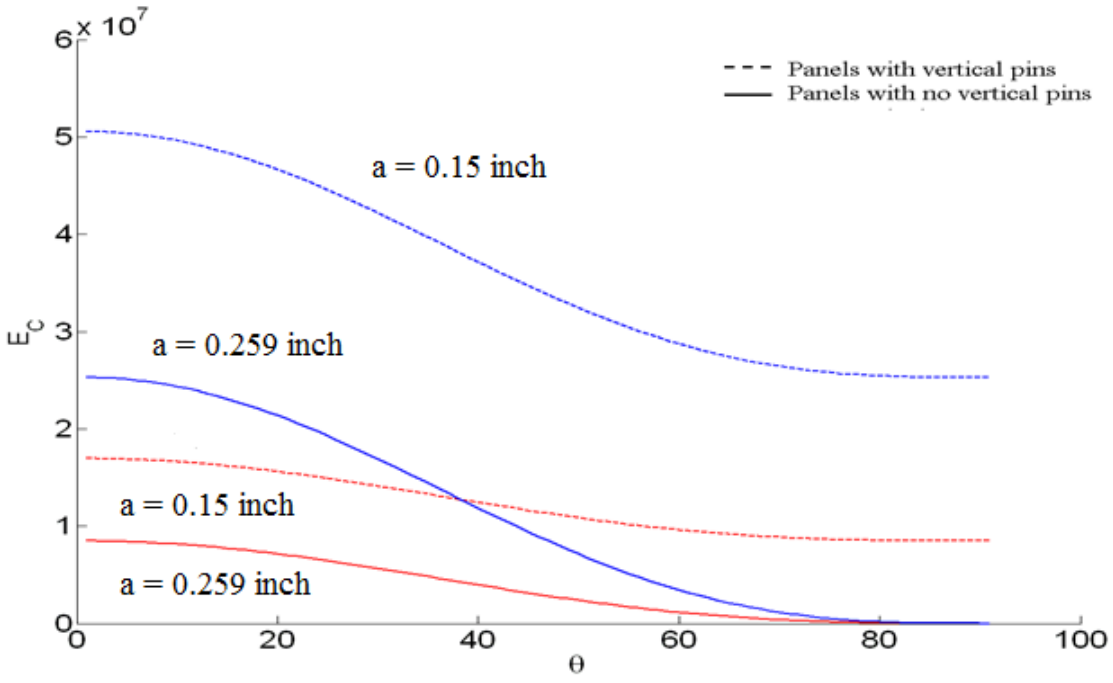

Figure 2.10: Compressive strengths of the core vs. insertion angle for different cell spacing and different types of panels.

For structures with simply supported ends, buckling occurs when the axial force equals,

$$F_a = \frac{EI\pi^2}{L^2} \tag{2.31}$$

The axial force in the pins in terms of the vertical displacement, δ is given by $F_a = EA\delta/h\cos^2\theta$. Equating the two expressions gives the value of δ at which the pins buckle. We get

$$\delta_{comp} = \frac{\pi^2 r^2}{4h} \tag{2.32}$$

This is exactly equal to one fourth of the buckling displacement of the structure with clamped ends. This is expected because the pins with simply supported ends buckle at one-fourth load value as that of pins with clamped ends.

For an infinite panel with no vertical pins and simply supported ends, the compressive buckling strength in terms of force per unit area (stress) is given by

$$\sigma_c = E\pi^3\beta^2\xi^2(\cos^3\theta) \tag{2.33}$$

The compressive buckling strength for an infinite panel with vertical pins and simply supported ends is given by

$$\sigma_c = E\pi^3\beta^2\xi^2(1+\cos^3\theta) \tag{2.34}$$

While making computational linear FE models of the sandwich structures, pins have been usually modeled with only clamped support ends for calculating stiffness and strengths of the structure. While the stiffness of the structure has a negligible dependence on the boundary conditions of the pin, the strength of the structure is four times higher in the case of clamped supports as compared with that with simple supports.

2.3.2 Shear

For a shear force in the x-direction, some of the oblique pins in the x-z plane are under compression while others are in tension and all the other pins are under tension. The pins under tension stretch under tensile force until they are pulled out from the plate. The pullout force therefore becomes the criterion for failure and determines the strength of the panel. The pins under compressive force buckle before the other pins are pulled out, but these pins are expected to carry loads even after buckling until the entire structure fails. Figure 2.11 shows a pin under compressive force under tip displacement in the x direction corresponding to a shear load.

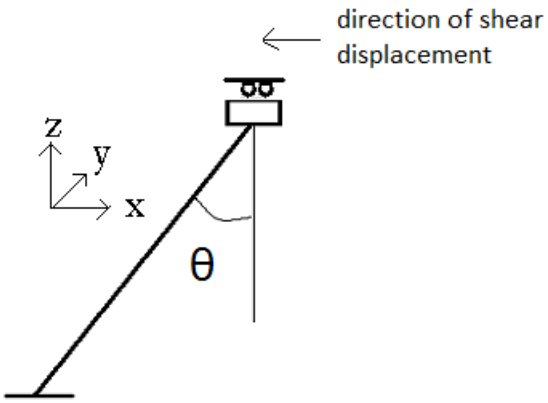

Figure 2.11: Oblique pin in the x-z plane which is under compression for a shear loading in the direction as shown.

At buckling for these pins,

$$u\cos\theta - v\sin\theta = 0 \tag{2.35}$$

$$\Phi = 0 \tag{2.36}$$

$$F_a = \frac{4EI\pi^2}{L^2} \tag{2.37}$$

Solving the above equations for unknown displacements u and v, the horizontal displacement at buckling for clamped boundary conditions can be determined as

$$\Delta_{shear} = \frac{\pi^2 r2}{L\sin\theta} = \frac{\pi^2 r^2 \cot(\theta)}{h} \tag{2.38}$$

The buckling displacement for simply supported ends can be shown to be equal to one-fourth this value, that is

$$\Delta_{shear} = \frac{\pi^2 r2}{4L\sin\theta} = \frac{\pi^2 r^2 \cot(\theta)}{4h} \tag{2.39}$$

The above shear displacements can be used as a lower bound estimate for the failure of the sandwich panels. Using these expressions, we get the shear buckling strength of the sandwich panels without vertical pins as,

$$\sigma_s = E\pi^3\beta^2\xi^2 \left(2(\sin^2\theta + 3\xi^2\cos^4\theta)\cos\theta + 24\cos^3\theta \cot\theta + 3\xi^2\cot\theta\right) \tag{2.40}$$

for clamped ends and

$$\sigma_s = E\pi^3\beta^2\xi^2 \left(2\sin^2\theta\cos\theta + 24\cos^3\theta \cot\theta\right) \tag{2.41}$$

for simply supported ends.

The above expressions are plotted for different cell intervals in Figure 2.12.

The shear buckling strength for sandwich panels with no vertical pins is given by

$$\sigma_s = E\pi^3\beta^2\xi^2 \left(2(\sin^2\theta + 3\xi^2\cos^4\theta)\cos\theta + 24\cos^3\theta \cot\theta\right) \tag{2.42}$$

for clamped supports, and

$$\sigma_s = E\pi^3\beta^2\xi^2 \left(2(\sin^2\theta)\cos\theta + 24\cos^3\theta \cot\theta\right) \tag{2.43}$$

for simple supports.

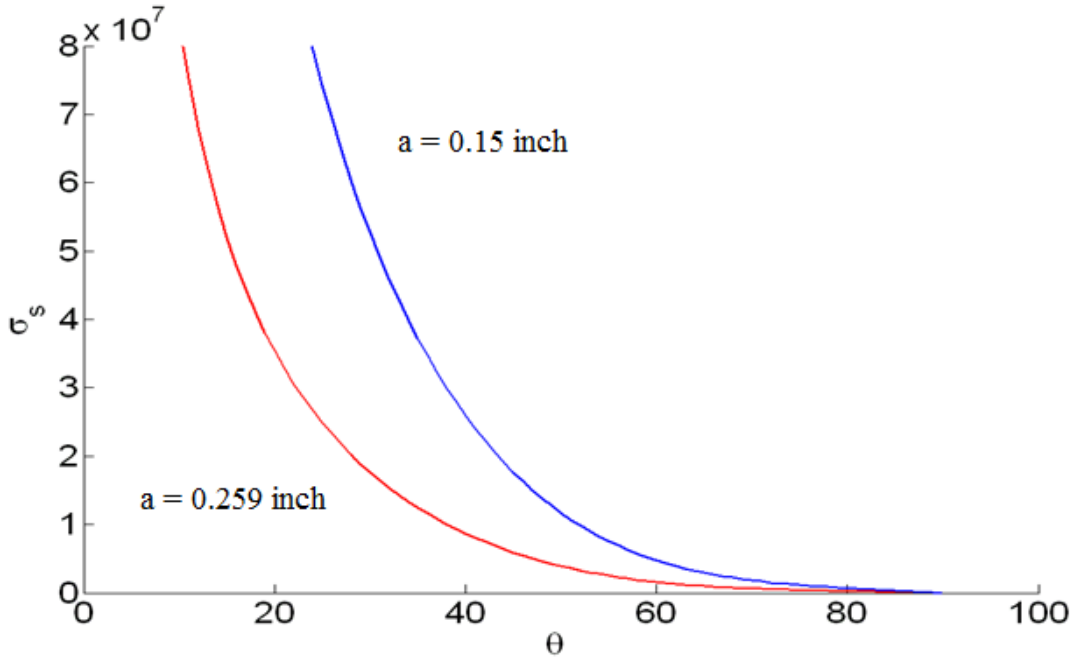

Figure 2.12: Shear buckling strengths of the core vs. insertion angle

Figure 2.13 shows the force-displacement curve for a panel under shear loading. The average force over a single unit cell is plotted versus the shear loading, for a 12 mm thick core and pin insertion angle equal to 35^0. A kink can be observed at a shear displacement value of 4.51×10^{-2} mm which is the buckling displacement under compression. Beyond this displacement these pins carry a constant force. The panel will fail ultimately when the pins under tensile force are pulled out.

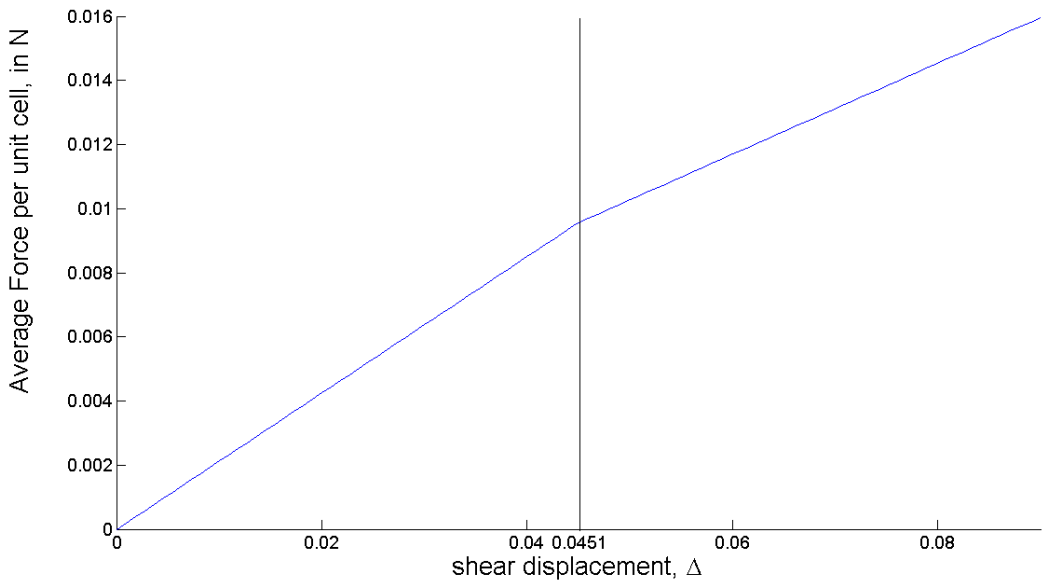

Figure 2.13: Force-displacement relation for a core under shear

For pins under tensile load the reaction forces at the end points are an important as they determine the pullout. If the shear displacement is along the x direction, then half of the oblique pins in the x-z plane are under tension, and the pins in the y-z plane, including the vertical pins are also under a tensile force. For the same amount of displacement, the oblique pins in the x-z plane will pull out first, due to larger reaction forces at the pin-face sheet interface. These pins also have much higher spring constants and are the main contributors to the stiffness and strength of the sandwich structure. Hence analyzing these pins for breakage of adhesive bonds with face sheets is an important study. Consider an oblique pin in the x-z plane, with a shear displacement, Δ in the x-direction. We must have

$$u\sin\theta - v\cos\theta = 0 \tag{2.44}$$

$$u\cos\theta + v\sin\theta = \Delta \tag{2.45}$$

$$\Phi = 0 \tag{2.46}$$

The above equations can be solved for unknown reaction forces, F_a and F_p. They are obtained as

$$F_a = EA\,\Delta\sin\theta\frac{\cos\theta}{h} \tag{2.47}$$

$$F_p = 3\xi^2\,EA\frac{\Delta\cos^2\theta}{h} \tag{2.48}$$

These forces can be converted into horizontal and vertical components, H and V as follows.

$$H = EA\,\Delta\frac{(\sin^2\theta + 3\xi^2\cos^4\theta)\cos\theta}{h} \tag{2.49}$$

$$V = EA\,\Delta\sin\theta\cos^2\theta\frac{(1+3\xi^2\cos^2\theta)}{h} \tag{2.50}$$

The quantities H/Δ , V/Δ and R/Δ (R is the magnitude of the net reaction force) which are measures of the reaction forces at the pin face-sheet interface, are plotted against insertion angles in Figure 2.14 below, for a single oblique pin inserted in a core 0.5 inches (12.7mm) thick.

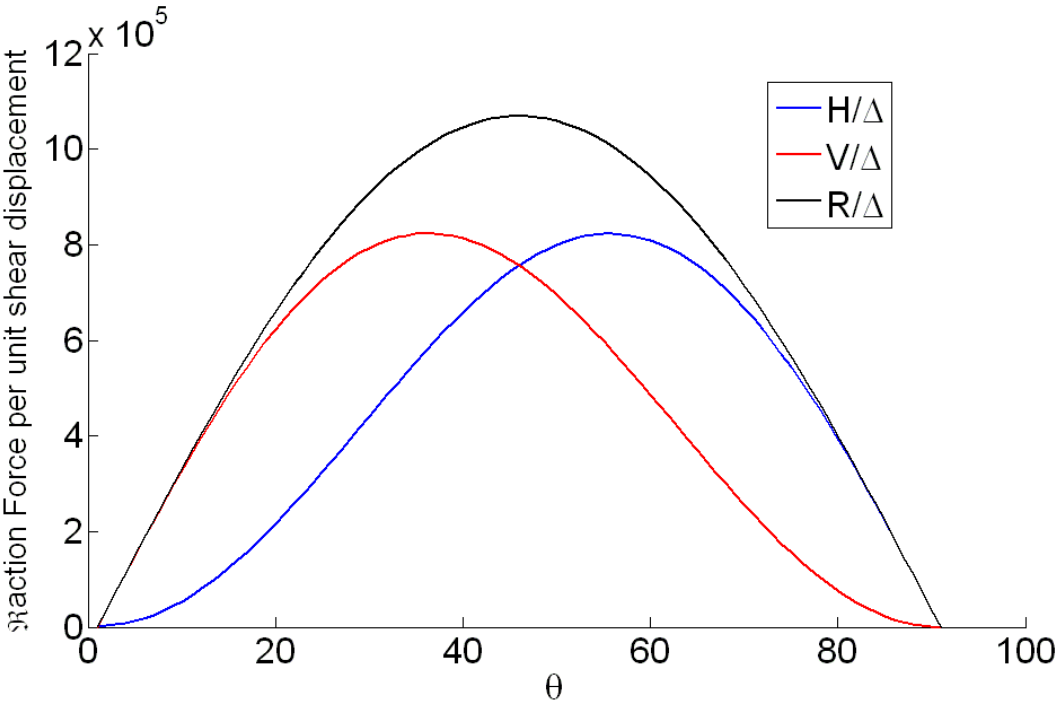

Figure 2.14: Reaction forces per unit shear displacement for a single oblique pin in x-z plane

2.4 Coupling

The above formulas for spring constants of the pins and the stiffness and the strengths of the sandwich panel were derived assuming that pins behave geometrically linear which does not include coupling between axial deformation and bending, as well as the non-linear effect due to large deformations. To confirm the validity of this assumption geometrically nonlinear analysis was carried out using ABAQUS for a typical oblique pin at an angle of 30^0 to the vertical clamped at both ends subjected to a compressive force. The core thickness is 0.75 inch (19.05 mm). The reaction forces at the pin ends obtained from a geometrically nonlinear analysis is plotted in Figure 2.15. Analysis was carried out until the buckling load of the pin. It is observed that the Force-displacement curve is very nearly linear. The slope of the graph is equal to 9.257 x 10^5 N/m which compares

very well with the spring constant obtained from Equation (2.7). Thus, the spring constants obtained from the no-coupling assumption matches with the values obtained from the non-linear analysis.

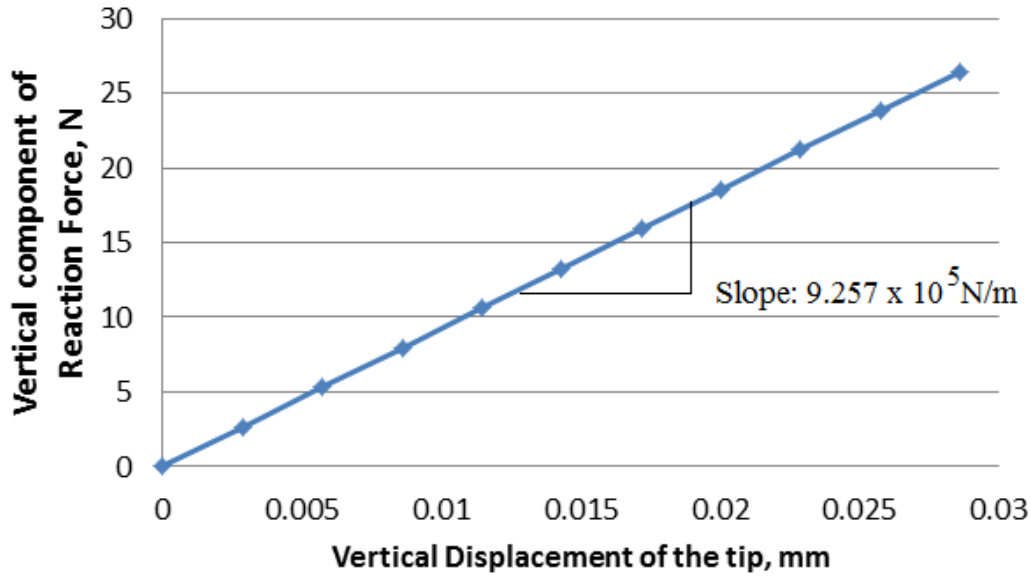

Figure 2.15: Force-displacement plot for a compressive load on a single oblique pin.

2.5 Effect of pin-foam interaction

In deriving the above expressions, the core stiffnesses were calculated by ignoring the effect of the foam. The foam used in the sandwich structures has typically a modulus equal to 36 MPa and the pins have a Young's modulus equal to 156.5GPa, which is several times the foam modulus. It is expected that the foam, being a very soft material, allows the pins to deform within easily and the foam follows the path of the pin deformations. The pin-foam interaction is negligible and the foam does not have a significant effect in the stiffness of the core. To verify this, we consider a 16 mm long oblique pin inclined at 30^0 to the vertical, embedded in a foam material 24 mm wide and 24 mm long as shown in Figure 2.16. The pins are modeled with 3-noded quadratic beam

elements along the length of the pin and the foam is modeled using 20 noded brick elements. The mesh on the foam is generated such that there exist nodes on the foam at the location of the nodes of the pin. The nodes of the foam at these locations are then tied to the respective nodes of the pin, allowing the foam at the line of contact to deform along the path of the pin only. The compressive stiffness of this model is obtained by fixing the bottom surface of the foam and applying a uniform unit vertical displacement on the top surface. This compressive stiffness obtained from the FEM analysis thus is compared with the model that ignores the pin-foam interaction. The compressive stiffnesses of the two models are respectively equal to 31.27 MPa and 30.62 MPa. It is observed that the pin-foam interaction increases the compressive stiffness of the model by only 2.1%. It may be noted that the pin-foam interaction would be larger for foams with higher elastic modulus.

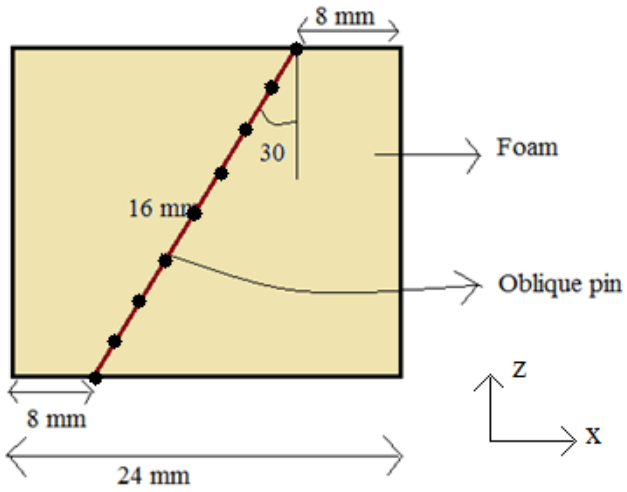

Figure 2.16: Side view of an oblique pin embedded inside foam shown with nodes on the pin

Chapter 3

Stiffness and Strength Models for Sandwich Specimens

3.1 Introduction

In this chapter, we develop models of the sandwich structures that allow us to predict the specimen response to compressive and shear loads. These models are constructed from the pin truss structure and the facesheets, without necessarily including the foam. If the foam is included in the model, the coupling between the pins and the foam is not modeled, and the foam is treated as an independent component attached to the facesheets.

3.2 Developing models of predicted specimen response for compression loading

3.2.1 Model 1: Infinite panel with no pin facesheet interaction

In the previous chapter, we derived expressions for the core stiffness of an infinite panel without considering the facesheets. When the facesheets are included in the model, the stiffness of the model can be computed by using a springs in series model. For a sandwich structure in compression loading, consider the arrangement shown in Figure 3.1. It shows an equivalent springs model for a sandwich structure that includes facesheets but does not have the foam on it. K^f is the spring constant of the facesheets and K^c is the spring constant of the core truss structure derived in the previous chapter. Neglecting the effect of Poisson's coupling between the loading and the transverse directions, we can write the spring constant of the facesheets, for compressive loading, as $K^f = E_3^f A^{fc}/ h^f$, where E_3 is the modulus of the facesheets in the loading direction (z direction) and A^{fc} is the area of the facesheets and h^f is the thickness of the facesheets.

The equivalent spring constant of the series arrangement as shown in Figure 3.1 is given by

$$\frac{1}{\mathrm{K}^{specimen}} = \frac{1}{\mathrm{K}^{f}} + \frac{1}{\mathrm{K}^{core}} + \frac{1}{\mathrm{K}^{f}} \tag{3.1}$$

The stiffness of the specimen in compression direction is then given by

$$E^{specimen} = \frac{h^{specimen}}{\frac{2h^{f}}{E_3{}^{f}} + \frac{h^{c}}{E^{c}}} \tag{3.2}$$

where, E^c is the core stiffness from the pin truss structure derived in the previous chapter, h^c is the core thickness and h^{total} is the total thickness of the specimen, that is $h^{total} = h^c + 2h^f$

The above expression can be be simplified as

$$E^{specimen} = \frac{E^{c}h^{\mathrm{total}}}{h^{c}} \frac{1}{1+\varepsilon} \approx \frac{E^{c}h^{\mathrm{total}}}{h^{c}} \tag{3.3}$$

where

$$\varepsilon = \frac{E^{c}}{E^{f}} \frac{2h^{f}}{h^{c}} \ll 1 \tag{3.4}$$

for sandwich structures with low pin density and low facesheet thickness.

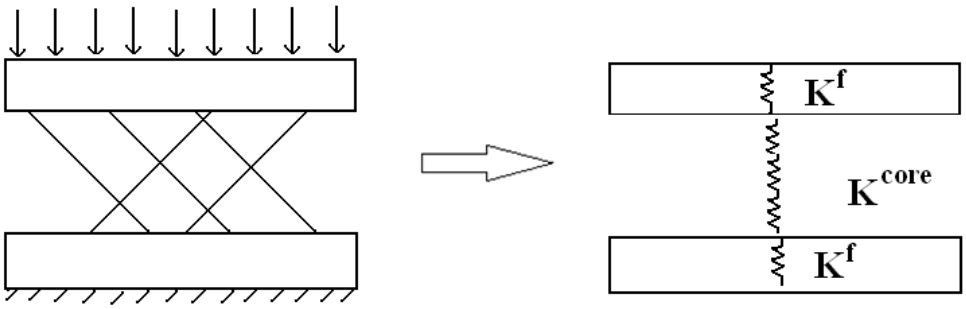

Figure 3.1 Equivalent spring arrangement for a compression loading on a sandwich structure

3.2.2 Model 2: Finite panel with no pin facesheet interaction

For a finite panel with no pin-facesheet interaction, the same formulas above hold for obtaining the stiffness of the structure. However, in the finite case, the core stiffness is given by

$$E^c = (N_O K_0 + N_V K_V) h^{\text{total}} / A^{fc} \tag{3.5}$$

where N_O and N_V are the number of oblique and vertical pins in the structure and K_O and K_V are the spring constant of the oblique and the vertical pins. Substituting the expressions for spring constants for oblique and vertical pins from Equation (2.7) we obtain the core modulus for a finite plate as

$$E^c = \frac{\text{EA}^{\text{fc}}}{\text{h}^{\text{total}}} (N_O (1 + 3\xi^2 \sin^2 \theta) \cos^3 \theta + N_V) \tag{3.6}$$

As we shall see, the number of pins in the structure not only depends on the pin density (cell spacing), but other factors such as the location of the cutting edges. The influence of both these parameters is studied in Section 5.1.

3.2.3 Model 3: Finite panel with pin facesheet interaction

The above two models do not account for the pin facesheet interaction. The pin modulus is very high (156.5 GPa for T650-35/8606 material) compared with the facesheet modulus in the transverse direction (12.96 GPa for AEC facesheets). This will allow the facesheets to have large local z-deformations near the points of contact with the pins, and the displacements on the upper surface of the face-sheets will not be conveyed to the end points of the pin. The stiffness of the model thus could differ significantly from the facesheet models above. In the computational models, twenty-node quadratic brick

elements (C3D20) are used to model the facesheets. This element allows the top surface and the bottom surface of the face-sheets to deform independently and also allow local deformations inside the facesheets.

In all these models, the analysis does not capture the influence of reveal length, as the pins are modeled with point contacts with the face-sheets without any reveal lengths. In addition the interaction between the foam and the pins is not modeled.

3.2.3.1 Analytical Model including pin facesheet interaction:

The facesheets offer some resistance to the pin penetration through the facesheet modulus. Thus the pin-facesheet interaction offers some resistance to the applied load in addition to the reinforcing pins and the facesheets. A simple springs model has been developed including this interaction resistance. Figure 3.2 shows a schematic which includes a spring for the pin facesheet interaction, of spring constant k^{int}. The interaction effect can be imagined as a consequence of a spring attached to every single pin in the model at both ends through the facesheets. It is expected that the spring constant of the interaction would depend mainly on the facesheet thickness and the pin lengths. The effect of different parameters on the interaction spring constants is studied in Section 5.2.

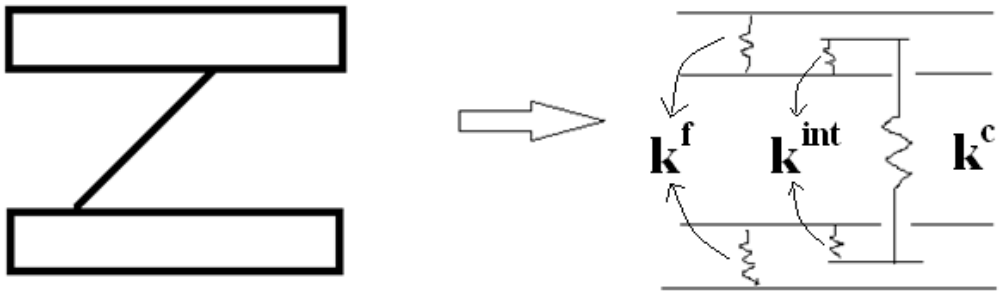

Figure 3.2: A schematic showing a springs model incorporating the penetration effect from pin-facesheet interaction.

Following the path of the springs, it can be observed that the interaction springs are in series with the equivalent springs of the facesheet and the pin. For the sake of simplicity, we consider models with oblique pins only. Let k^{int} denote the interaction spring constant for a single pin and K^{int} denote the interaction spring constant for the entire truss structure given by $K^{int} = N_{total}\, k^{int}$, where N_{total} is the total number of pins in the mode. The effective spring constant of the specimen may thus be derived as

$$\frac{1}{K^{specimen}} = \frac{2}{K^f} + \frac{2}{K^{int}} + \frac{1}{K^c} \tag{3.7}$$

or,

$$K^{specimen} = \frac{K^f K^{int} K^c}{2K^{int}K^c + 2K^f K^c + K^f K^{int}} \tag{3.8}$$

Note that for Models 1 and 2, where the interaction effect has been ignored, the interaction spring constant is essentially assumed to be infinitely large. In these cases, the spring constant of the specimen is simply given by

$$K^{specimen} = \frac{K^f K^c}{K^f + 2K^c} \tag{3.9}$$

By adding a spring in series, the effective spring constant of the model reduces. By simple algebra, it can be shown that

$$\frac{K^f K^c}{K^f + 2K^c} > \frac{K^f K^{int} K^c}{2K^{int} K^c + 2K^f K^c + K^f K^{int}} \tag{3.10}$$

Hence, the interaction models always have lower spring constants, and hence lower stiffness compared to that of the models that do not include interaction. If the interaction spring constant is small, then penetration displacements are larger and the stiffnesses of the models 2 and 3 differ hugely.

3.2.4 Model 4a: Finite model with adhesive layer and pin-adhesive interaction:

In this model, an adhesive layer is modeled between the facesheets and the core to attach the reveal lengths of the pins to the facesheets. However, the reveal lengths of the pins are not physically modeled. A schematic is shown in Figure 3.3. The compressive modulus of this model further drops from the value corresponding to Model 4 because of an additional spring in series. The effective spring constant of the specimen may thus be derived as

$$\frac{1}{K^{specimen}} = \frac{2}{K^f} + \frac{2}{K^{int-a}} + \frac{2}{K^a} + \frac{1}{K^c} \tag{3.11}$$

Here $K^{int\text{-}a}$ is the interaction spring constant, between the adhesive layer and the pin, and Ka is the spring constant corresponding to the adhesive layer, given by $K^a = E^a A^{fc}/ h^a$, where the superscripts ‘a’ refers to the adhesive layer. It is expected that the interaction spring constant, $K^{int\text{-}a}$ will be smaller than the corresponding value for K^{in} because the pins now penetrate into a much softer adhesive layer, allowing a larger degree of penetration.

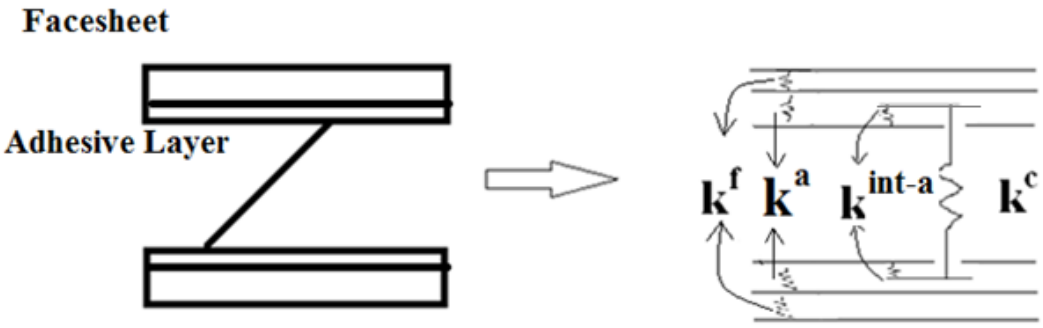

Figure 3.3: A schematic showing a springs model including the adhesive layer incorporating the penetration effect from pin-adhesive interaction.

3.2.4.1 Model 4b: Adhesive layer yielding

Since the adhesive layer is much softer than the facesheets, the pin penetration onto the adhesive layers can cause adhesive yielding. The Von-Mises criterion is used in the FEM analysis to obtain this critical point. The modulus of the adhesive layer material drops after it yields. The stress-strain relation for the adhesive material may be represented by a bilinear relation as shown in Figure 3.4. It is expected that after the adhesive layer yields, the pins can penetrate more easily into the adhesive layers, and the interaction spring constant also decreases hugely. The compressive modulus of the sandwich structure thus changes after adhesive yielding, as the modulus is calculated for the new value of the adhesive spring constant and the interaction spring constant. The decrease in the compressive modulus of the specimen after adhesive yielding manifests a kink in the stress-strain graph of the specimens.

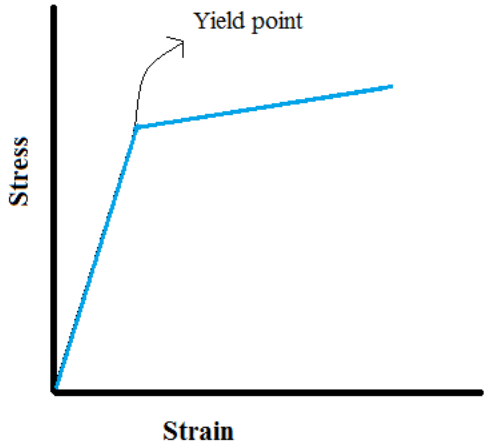

Figure 3.4: Stress-strain plot for adhesive layer assuming a bilinear relation, with different moduli before and after yielding

3.2.5 Model 5: Post buckling Analysis

In Chapter 2, the strength of the sandwich panels was calculated assuming that the model attains failure at the point of buckling of the pins when the axial force in the pins equals its first critical load. Even though the pins buckle at the critical load, they are still expected to carry some load after that. Geometrically non-linear analysis will be needed for estimating large deformations and the stiffness of the pin after the first critical load. In such computational models, it is necessary to include geometrical imperfections in the beam to compute the post critical load effects.

3.3 Developing models of predicted specimen response for shear loading

The analogy between compression and shear loading conditions on the sandwich specimen is straightforward. The models used for compression above may be extended for the shear loading conditions as well.

3.3.1 Model 1: Infinite panel with no pin-facesheet interaction

The equivalent springs model for a shear loading condition on the sandwich structure with no foam is shown in Figure 3.5.

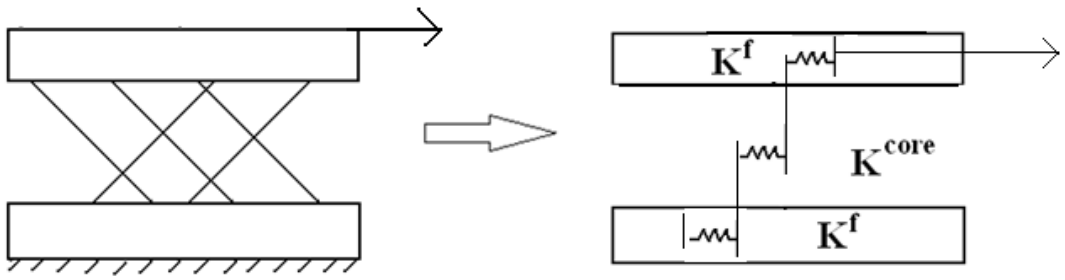

Figure 3.5: Equivalent spring arrangement for a shear loading on a sandwich structure

The equivalent spring constant of the series arrangement as shown in Figure 3.5 is given by

$$\frac{1}{\mathrm{K}^{specimen}} = \frac{1}{\mathrm{K}^{f}} + \frac{1}{\mathrm{K}^{core}} + \frac{1}{\mathrm{K}^{f}} \tag{3.12}$$

where the spring constant of the facesheets, for shear loading, as $K^f = E_1^f A^{fc}/ h^f$, where E_1 is the modulus of the facesheets in the loading direction (x direction) and A^{fc} is the area of the facesheets and h^f is the thickness of the facesheets.

The stiffness of the specimen in shear direction is then given by

$$G^{specimen} = \frac{h^{specimen}}{\frac{2h^f}{E_1{}^f} + \frac{h^c}{G^c}} \tag{3.13}$$

where, G^c is the core stiffness from the pin truss structure derived in the previous chapter.

The above expression can be be simplified as

$$G^{specimen} = \frac{G^c h^{specimen}}{h^c} \frac{1}{1+\varepsilon} \approx \frac{G^c h^{specimen}}{h^c} \tag{3.14}$$

where

$$\varepsilon = \frac{G^c}{{E_1}^f}\frac{2h^f}{h^c} \ll 1 \tag{3.15}$$

is valid for most sandwich structures because the facesheets are very stiff in the loading direction, i.e., ${E_1}^f$ is a large quantity.

3.3.2 Model 2: Finite panel with no pin facesheet interaction

For a finite panel with no pin-facesheet interaction, the same formulas above hold for obtaining the stiffness of the structure. However, in the finite case, the core stiffness is given by

$$E^c = N_{Ox}K_{0x} + N_{Oy}K_{0y} + N_V K_V \tag{3.16}$$

where N_{Ox}, N_{Oy} and N_V are the number of oblique pins in the loading direction, in transverse direction and vertical pins in the structure and K_{0x}, $K_{0y}$and K_V are the spring constants of the respective pins. Substituting the expressions for spring constants for oblique and vertical pins from Equation (2.11), we obtain the core modulus for a finite plate as

$$G^c = \frac{\mathrm{EA}}{\mathrm{h}}(N_{Ox}(\sin^2\theta + 3\xi^2\cos^4\theta)\cos\theta + N_V 3\xi^2) + 12N_{Oy}\mathrm{EI}\cos^3\theta/\mathrm{h}^3) \tag{3.17}$$

3.3.3 Model 3: Finite panel with pin facesheet interaction

The penetration of pins into facesheets in shear loading affects the shear stiffness of the sandwich structure as well. The penetration displacements from the oblique pins in the loading direction and the ones in the transverse direction are different and both are

captured by the FEM model. Computational models using brick elements for the facesheets have been constructed to include the flexibility effects of the facesheets. However, addition the interaction between the foam and the pins is not modeled.

3.3.3.1 Analytical Model including pin facesheet interaction:

Figure 3.6 shows a schematic which includes a spring for the pin facesheet interaction, of spring constant k^{int}, for a sandwich structure under shear. The effective spring constant of the specimen is

$$\frac{1}{K^{specimen}} = \frac{2}{K^f} + \frac{2}{K^{int}} + \frac{1}{K^c} \tag{3.18}$$

or,

$$K^{specimen} = \frac{K^f K^{int} K^c}{2K^{int}K^c + 2K^f K^c + K^f K^{int}} \tag{3.19}$$

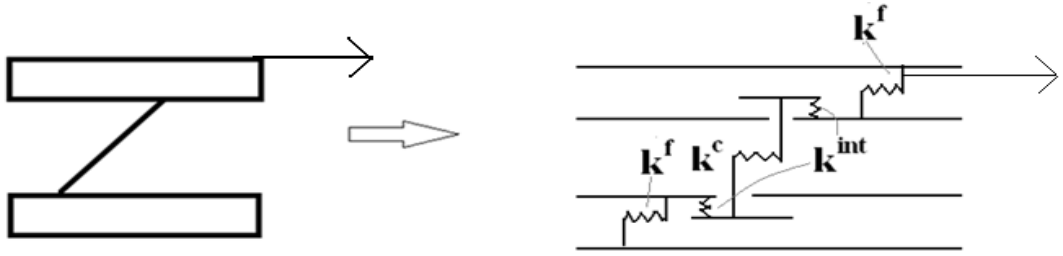

Figure 3.6: A schematic showing a springs model incorporating the penetration effect from pin-facesheet interaction, for shear loading.

The interaction model for shear has lower spring constants and hence lower shear moduli when compared to that of the models that do not include interaction.

3.3.4 Model 4a, 4b: Finite model with adhesive layer and pin-adhesive interaction:

Figure 3.7 shows a schematic which includes the adhesive layer. The effective spring constant of the specimen is given by

$$\frac{1}{K^{specimen}} = \frac{2}{K^f} + \frac{2}{K^{int-a}} + \frac{2}{K^a} + \frac{1}{K^c} \tag{3.20}$$

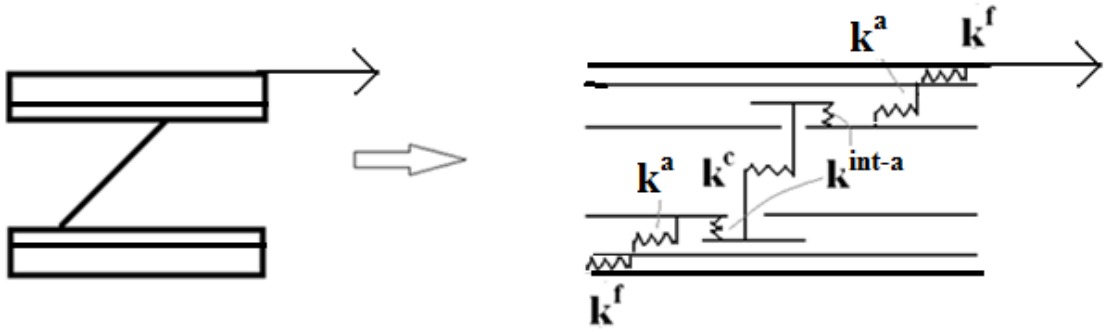

Figure 3.7: A schematic showing a springs model including the adhesive layer incorporating the penetration effect from pin-adhesive interaction, for shear loading.

The values K^a, the spring constant of the adhesive layer and K^{int-a}, the adhesive-pin interaction spring constant are expected to change after adhesive yielding thus affecting the shear modulus of the specimen too. Model 4b has the adhesive layer post yielding.

Chapter 4

Correlations with Experimental Results

In this chapter, we compare the experimental results obtained on sandwich structures constructed and tested at UMD by Dr. Hugh Bruck's composite research group with our simulations.

4.1 UMD low density specimen

Figure 4.1 is a sandwich specimen manufactured and tested under compression at UMD. The foam core for the sandwich specimen was obtained from AEC and the facesheets were ordered from Dragonplate. Epoxy adhesive was used to adhere the foam to the facesheets at UMD. Specimens of sizes 3"x3", 2"x2", and 1"x1" were tested under compression. The properties of the different components of the sandwich structure are given below, which correspond to a pin density of approximately 0.9 lb/ft^3.

Figure 4.1: Sandwich specimen of low pin density tested under compression. Snapshot taken from experimental set-up at Dr.Hugh Bruck's research group, UMD.

Core:

Pin radius: 0.235 mm, Pin insertion angle = 30^0, Pin spacing = 10 mm,

Core thickness = 12.75 mm

Pin modulus = 156.5 GPa, $\upsilon = 0.23$

Facesheet:

Facesheet thickness: 1mm, each

Ply configuration = $[0/90/45/-45]_s$

$E_L = 156.5$ GPa, $E_T = 12.96$ GPa, $G_{LT} = 6.96$ GPa, $G_{TT} = 4.3$ GPa, $\upsilon_{LT} = 0.23$, $\upsilon_{TT} = 0.5$

Adhesive Layer:

Thickness: 0.0235mm = $1/10^{th}$ the pin radius.

Epoxy Young's modulus: 3.17 GPa, $\upsilon = 0.35$

Epoxy compression yield strength: 79 MPa

4.1.1 Experimental Results

Test results using the 3"x3" specimens are presented in Figure 4.2. Specimens were tested by repeated loading to understand the effects of the nonlinear response on the elastic response of the specimen. The modulus is observed to vary throughout the test, and changes after nonlinear deformation. Initially during the first cycle of loading it exhibits high stiffness of around 580 MPa up until 1 MPa, where it transitions to 100 MPa. However, after the repeated loading the initial stiffness decreases to 160 MPa before transitioning to 40 MPa at the load level where the previous loading was terminated. Compression tests performed with sandwich specimens that were 2"x2" size

in the smaller load frames have the stress-strain curve as shown in Figure 4.3. The initial modulus under compression was determined to be around 500 MPa, about which was similar to the larger specimen. The maximum stress was found to be around 2.2 MPa, which was also similar to the larger compression specimen. The stress-strain response under compression for the 1”x1” specimen is shown in Figure 4.4.

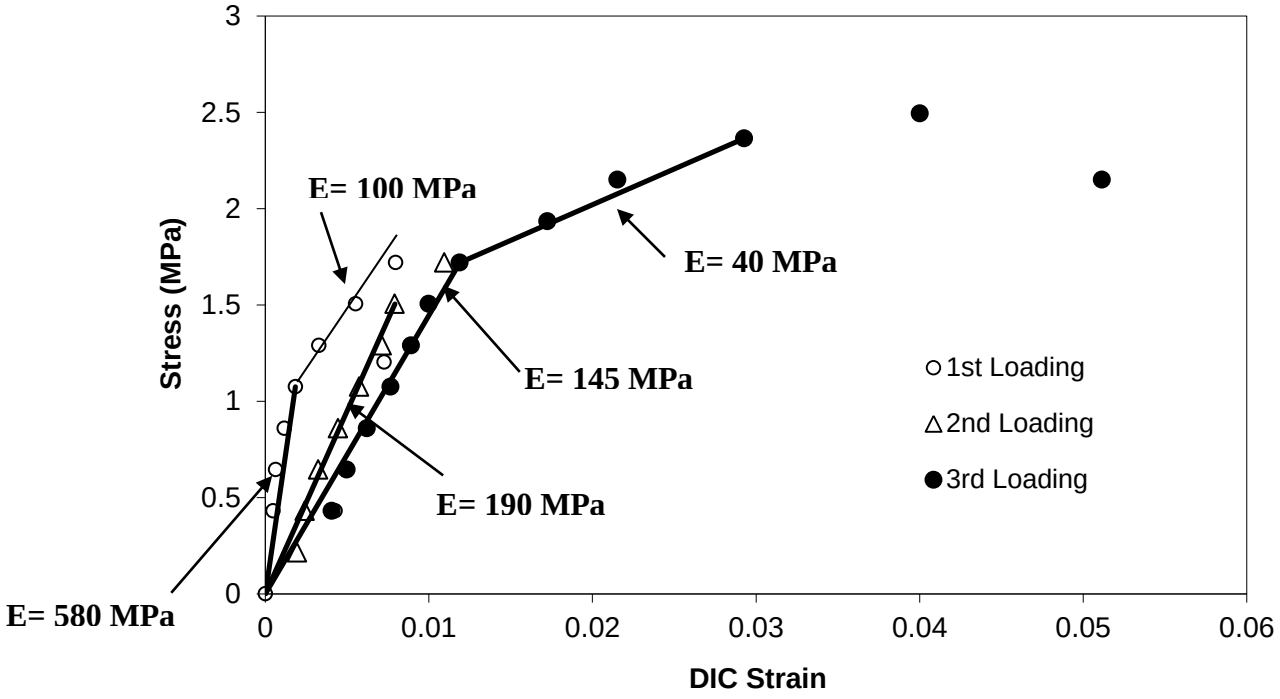

Figure 4.2 Compression behavior of 3”x3” sandwich specimen in the large load frame under repeated loading

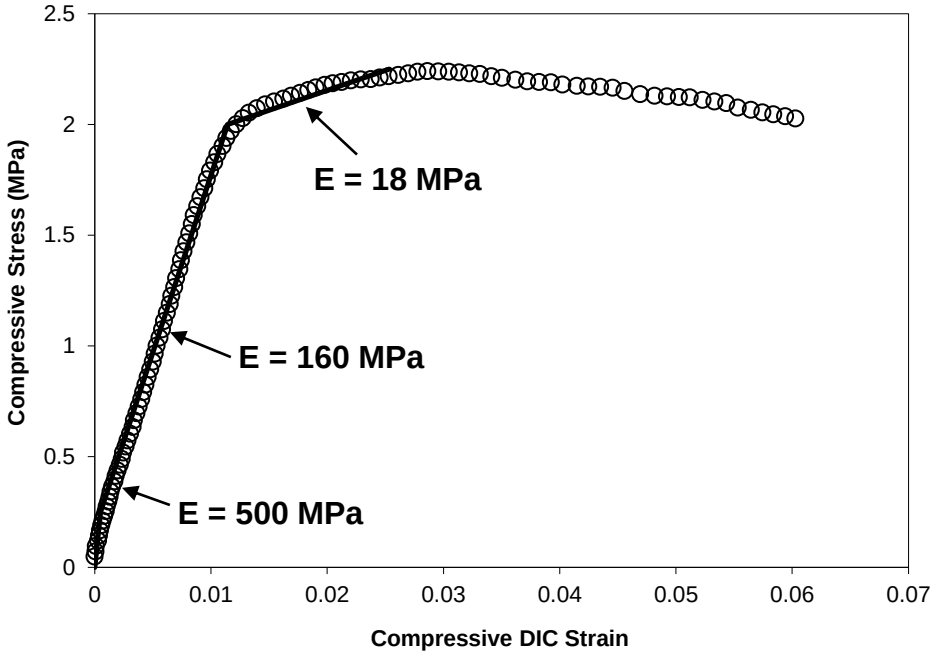

Figure 4.3 Compression behavior of 2"X2" sandwich specimens

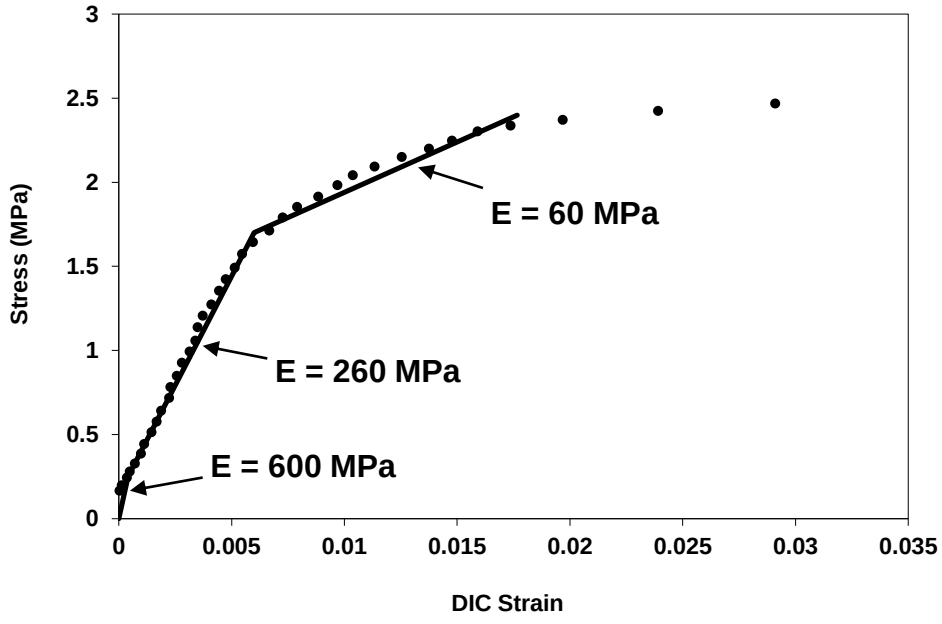

Figure 4.4 Compression stress-strain response of 1"x1" sandwich specimens

4.1.2 FE Models

Computational finite element models were developed as described in the previous chapter. To include the pin-facesheet interaction effects in model 3, twenty-node quadratic brick elements (C3D20) were used to model the facesheets. In modeling the different specimens of finite size, the cutting edges on one side were placed such that the reveal lengths of the boundary pins on that side are accommodated inside the specimen. This is shown in Figure 4.5, where the left and the bottom cutting edges are shown with the first pin at the boundary positioned at a distance of 2 mm (reveal length) from both the edges. The pins on the other edges (right and top), however, are included in the model, even at very close distances to the cutting edges. Such closely located boundary pins may fall out during loading, resulting in dropping of the compressive modulus of the specimen. Figure 4.6 shows the isometric view of the finite element model for the 3”x3” specimen.

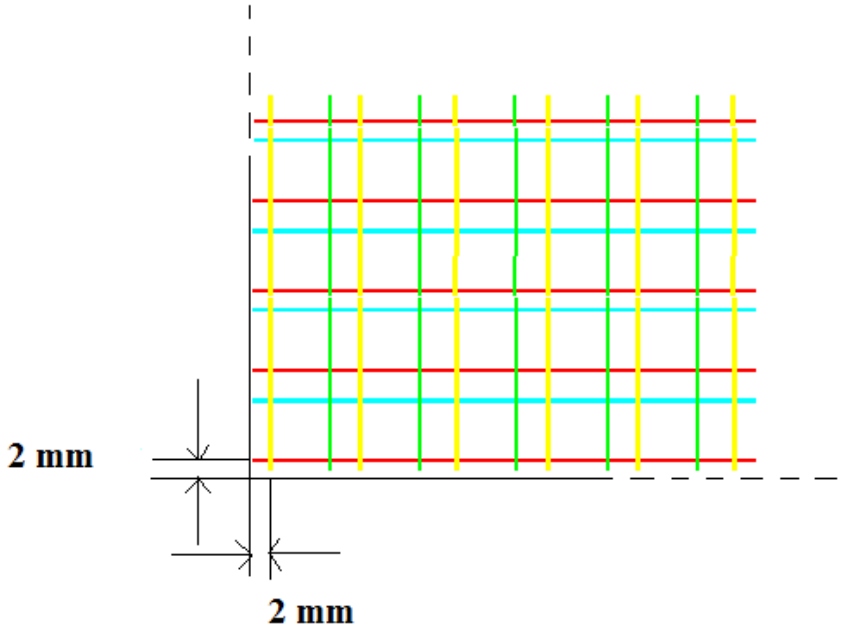

Figure 4.5. Top view of a sandwich panel shown with left and bottom cutting edges

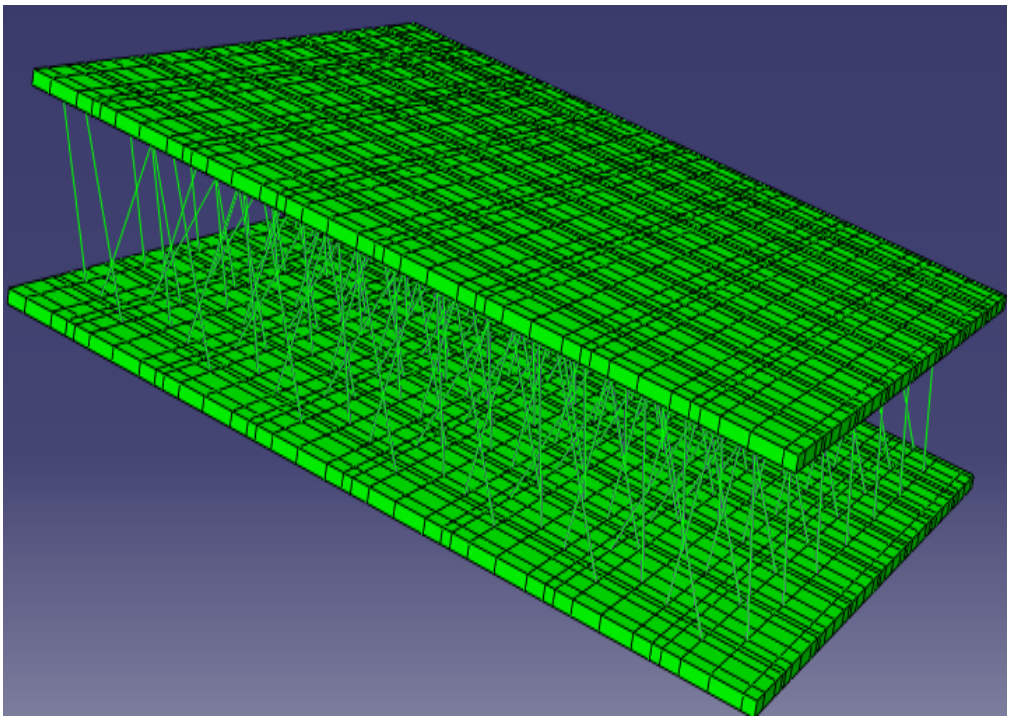

Figure 4.6: Isometric view of the finite element model for the 3”x3” specimen.

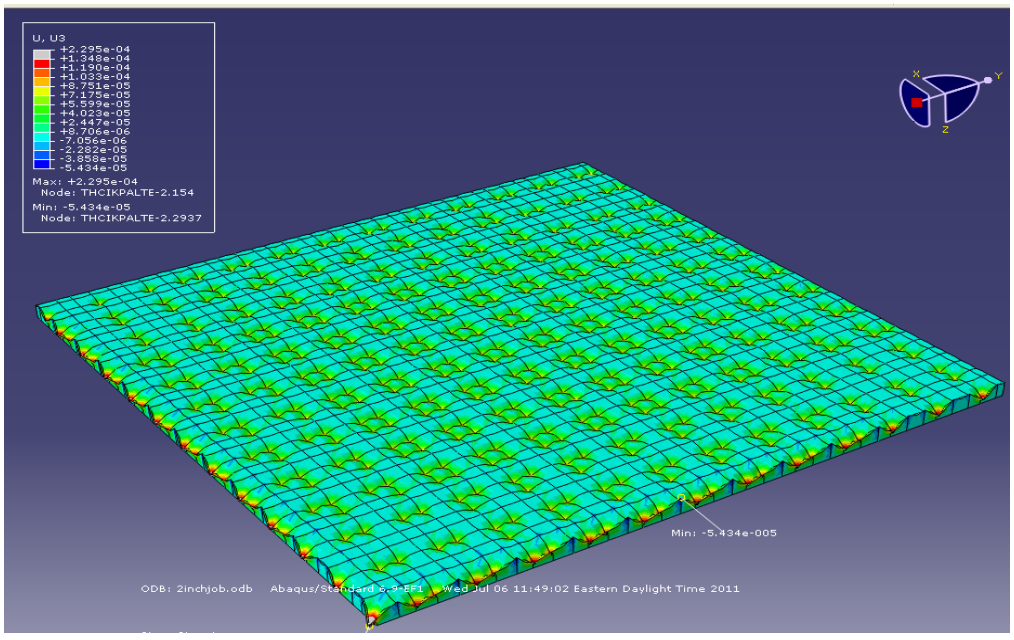

Figure 4.7: Vertical displacement field on the top of the bottom facesheet of a typical sandwich specimen, showing pin-facesheet interaction effects via pin penetration under compressive loading

4.1.3 Computational Results

4.1.3.1 Compressive Stiffness

The results for the compressive stiffness of the models obtained are tabulated below in Table 4.1. Model 1 is the infinite panel model and has the highest stiffness. Model 2 is a finite sized model and has a smaller compressive stiffness than model 1, owing to size effect. Model 3 incorporates the pin facesheet interaction and has lower compressive stiffness compared to Model 2 owing to the interaction effects. Figure 4.7 shows the vertical displacement field of a typical facesheet including the penetration displacements from the pins. The compressive stiffness of this model (545 MPa, 562 MPa and 573 MPa for the 3"x3", 2"x2" and 1"x1" specimens respectively) compares reasonably well with the experimental values obtained from the first slope of the stress-strain curve (580 MPa, 500 MPa and 600 MPa respectively) in Figures 4.2-4.4 for the sandwich specimens. The interaction spring constant of the model can be obtained by comparing the stiffness values, and hence spring constants of Models 2 and 3. Model 3 has lower stiffness and hence lower spring constant as compared to Model 2. The difference in spring constant of the model is due to inclusion of the interaction springs in series, as shown in Figure 3.1. The interaction spring constant of a single pin can be derived as

$$k^{int} = \frac{2A^{fc}E_2E_3}{N_{pins}h^{total}(E_2 - E_3)} \tag{4.1}$$

where A^{fc} is the cross sectional area of the facesheets, h^{total} is the total thickness of the specimen, N_{pins} is equal to the number of pins in the model and E_2 and E_3 are the stiffnesses of models 2 and 3 respectively. The interaction spring constant of each pin in the model is provided in the Table 4.2.

Model	Description	Compressive Modulus, MPa		
		3" x 3"	2"x2"	1"x1"
Model 1	Infinite panel with no pin-facesheet interaction	842	842	842
Model 2	Finite panel with no pin-facesheet interaction	708	732	780
Model 3	Finite panel with pin-facesheet interaction,	545	562	573
Model 4a	Finite panel with adhesive layer included, before adhesive yielding	511	510	467
Model 4b	Finite panel with adhesive layer included, after adhesive yielding	234	225	149
UMD Experiments	Phase 1	580	500	600
	Phase 2	100	160	260

Table 4.1: Compressive stiffness of different models corresponding to low density UMD specimen

In Model 4a, an adhesive layer is modeled between the facesheets and the core to attach the reveal lengths of the pins to the facesheets. The thickness of the adhesive layer in

Model 4 was chosen as a very small value, equal to one-tenth the radius of the pin, (i.e., thickness = 0.0235 mm). It may be observed from Table 4.1 that the compressive modulus further drops from Model 3 to Model 4. This is because the pins now penetrate into a much softer adhesive layer, allowing a larger degree of penetration and thus a further drop in compressive modulus.

Model	**Type of interaction spring constant**	**Interaction Spring Constant, MPa**		
		3" x 3"	**2"x2"**	**1"x1"**
Model 3	k^{int}	9.55	9.16	7.66
Model 4a	k^{int-a}	7.42	6.38	4.13
Model 4b	k^{int-a}	1.41	1.23	0.66

Table 4.2: Interaction Spring Constants of different interaction models for low density UMD specimen

The interaction spring constant for the interaction between the adhesive layer and the facesheet, can be derived as

$$k^{int-a} = \frac{2A^{fc}}{N_{pins}h^{total}}\left(\frac{1}{E_4} - \frac{1}{E_2} - \frac{2\,h^{adh}}{E_{adh}h^{total}}\right)^{-1} \tag{4.2}$$

where E_{adh} and h^{adh} represent the modulus and the thickness of the adhesive layer.

The interaction spring constants calculated thus for Models 4a and 4b are given in Table 4.2.

For Model 4a, the stresses in the adhesive layer for a given compressive load are obtained from the FE models. The stresses in the adhesive layer increases as the load on the structure is increased and the adhesive layer reached the yield strength first at the points of contact of the boundary pins with the adhesive layer. Using, the Von-Mises criterion to obtain this critical point, we can estimate the load on the structure at which the adhesive layer experiences yielding as shown in Table 4.3.

Specimen Size	**Loading at Adhesive Yield (MPa)**
3"x3"	1.29
2"x2"	1.01
1"x1"	1.04

Table 4.3. Load (stress) on the sandwich specimen at which adhesive yields

The modulus of the adhesive layer material (Epoxy) drops after it yields. The stress-strain relation for the epoxy material may be represented by a bilinear relation as shown in Figure 3.4. Data for the epoxy material properties after yielding was not available. Accordingly, a model (Model 4b) in which the modulus value after yielding was arbitrarily chosen as one-tenth the elastic modulus of the epoxy was considered to appreciate the effect of yielding on the sandwich compressive modulus. The compressive moduli of the specimen obtained thus are included in Table 4.1. The interaction spring constants after adhesive yielding are calculated from. Equation (4.2).

4.1.3.2 Compressive Strengths

Table 4.4 enlists the results obtained for compressive stregnths for different models based on pin buckling, assuming clamped boundary conditions at the pin ends. The compressive strengths for Models 1 and 2 are obtained analytically from Equations (2.15) and (2.21). Model 1 has higher compressive strength than Model 2, due to size effect. For model 3, the compressive strength is obtained by calculating the load on the structure when the last pin buckles. This is obtained by calculating the axial force in each pin for a small vertical displacement and then estimating the load on the structure when the axial force equals the buckling load in the pin carrying the least axial force (as this pin will buckle the latest). It is observed that the pin buckling strengths of model 2 and 3 are nearly the same, even though the models have considerably different compressive moduli. This is because the buckling strength of the structure is dependent on the axial force in the pins. Model 3 has a lower compressive stiffness, which allows the pins to deform more than the pins in Model 2, before the axial force equals the buckling force. The pin penetration into the facesheet in model 3 makes the model softer hence allowing for more vertical displacements before buckling.

Model	Description	Compressive Strengths, MPa		
		3" x 3"	2"x2"	1"x1"
Model 1	Infinite panel with no pin-facesheet interaction	2.37	2.37	2.37
Model 2	Finite panel with no pin-facesheet interaction	1.99	2.06	2.20
Model 3	Finite panel with pin-facesheet interaction	1.95	2.04	2.19
UMD Experiments	Position of 1st kink	1.0	0.4	0.2
	Position of 2nd kink	2.2	2.2	2.2

Table 4.4. Buckling strengths of the sandwich specimens obtained for different FE models

4.1.3.2 Non-linear Analysis

The pins of the sandwich structure carry some load on them even after they buckle at their critical load. To obtain the stiffness of the structure after the critical load of the pin, a geometric non-linear analysis must be carried out to account for its large deformations. Geometrical imperfections are necessary to be introduced to capture the bending deformations on the pin. In this section, a critical load analysis is performed on a single pin with clamped ends with different degrees of geometrical imperfections. Consider a two dimensional beam with clamped boundary conditions at its ends subjected to axial force at one end. Imperfections are introduced to the geometry of the beam to study the effect of large forces. The imperfections are of the form $\varepsilon(x) = k\,(1-\cos(2\pi x/L))$, the first mode shape of the beam where k is the degree of imperfection. Three degrees of

imperfection are studied here, namely k = L/1000, L/500, L/100 to compare the variation of the stiffness with the degree of geometrical imperfection. A pin of length 14.72 mm which is typical of reinforcing pins of UMD samples of low density is modeled here. The pin has a Young's modulus equal to 156.5 GPa and a Poisson's ratio of 0.23.

The critical load of a clamped beam of length L are given by the formula,

$$F = \frac{4\pi^2 EI}{L^2} \tag{4.3}$$

The first critical load (buckling load) of the beam above obtained from Equation 4.3 is 68.3 N. A geometrically non-linear analysis is carried out on the pin for loads beyond the first critical load, and the load displacement curves for different degrees of imperfections are plotted in Figures 4.8 and 4.9 below. Figure 4.8 is the plot of the tip axial displacement of the pin, δ with axial force. Figure 4.9 is the plot of the bending displacement at the center of the beam, w, with axial force acting at the pin end. It can be seen from Figure 4.8, that the slope of the graph F vs. δ, becomes really small at the first critical load value which means that the spring constant of the pin drops down dramatically at the first critical load. This phenomenon will manifest as the second kink in the graph of stress versus strain of the whole sandwich specimen, where the slope of the graph will drop down drastically. It may be observed that the stress-strain curve has nearly the shape and equal slopes at the first critical load, for degrees of imperfections equal to L/1000 and L/500, indicating that the non-linear analysis of the sandwich structures may be carried out for either degree of imperfection.

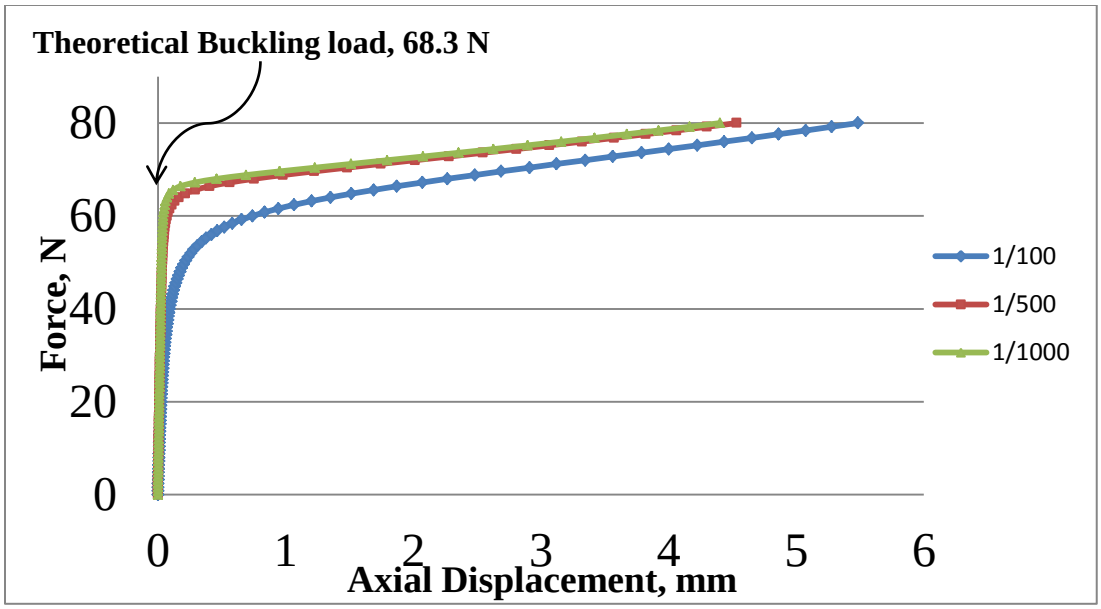

Figure 4.8: Plot of axial displacement, δ at the tip of the pin with geometric imperfections of varying degree with axial force acting at the tip, F

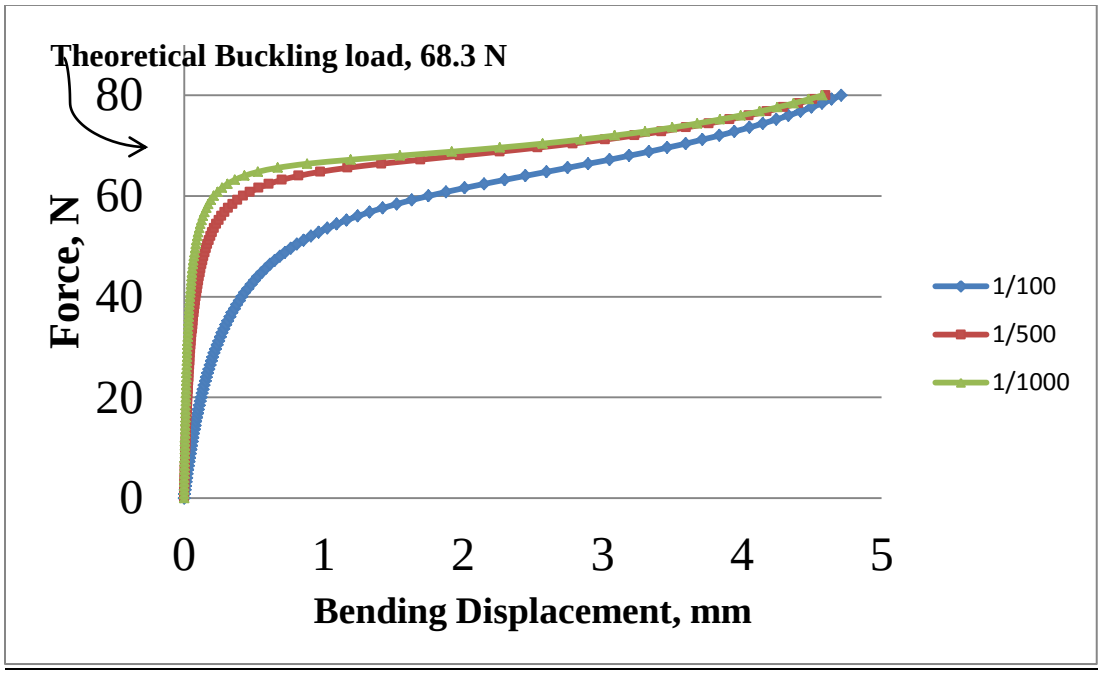

Figure 4.9: Plot of bending displacement, w at the center of the pin with geometric imperfections of varying degree with axial force acting at the tip, F

By comparing the slopes before and after buckling of the pin in Figure 4.8, we can estimate the stiffness of the sandwich structure after the second kink.

The buckling strengths above provide the onset of failure for the sandwich specimens. A summary of the compressive behavior for a 2”x2” specimen predicted by the model due to adhesive yielding from Model 4a and pin buckling from Model 4b can be seen in Figure 4.10. It is observed that the compressive stress-strain behavior is similar to the experimental values in Figure 4.10 for the initial onset of failure due to adhesive failure but not the maximum load bearing capacity that may be associated with pin buckling. The post buckling stiffnesses of the sandwich structure obtained are much smaller than experimental values as well. For lower pin density specimens such as these, the foam core may stabilize the structure to increase its strength. A study incorporating the foam core effect on the sandwich specimens will be needed to obtain a better estimate of the compressive strengths.

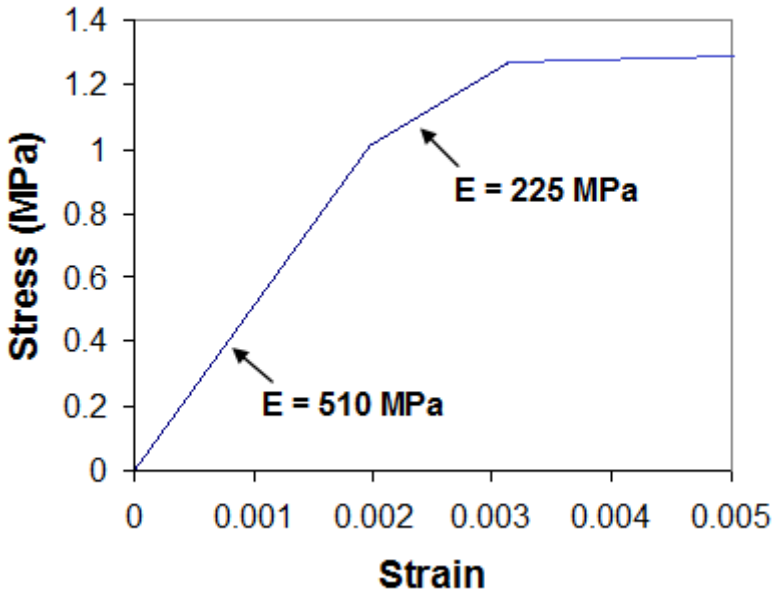

Figure 4.10: Summary of computational predictions for the compressive behavior of a 2"x2" specimen with failure using Model 4a for adhesive yielding and Model 4b for pin buckling at a pin density of approximately 0.9 lb/ft^3.

4.2 UMD 7pcf specimen

7lb/ft^{3}specimens provided by AEC were tested under compressive loading by Dr. Hugh Bruck's composite research group at UMD. Figure 4.11 is a sandwich specimen tested under compression load provided by AEC, of dimensions 2x2 inch^2. A schematic of the pin structure is shown in Figure 4.12.

The specimen properties as provided by AEC are given below.

Pin and core properties:

Pin radius: 0.235 mm, Pin insertion angle = 30^0, Pin spacing = 0.164" = 4.17 mm,

Core thickness = 0.75 inch = 19.05 mm, Core density = 7 lb/ft^3

E = 156.5 GPa and a Poisson's ratio of $\upsilon = 0.23$.

Facesheet properties:

Facesheet thickness: 1.27 mm

Ply configuration = $[0/90/45/-45]_s$

E_L = 156.5 GPa, E_T = 12.96 GPa, G_{LT} = 6.96 GPa, G_{TT} = 4.3 GPa, υ_{LT} = 0.23, υ_{TT} = 0.5.

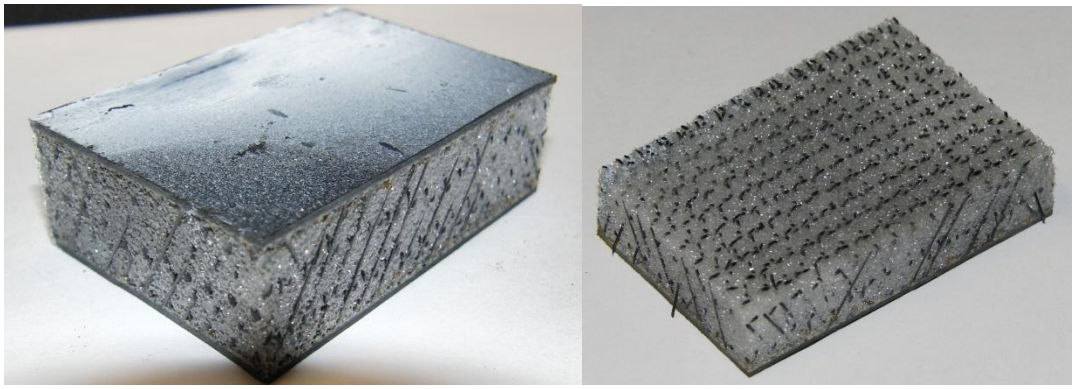

Figure 4.11: Pin configuration of 7pcf sandwich specimen (left) as received, (right) with top face sheet removed.

4.2.1 Experimental Results:

A compression test was conducted on the 2 inch specimen where the specimen was cyclically loaded to 3 MPa, and then loaded to failure. The results are plotted in the stress strain curve shown in Figure 4.13. These results indicate an initial modulus of 3052 MPa and then a transition to a modulus of 1926 MPa. However, at 6 MPa the specimen transitions to a modulus of 669 MPa to failure at 7.75 MPa. The cyclic loading response up to 3 MPa indicates perfectly elastic behavior. Thus, there appears to be a transition in

the elastic load bearing mechanisms for the pins after the 1 MPa load level is reached that is causing a reduction in the effective modulus.

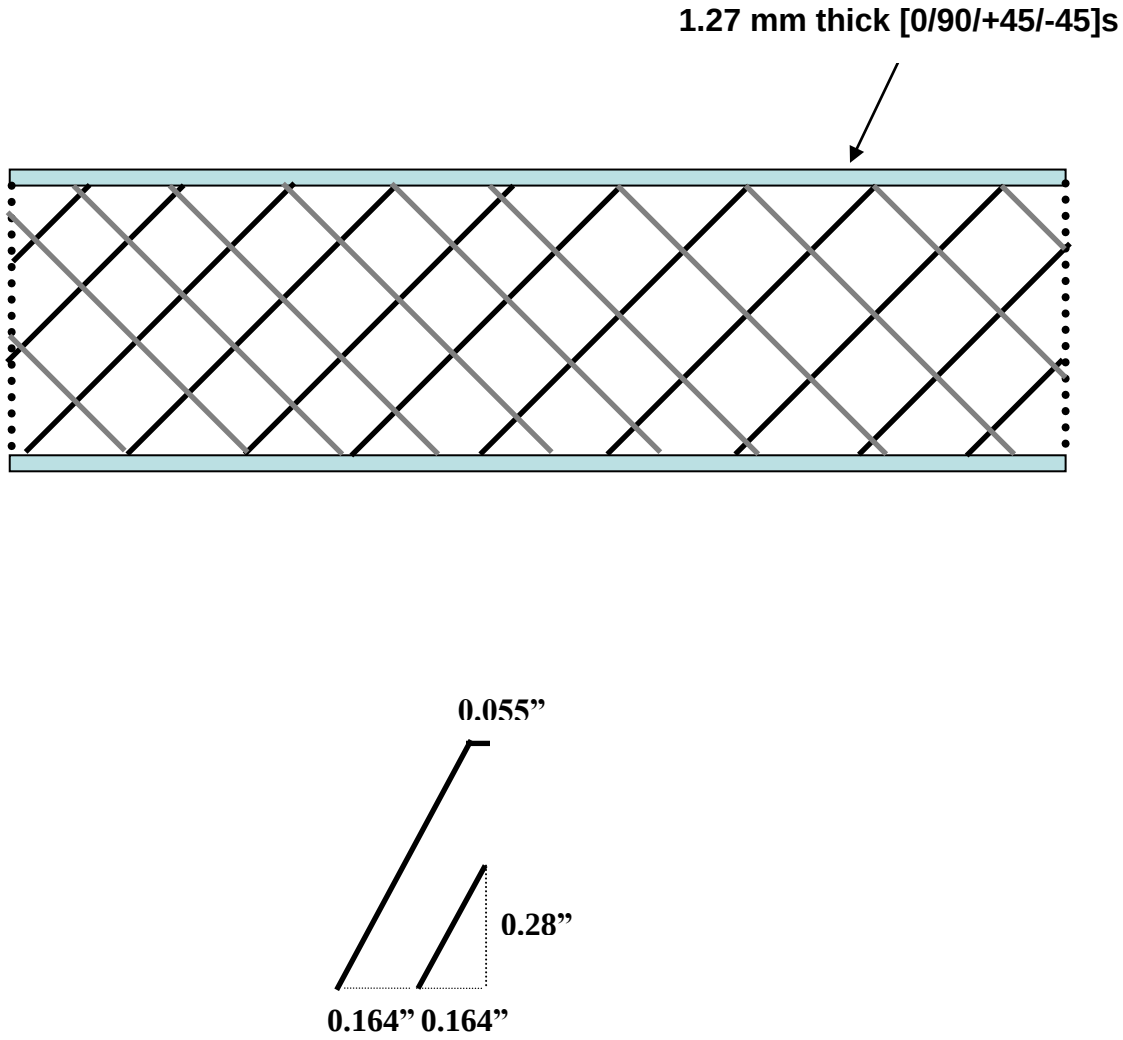

Figure 4.12: Schematic diagram of the pin configuration for the tested specimen.

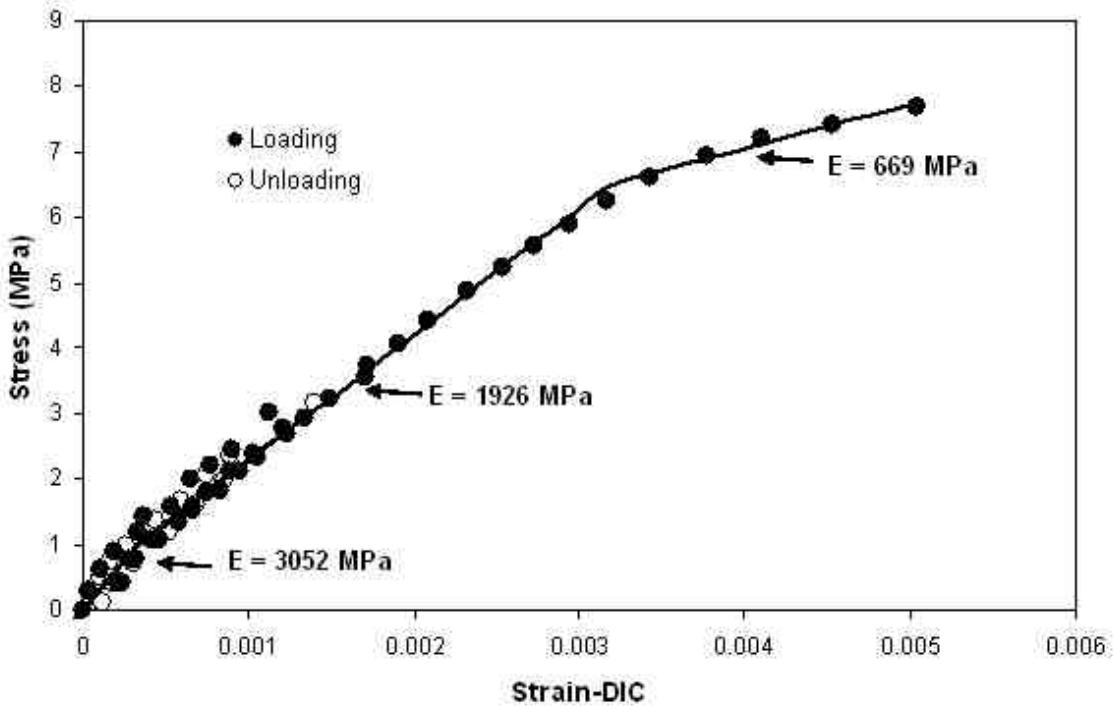

Figure 4.13. Repeated loading of UMD 7pcf specimen to 3 MPa and then loading to failure

4.2.2 FEM Models

Figure 4.14 shows the cross section of the bottom facesheet with the grid lines in it. The red point marked at the left bottom indicates the first pin that originates from the bottom facesheet and travels in the positive x direction till it terminates at the top facesheet. This point is situated at a distance 1.4 mm, both vertically and horizontally from the bottom left vertex of the facesheet to allow for the inclusion of reveal length of the pin in the model. The other cutting edges of the model are decided by the length and the width of the specimen which equal 2 inch each.

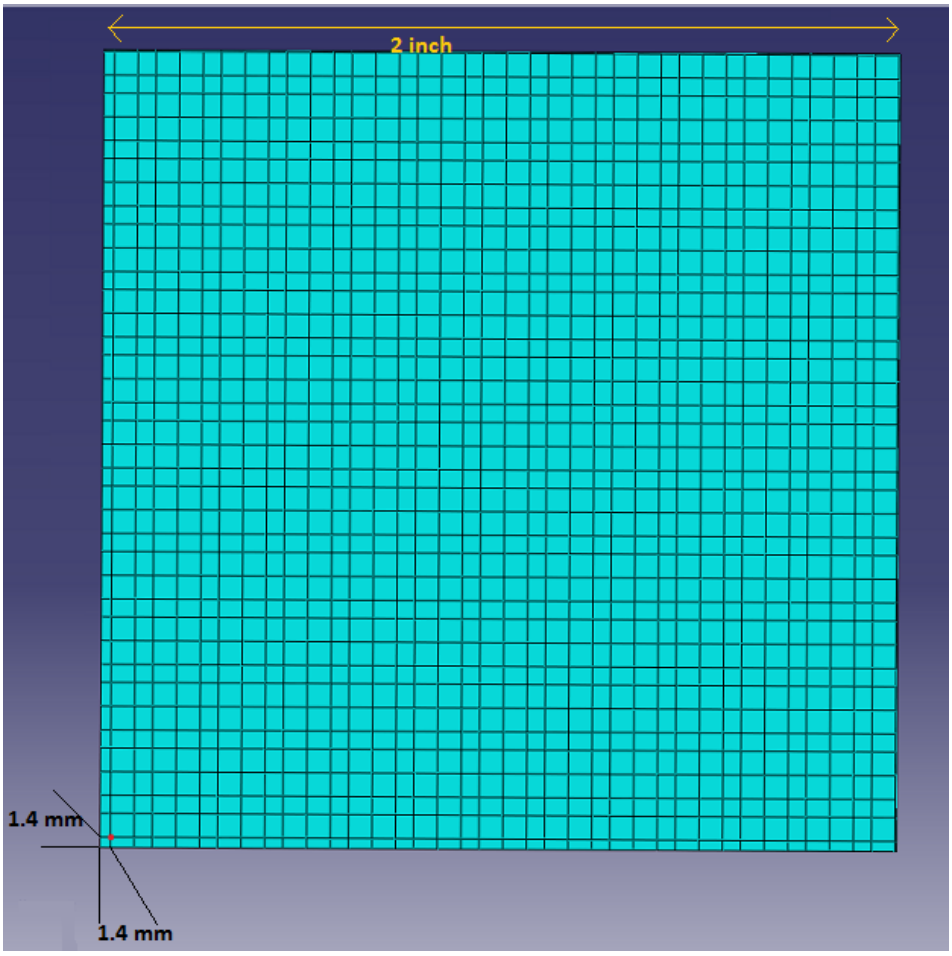

Figure 4.14: Cross section of the bottom facesheet of the 2inch specimen showing the mesh and the location of the point on the facesheet from which the first pin originates.

4.1.3 Computational Results

4.1.3.1 Compressive Stiffness and Strengths

The results for the compressive stiffness of the models obtained are tabulated below in Table 4.5. Adhesive layer is not considered in modeling this sandwich specimen. The compressive stiffness of Model 3 (2.96 GPa) compares very well with the experimentally value obtained from the first slope of the stress-strain curve (3.052 GPa) in Figure 4.13.

The interaction spring constant of the model was obtained from Equation. (4.1) as k^{int} = 4.384 N/m.

Model	**Description**	**Compressive Modulus, GPa**
Model 1	Infinite panel with no pin-facesheet interaction	4.15
Model 2	Finite panel with no pin-facesheet interaction	3.67
Model 3	Finite panel with pin-facesheet interaction	2.96
UMD Experiments	Experimental Results	1st segment – 3.052 2nd segment – 1.926

Table 4.5: Compressive stiffness of different models corresponding to 7pcf UMD specimen

Model	Description	Compressive Strength, MPa
Model 1	Infinite panel with no pin-facesheet interaction	6.08
Model 2	Finite panel with no pin-facesheet interaction	5.02
Model 3	Finite panel with pin-facesheet interaction	Average estimate - 4.88 Upper Bound Estimate-5.76
UMD Experiments	Experimental Results	7.75 (Onset of the 3rd segment – 6.1)

Table 4.6: Compressive strength of different models corresponding to 7pcf UMD specimen

The compressive strengths of models 1, 2 and 3 obtained for this specimen based on pin buckling is tabulated in Table 4.6. The buckling strength of model 3 compares reasonably with the experiments.

Chapter 5

Parametric Studies

In this chapter, we study the influence of different parameters that affect the properties of the sandwich structures.

5.1 Size Effect and Scatter

To derive the expressions for the compressive and shear stiffnesses of the finite core panels, consider a typical sandwich pin structure shown in Figure 5.1. Of the four sets of `oblique pins, only the two sets running along the x direction are shown in Figure 5.1, which is the projection of the sandwich core on the XZ plane. Red lines in Figure 5.1 are pins running in the positive-x direction and blue lines are pins running in the opposite direction. The red lines originate from their points of contact with the bottom facesheet represented by circles and terminate at points represented by x's on the top facesheet. The blue lines run from points represented by squares on the bottom facesheet to points represented by diamonds on the top facesheet. Points of similar kind are all separated by a distance equal to the cell spacing, 'a'. In Figure 5.1, we assign x-coordinates to different points of contact on the top and bottom facesheets. Choose a point represented by a circle on the bottom facesheet as the origin. Then the other circles have coordinates of the form 'na' where n is an integer, as shown in the figure. Let 'b' represent the coordinate of the point represented by a square on the immediate right of the origin. Let c and d denote the coordinates of the other ends of the pin starting from the origin and the point with coordinate 'b'. The coordinates of other points are decided by their distance from these reference points as shown. We proceed to find the relation between these

coordinates. The parameter ‘a’ is equal to the cell spacing of the sandwich structure. While ‘b’ is an independent parameter, the quantities ‘c’ and ‘d’ are defined by the core geometry. We have,

$$c = h\tan(\theta) \tag{5.1}$$

$$d = b - h\tan(\theta) \tag{5.2}$$

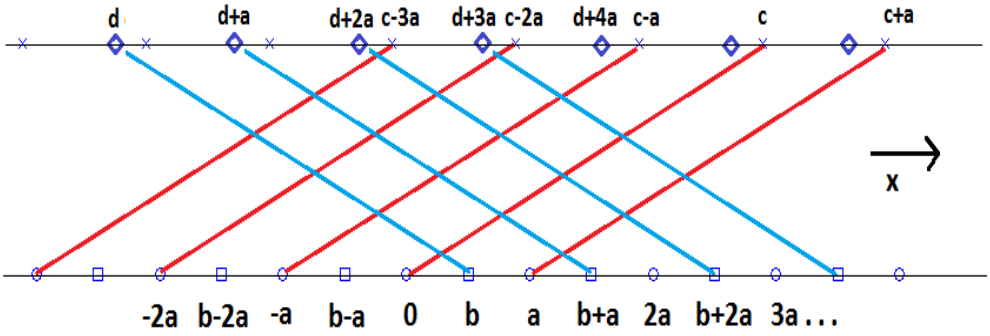

Figure 5.1: Side view of a tyical sandwich structure showing only pins in the xz plane.

In order to obtain the core stiffness of finite panels from the truss structure, the number of pins in the structure must be ascertained. This number will depend on the location of the cutting edges. We consider two kinds of cutting edge locations, which will result in maximum and minimum pin density. The core stiffness of the sandwich structure will lie between the values corresponding to these locations. For obtaining the panel with most number of pins and hence the maximum pin density, the cutting edges must be located right near the points of contact of the pins with facesheets. The minimum length of the sandwich panel that can include ‘n’ red pins in the structure is given by L_{min}= (n-1)a + htan(θ), as shown in Figure 5.2. This is also equal to the minimum length of the sandwich structure required to include n blue pins in structure. Since the cuts for the minimum lengths for including the red and the blue pins have to be made at different locations, the

minimum length of the sandwich panel that can include 'n' pins of both kinds is not equal to L_{min}, but given by $L = L_{min} + e = (n-1)a + h\tan(\theta) + e$, where e is the distance between the two cutting edge locations given by the formula,

$$e = \min\begin{Bmatrix} e_1 \\ e_2 \end{Bmatrix} \tag{5.3}$$

e_1 and e_2 are the distance between the cutting edges on either sides given by the following formulas.

$$e_1 = d + m_1 a \tag{5.4}$$

$$e_2 = b - (d + m_2 a) \tag{5.5}$$

where m_1 is the smallest natural number such that the quantity $d + m_1 a$ is positive.

where m_2 is the smallest natural number such that the quantity $b - (d + m_2 a)$ is positive. The two scenarios where e equals e_1 and e_2 respectively are shown in Figure 5.3 and 5.4 respectively. The pins excluded from the model, outside the cutting edges are drawn by dotted lines.

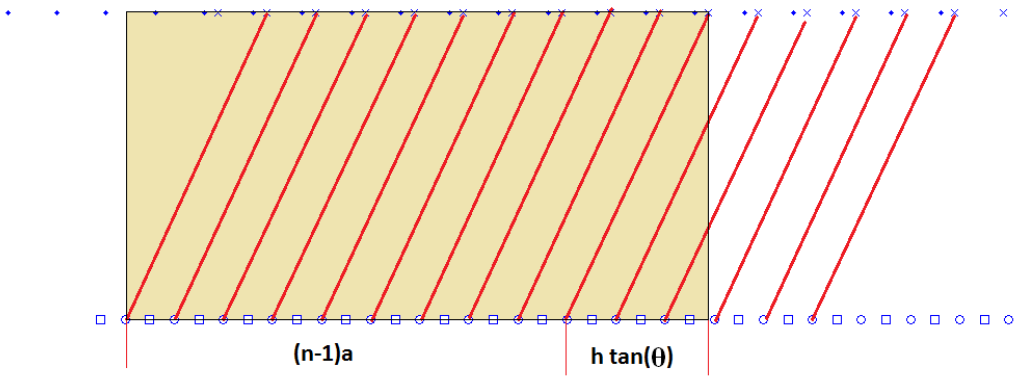

Figure 5.2: Minimum length of the sandwich structure needed to include n red pins

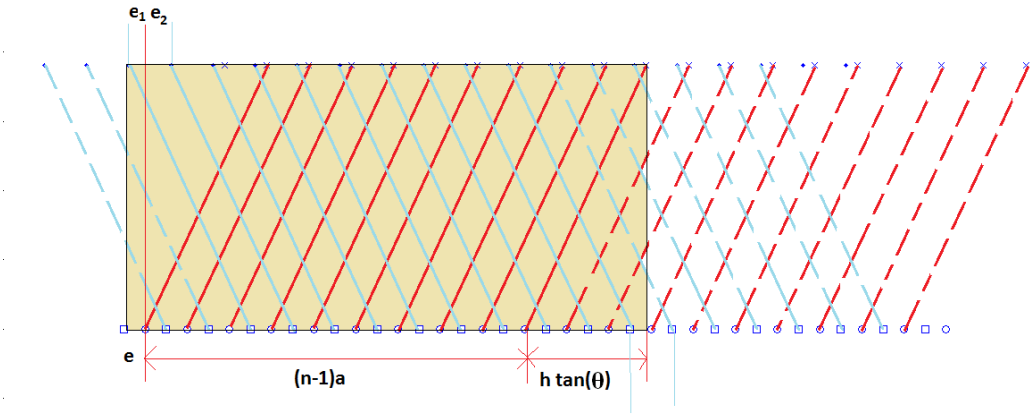

Figure 5.3: Minimum length of the sandwich structure to include n red pins and n blue pins, where $e=e_1$

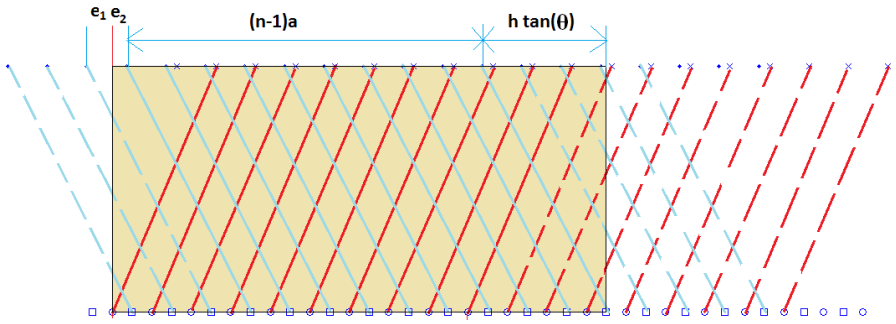

Figure 5.4: Minimum length of the sandwich structure to include n red pins and n blue pins, where $e=e_2$

To accommodate reveal lengths of the pins, the size of the sandwich specimen must equal a little more than the length derived above. The length of the sandwich specimen must equal $L_1 = L + 2\rho$, where ρ is the reveal length of the pins. If we allow the width of the specimen to equal the length and make cuts at appropriate locations, then there will be n pins of each kind in the structure. This kind of arrangement and cutting edge locations accounts for maximum pin density. We proceed to calculate the stiffness for a square

panel with each side length equal to L_1. The number of pins in the structure is equal to 4n, and the cross-sectional area of the facesheets is equal to $(L_1)^2$. The pin density of the structure is thus equal to $4n/(L_1)^2$. The compressive stiffness of the structure then equals

$$E_c^{max} = \frac{4nK_c h_{core}}{(L_1)^2} \tag{5.6}$$

where Kc is the spring constant of a single oblique pin given by Equation (2.7).

Note from Figure 5.3 and 5.4 that if the cuts were made just near the points of contact of the pins with the facesheets such that the boundary pins are not included in the model, then this will result in a sandwich specimen with minimum pin density. The length and width of the specimen will equal L and it will include (n-1) pins of each kind. The compressive stiffness of the structure would equal

$$E_c^{min} = \frac{4(n-1)K_c h_{core}}{(L)^2} \tag{5.7}$$

The theoretical values of compressive and shear modulus obtained for Model 1, from Equations(2.13)-(2.20) are for infinite sized panels while real panels are finite sized. The moduli from Equations (5.6) and (5.7) correspond to finite sized cores. This is used in computing the stiffness values of Model 2. Comparing the compressive moduli of Model 1 and 2 we can read the size effect on the model stiffness. In the next section, models 1 and 2, for certain constructions are compared for estimating the size effect. Finite models of different sizes are compared to examine the size effect in the next section. The stiffness values obtained for Model 2 were computationally verified by performing calculations for the models with artificially high modulus on facesheets. The size effect, as we shall see is a reason for scatter of the experimentally obtained values for stiffness of the models.

Since the moduli of the models depend on the number of pins in the sample, the position of the cutting edges becomes an important factor in determining the moduli. Two same sized specimens can have different moduli for different locations of the cutting edges.

5.1.1 Moduli variation with size for compressive loading:

In this section, we examine the combined effect of specimen size and position of cutting edges in influencing the modulus of the specimen. We consider models with square cross-sections (equal length and width) to study the effect of the side length of the model on the compressive modulus. In general, we expect that the moduli of the finite model increase as the size of the model increases. However, the variation is not strictly monotonic because the variation of pin density is not. The pin density tends to decrease with increase in size momentarily when the model size is such that it just includes a row of pins at its boundary, until the next row of pins can be accommodated. In essence, then, we have a highly zigzag variation of the pin density with specimen size. For better understanding, we study three different size patterns, corresponding to three different locations of the cutting edges.

Consider a typical sandwich model with different pins laid down as shown in Figure 5.5. The red and the blue lines represent the oblique pins in the ‘x’ direction, and the yellow and the green pins represent the oblique pins in the ‘y’ direction. The red pins begin at the top plate and proceed in the positive x direction till they meet the bottom plate. The blue pins originate at the top plate and run along the negative x direction. The green and the yellow pins begin at the top plate and run along the positive y and negative y directions respectively till they meet the bottom plate. In Figure 5.5, only the left and the bottom

edges of the model are shown. The first row of pins begins at a distance 3mm from the defined edge, as shown. The position of other edges of the model depends on the size of the model.

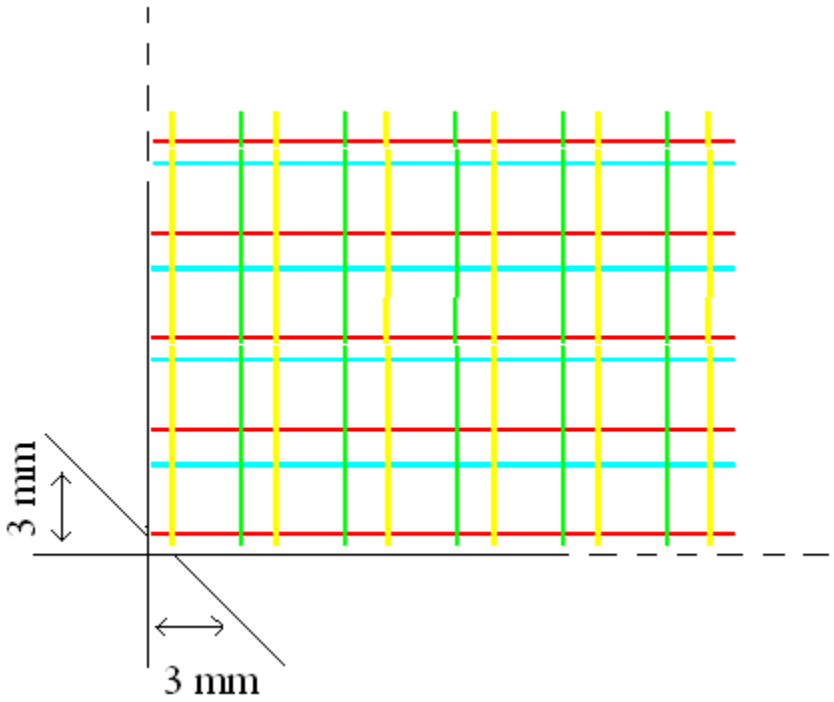

Figure 5.5: Top view of a sandwich panel shown with left and bottom cutting edges.

For the study of size effect, we consider three different types of positions for the right and the top cutting edges that give rise to an upper bound, lower bound and an intermediate values for the moduli of the model.

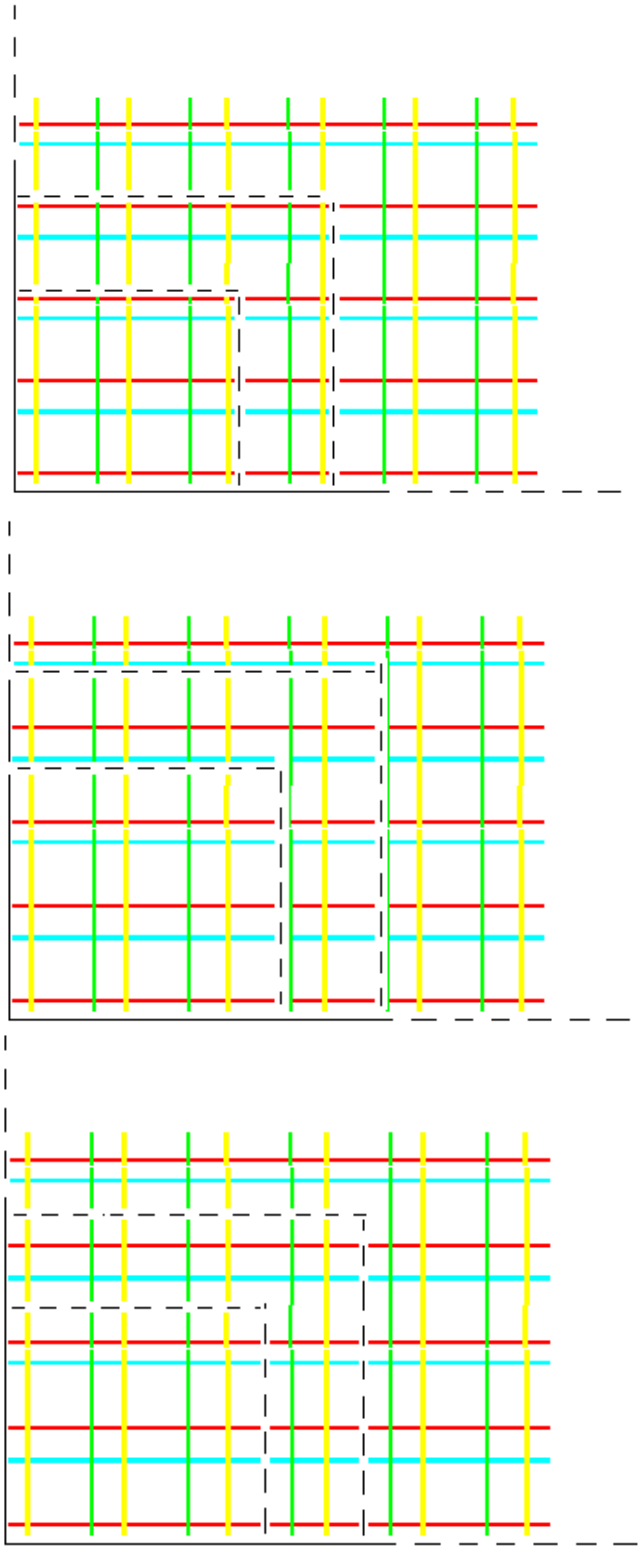

Figure 5.6 (a), (b), (c): Top views of sandwich models with three cutting patterns giving rise to models with different pin densities.

Figure 5.6 shows three different patterns of cutting edges. The cutting edge pattern in Figure 5.6(a) includes the last row of pins that can be accommodated near the right and top boundaries making it a high pin-density model. This type of cutting edge pattern will result in the model having higher moduli and the upper bound of the specimen moduli are obtained from this pattern. Figure 5.6(b) excludes the pins near the boundary and this kind of cut gives rise to models with lower moduli (lower bound). Figure 5.6(c) shows cutting edges in between the two extremes, and an intermediate value estimate is obtained from this kind of cutting pattern.

Calculations were carried out for a typical sandwich specimen with low core density (4.5 lb/ft^3) having the following configuration.

Pin and core properties:

Pin radius: 0.235 mm, Pin modulus, E = 156.5 GPa, Poisson's ratio, $\upsilon = 0.23$

Pin insertion angle = 35^0, Pin spacing = 0.243" = 6.17 mm, Core thickness = 0.5 inch = 12.7 mm

Facesheet properties:

Facesheet thickness: 1.104 mm

Ply configuration = [0/45/90]

E_L = 156.5 GPa, E_T = 12.96 GPa, G_{LT} = 6.96 GPa, G_{TT} = 4.3 GPa, $\upsilon_{LT} = 0.23$, $\upsilon_{TT} = 0.5$

The blue dots in Figure 5.7 show the variation with size, of the moduli of the finite models for these three cutting patterns, relative to moduli of the infinite model. As expected, moduli for all three cutting patterns approach the value for the infinite model as the size increases.

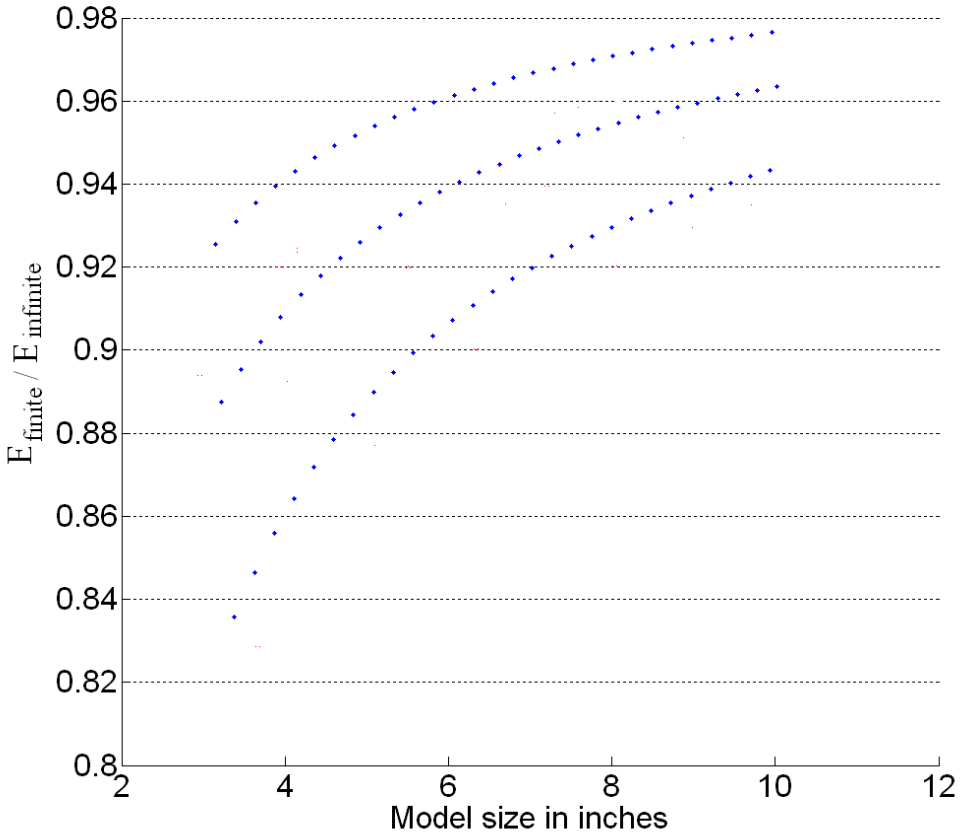

Figure 5.7: Variation of compressive modulus with specimen size for the a typical sandwich configuration of core density equal to 4.5 lb/ft^3

5.1.2 Moduli variation with size for shear loading:

The sandwich specimens tested for shear do not have square cross sections typically. We examine the shear modulus sensitivity to the specimen size in the length and width directions.

5.1.2.1 Width sensitivity:

To study the effect of the specimen size in the width direction, we allow the length of the specimen to remain fixed at 6.1 inches and vary the model width. One of the edges of the

model is predefined and the modulus of the model will vary depending on the location of the upper cutting edge. Following the same procedure as in the compression case, three different cutting patterns emerge as shown in Figure 5.8. Note that the shear loading is along the length direction.

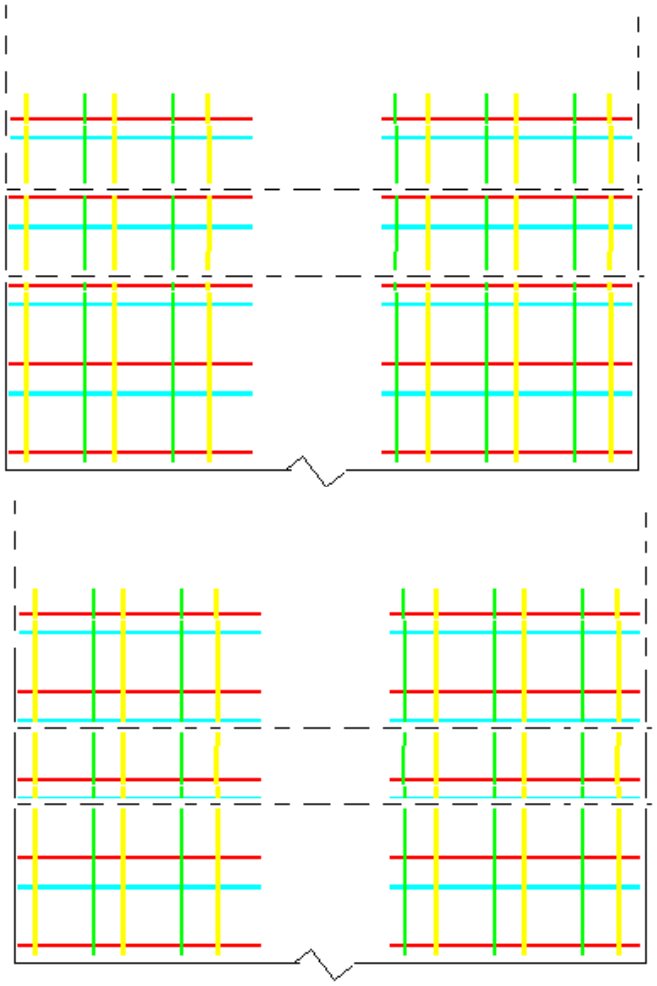

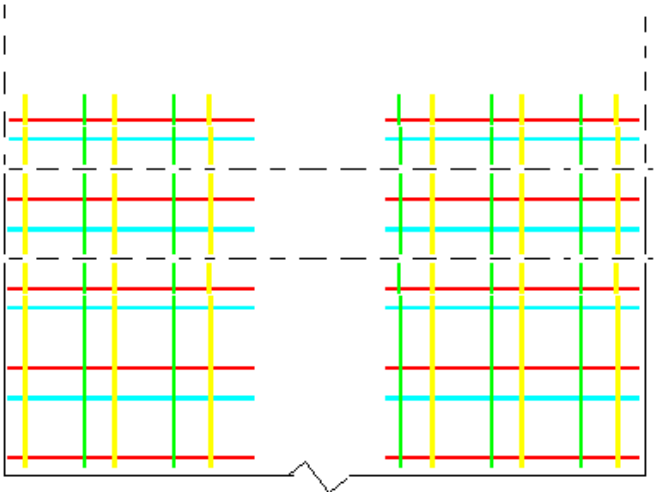

Figure 5.8 (a), (b) and (c): Top view of three different cutting patterns for a sandwich panel of varying length resulting in models of high, low and intermediate pin density

The shear moduli of the models corresponding to these cutting patterns are plotted in Figure 5.9. We observe that the high pin-density models have nearly same moduli for different sizes. We also observe that, for the MR&D sample size, which is 6.1in x 3.1 in, about 90% of the modulus of the infinite model is achieved for all the three cutting patterns.

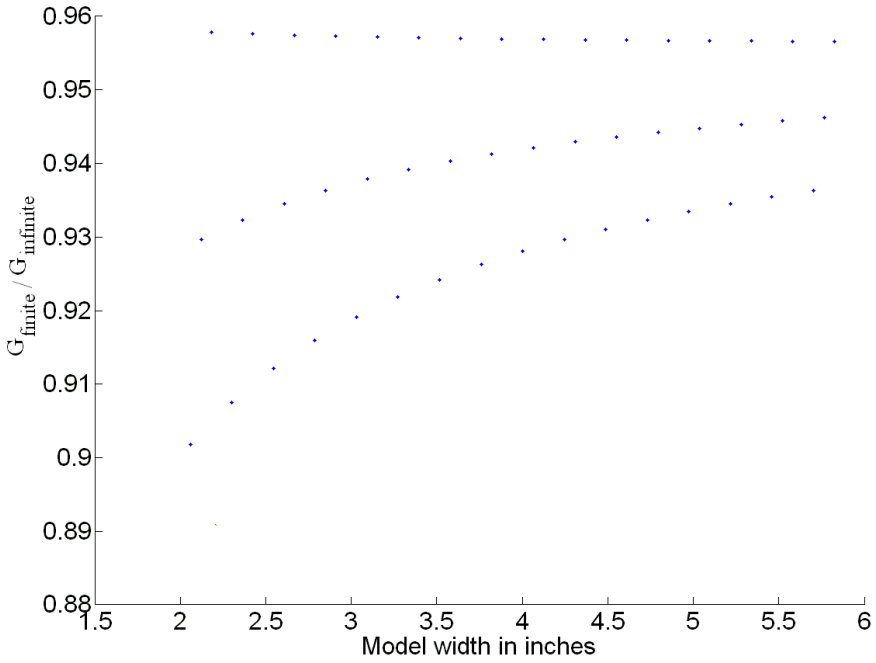

Figure 5.9: Variation of shear modulus with specimen width for a typical sandwich configuration of core density equal to equal to 4.5 lb/ft^3

5.1.2.2 Length sensitivity:

To study the effect of the specimen size in the length direction, we keep the width of the specimen fixed at 2.1 inches and vary the model length. The locations of three cutting edges of the model are predefined and thus the modulus of the model will vary depending on the location of the right cutting edge. The three different cutting patterns giving rise to upper bound, lower bound and intermediate estimate for the pin density are shown in Figure 5.10.

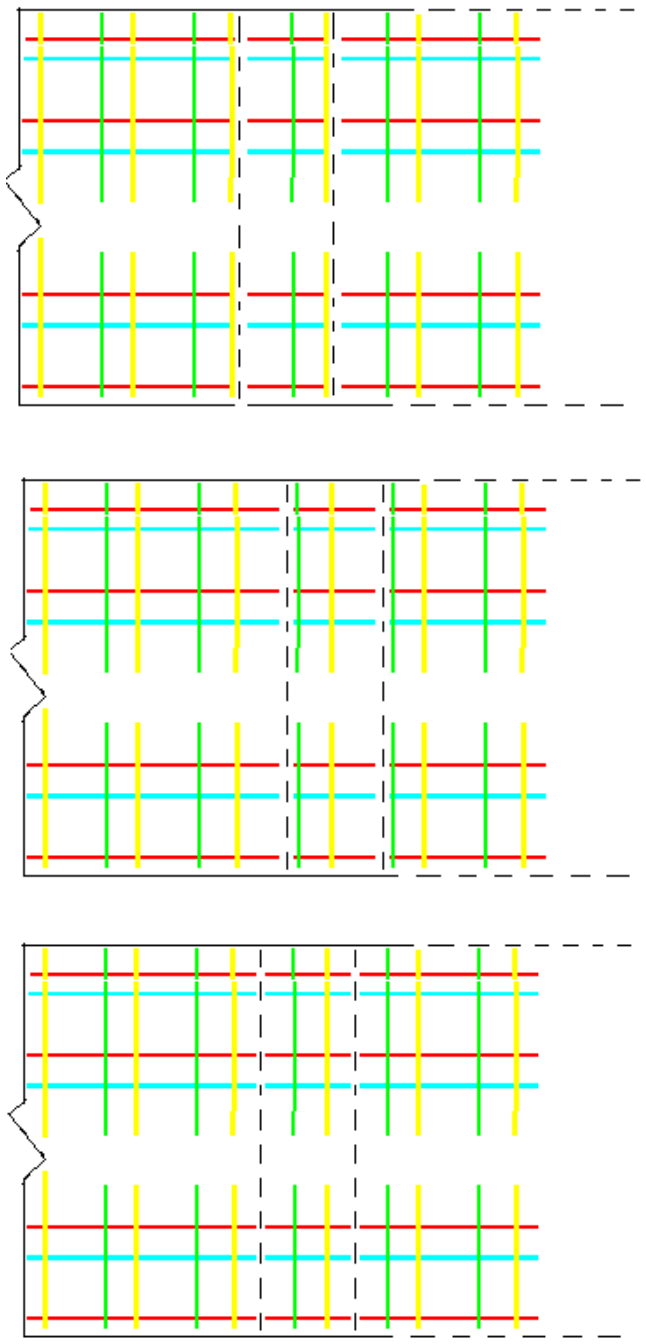

Figure 5.10 (a), (b) and (c): Top view of three different cutting patterns for a sandwich panel with varying length resulting in models of high, low and intermediate pin density

The shear moduli of the models obtained from these cutting patterns are plotted in the Figure 5.11. The variation is more drastic for the upper-bound model compared to that in the width-sensitivity analysis. It can also be observed that, since the width is fixed at a constant small value (3.1 in), only a fixed number of rows of pins can be accommodated in the width direction. Accordingly, the modulus does not increase beyond a certain value with the increase in length only.

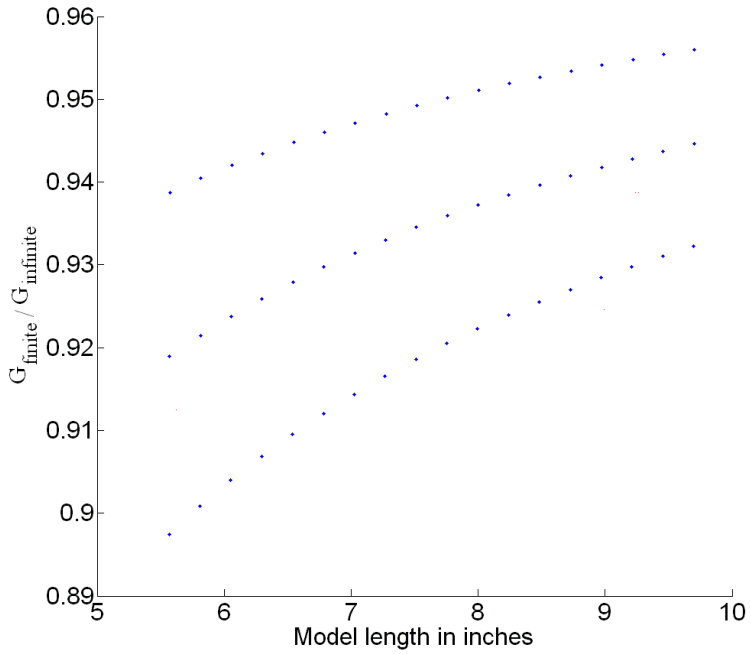

Figure 5.11: Variation of shear modulus with specimen length for the for a typical sandwich configuration of core density equal to equal to 4.5 lb/ft^3

5.2 Dependence of Interaction Spring Constant, k^{int} on different parameters:

In the following sections, we consider the influence of each parameter on interaction spring constant, k^{int}. In doing so, we use non-linear computational FE models on typical sandwich constuctions or unit cells to compare with rigid facesheet models.

To evaluate the effect of different parameters in influencing the extent of pin-facesheet interaction through penetration displacements, we consider the following computational model of a typical sandwich structure. In the sections that follow we compare the interaction spring constant of this computational model with another one similar to this model differing only in one single parameter. Figure 5.12 shows the arrangement of the pins and the facesheets in the model. Only 4 pins are included in the model for the sake of brevity. This model is representative of a typical sandwich structure of density 7pcf, used and tested at UMD. The pins are 22 mm long, inclined at 30^0 to the vertical. The pin modulus and Young's modulus are equal to 156.5 GPa and 0.23 respectively. Figure 5.13 shows the top view of the assembly and the projections of the pins on this view are depicted as well. The pin spacing is equal to 3.81 mm (0.15 inches) and the facesheets themselves are 30 mm long on each side. The facesheets are 1.27 mm (0.05 inches) thick and have the composite layup $[0/90/45/-45]_s$ with ply properties thus: $E_1 = 156.5$ GPa, $E_2 = E_3 = 12.96$ GPa, $G_{12} = G_{13} = 6.96$ GPa, $G_{23} = 4.3$ GPa, $\nu_{12} = \nu_{13} = 0.23$, $\nu_{23} = 0.5$. The displacements and the rotations of the pins are tied at the points of contact on the facesheets of the sandwich structure. The pins are modeled as quadratic B32 elements and the facesheets as 20 noded brick elements, C3D20. The bottom surface of the bottom facesheet is clamped and a unit displacement is applied on the top surface of the top facesheet uniformly. The stiffness of the structure is obtained by computing the reaction force in the vertical direction. Equation (4.1) is used to compute the interaction spring constant from the stiffness of the model. The interaction spring constant is always reported per single pin in the following sections. If the interaction spring constant for a

single pin, k^{int} is large, then the penetration displacements are smaller and the model is close to the rigid plate model.

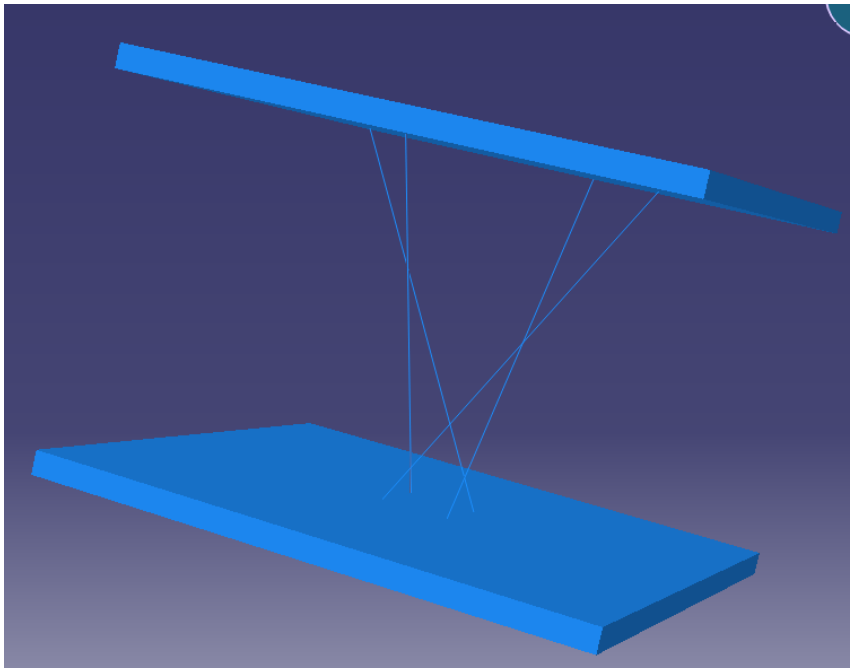

Figure 5.12: Model of a sandwich structure with 4 pins used to estimate the effect of different parameters in influencing the interaction spring constant.

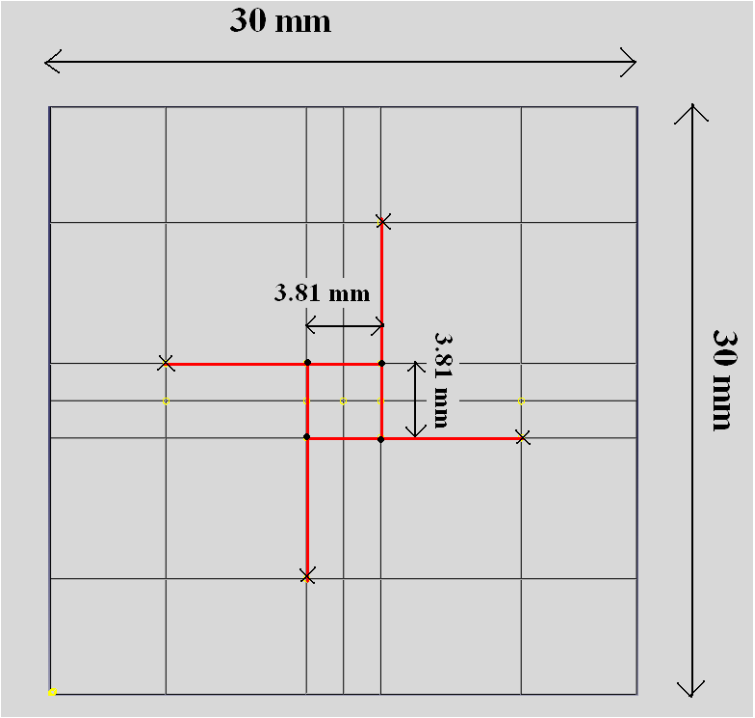

Figure 5.13: Top view of the sandwich model with 4 pins showing the pin projections and different dimensions on the facesheet

5.2.1 Facesheet Thickness

Two computational models are modeled in addition to the one above to study the effect of facesheet thickness on the interaction. They have facesheet thicknesses of 0.635 mm and 1.8 mm as compared with 1.27 mm on the above model. Table 5.1 compares the interaction spring constant for these models.

Facesheet Thickness	**Interaction Spring constant per pin, k^{int}**
0.635 mm	6.19×10^6 N/m
1.27 mm	8.53×10^6 N/m
1.8 mm	9.97×10^6 N/m

Table 5.1: Interaction spring constants for three models with different facesheet thicknesses.

It is observed that the facesheet thickness has a significant effect on pin-facesheet interaction. Thinner facesheets have smaller interaction spring constants and this higher interaction potential. This pattern is also corroborated by smaller penetration displacements on thicker facesheets. For thinner facesheets the two surfaces of the facesheets are closer to each other and the effect of the boundary conditions on one side of the facesheet results in a greater penetration displacements and thus greater interaction potential.

5.2.2 Core Thickness

Core thickness has a significant effect on the interaction potential. To study the effect of core thickness, a model with 12.7 mm (0.5 inch) thick is constructed. This core thickness value is typical of sandwich structures with lower pin densities. Since the core thickness also affects the pin lengths, the pin spring constants are themselves different in the two models. The interaction potential is compared by comparing the ratio of the interaction spring constant, k^{int}, and the pin spring constant, k^{pin} in Table 5.2.

Core Thickness	**Interaction Spring constant per pin, k^{int}**	**Pin Spring constant k^{pin}**	**Ratio k^{int} /k^{pin}**
19.05mm (0.75 inch)	8.53 x 10^6 N/m	0.926 x 10^6 N/m	9.24
12.7mm (0.5 inch)	9.82 x 10^6 N/m	1.389 x 10^6 N/m	7.07

Table 5.2: Interaction spring constants for models with different core thicknesses

It is observed that the interaction spring constant is a smaller multiple of the pin spring constant for the model with lower core thicknesses, i.e., the ratio k^{int} /k^{pin} is smaller, indicating a higher interaction potential. This is because the pins in the model with lower core thickness have higher spring constants and thus penetrate deeper into the facesheets.

5.2.3 Pin Angle

Another important parameter influencing pin-facesheet interaction is the pin orientation. Here we consider two typical pin angles to study the effect. Vertical pins and oblique pins inclined at 30^0 degrees to the vertical are compared. An isometric view of the model with 4 vertical pins is shown in Figure 5.14.

Pin Insertion Angle	**Interaction Spring constant per pin, k^{int}**	**Pin Spring constant k^{pin}**	**Ratio k^{int} /k^{pin}**
30^0 (Oblique pins)	8.53 x 10^6 N/m	0.926 x 10^6 N/m	9.24
0^0 (Vertical pins)	10.12x 10^6 N/m	1.425 x 10^6 N/m	7.09

Table 5.3: Interaction spring constants for models with different pin insertion angles

It can be observed from Table 5.3 that vertical pins have smaller interaction spring constants as a multiple of the pin constants. This means that the vertical pins have a greater interaction potential, which is because the vertical pin has a higher spring constant and hence can penetrate deeper into the facesheets.

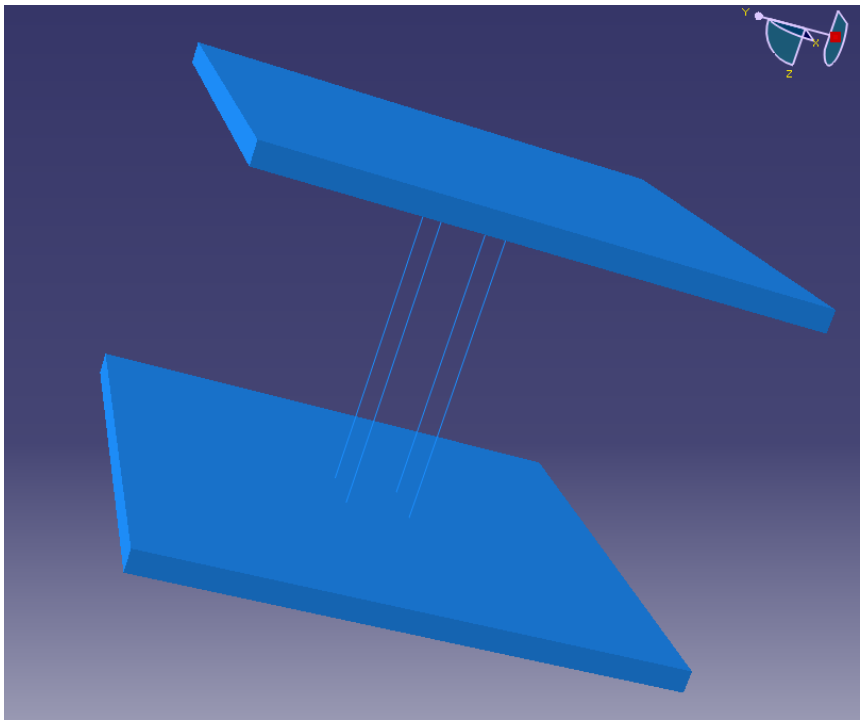

Figure 5.14: A sandwich model containing only vertical pins separated by pin spacing of 3.81 mm.

5.2.4 Pin Proximity

The penetration displacements of the pin into the facesheets depend on the pin surroundings as well. If the pins are closely packed then the neighboring pins have an effect on the penetration of the pins. To study the effect of the neighboring pins, a computational model is developed with 4 pins as above, spaced at 8mm away from each

other on the bottom plate, as shown in Figure 5.15. The interaction spring constant of each model is given in Table 5.4.

Distance between adjacent pins	**Interaction Spring constant per pin, k^{int}**
3.81 mm	8.53 x 10^6 N/m
8 mm	10.51 x 10^6 N/m

Table 5.4: Interaction spring constants for models with different pin proximities

It can be observed from Table 5.5 that the model with pins packed closer to each other has a lower interaction spring constant and thus higher interaction potential.

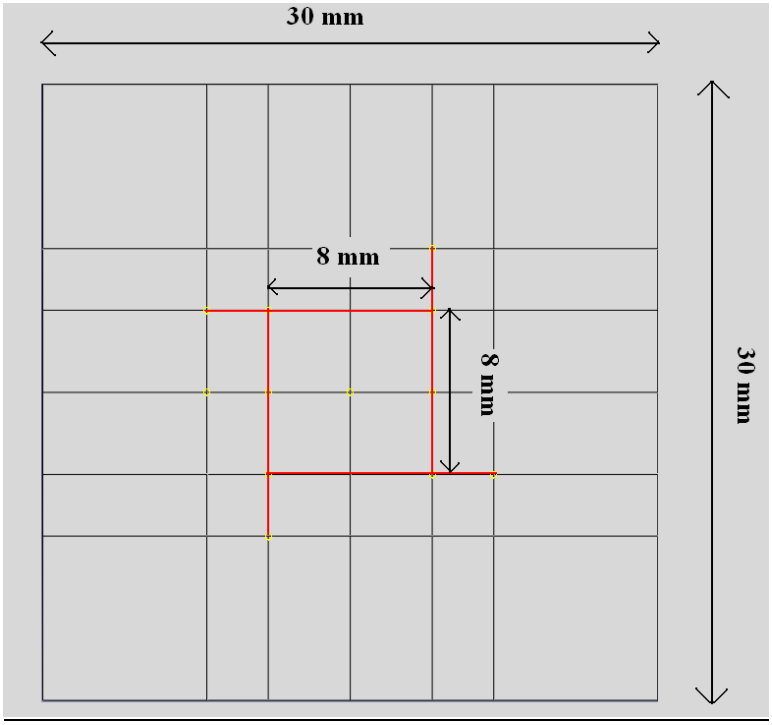

Figure 5.15: Top view of the sandwich model with 4 pins spaced at 8 mm from each other on the bottom plate.

5.2.5 Comparison of interaction spring constant for compression and shear loading

The interaction springs in the sandwich models represent the resistance to loading offered from the pin-facesheet interaction in the form of penetration displacements. In this section we compare the interaction spring constants obtained for a model under compression and shear. Since the spring constants of the oblique pins are different in the x and y directions, we consider a 2 pin model as shown in Figure 5.16 below. The top view of the model is shown in Figure 5.17. Two models with core thicknesses 12.7 mm (0.5 inch) and 19.05 mm(0.75 inch) are constructed.

The interaction spring constants are obtained from the stiffness values obtained from the computational models incorporating facesheet flexibility and pin-facesheet interaction. Table 5.5 lists the values obtained. It is observed that the ratio of spring constants, k^{int}/k^{pin} is nearly the same for both the models in both the loading conditions.

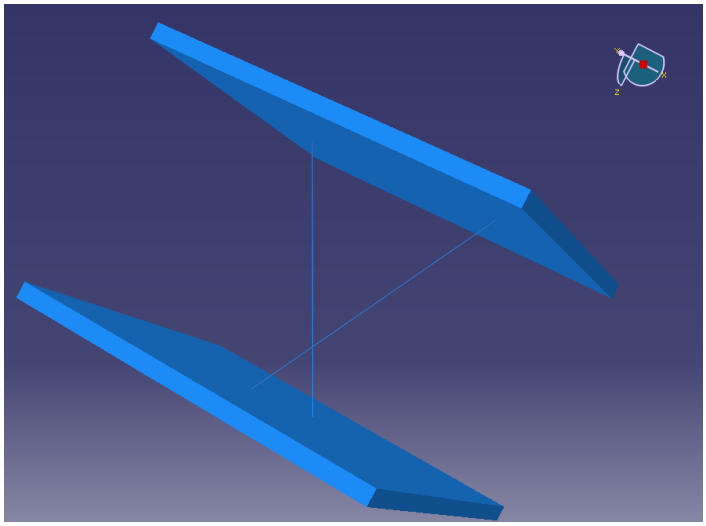

Figure 5.16: Model of a sandwich structure with 2 pins used to compare the interaction spring constant in compressive and shear loading conditions

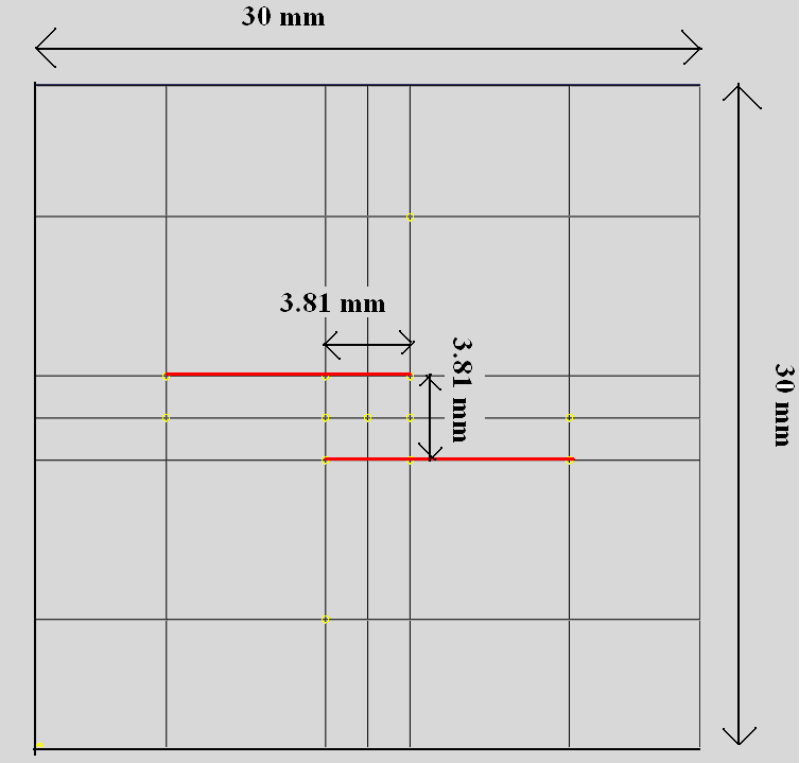

Figure 5.17: Top view of the sandwich model with 2 pins showing the pin projections and different dimensions on the facesheet

Loading	**Core Thickness**	**Pin Spring Constant, k^{pin}**	**Interaction Spring Constant per pin, k^{int}**	**Ratio k^{int}/ k^{pin}**
Compression	0.75 inch	9.26×10^5 N/m	1.04×10^6 N/m	11.22
Shear	0.75 inch	3.09×10^5 N/m	3.42×10^6 N/m	11.08
Compression	0.5 inch	1.39×10^6 N/m	7.91×10^6 N/m	11.39
Shear	0.5 inch	4.64×10^5 N/m	5.23×10^6 N/m	11.27

Table 5.5: Interaction spring constants for the same sandwich structure under compression and shear loading conditions.

5.2.6 Other Factors

The above parameters are the main factors of influence of the interaction spring constant and the interaction potential of a sandwich model. Other minor influencing factors may include size of the specimen, direction of loading, pin locations based on cutting edges etc.

5.3 Influence of adhesive modulus

In Section 4.1, we studied low density UMD sandwich specimens and compared the compressive moduli of Models 1, 2, 3 and 4for them. In Section 4.1.3.2, we examined Model 4b, which is the model including the adhesive layer post yielding. Since data for post yield modulus of the adhesive modulus was not available, we arbitrarily chose the post yield modulus of the adhesive layer as one-tenth its original modulus. Since the adhesive modulus (post-yield) value was chosen arbitrarily, it is important to study the influence of these parameters on the compressive modulus of the specimen. We analyze the influence of adhesive modulus on UMD low density specimen of size 2”x2”. Figures (5.18)-(5.21) show the influence of the adhesive modulus on the sandwich specimen modulus, maximum pin penetration displacements and interaction spring constants respectively. The adhesive modulus is normalized with respect to epoxy modulus, E_{epoxy} = 3.17 GPa. The penetration displacements are calculated for a unit displacement (1 mm) applied on the top facesheet. The shear modulus, interaction spring constant and the penetration displacements are normalized with respect to their values when the adhesive modulus equals E_{epoxy}, i.e, 636 MPa, 1.76 GPa and 0.0546 mm. Figure 5.18 shows how

the specimen modulus varies with the penetration displacements and interaction spring constant for the different values of adhesive modulus used in the model. It is observed that these curves are fairly smooth and can be used to predict the properties of the sandwich structure.

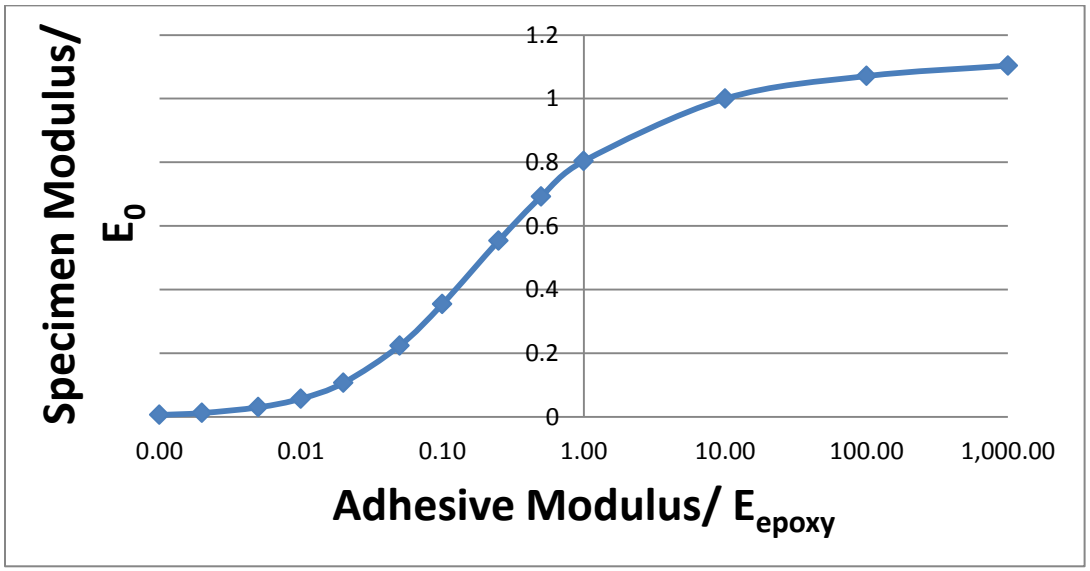

Figure 5.18: Variation of sandwich specimen modulus with adhesive modulus.

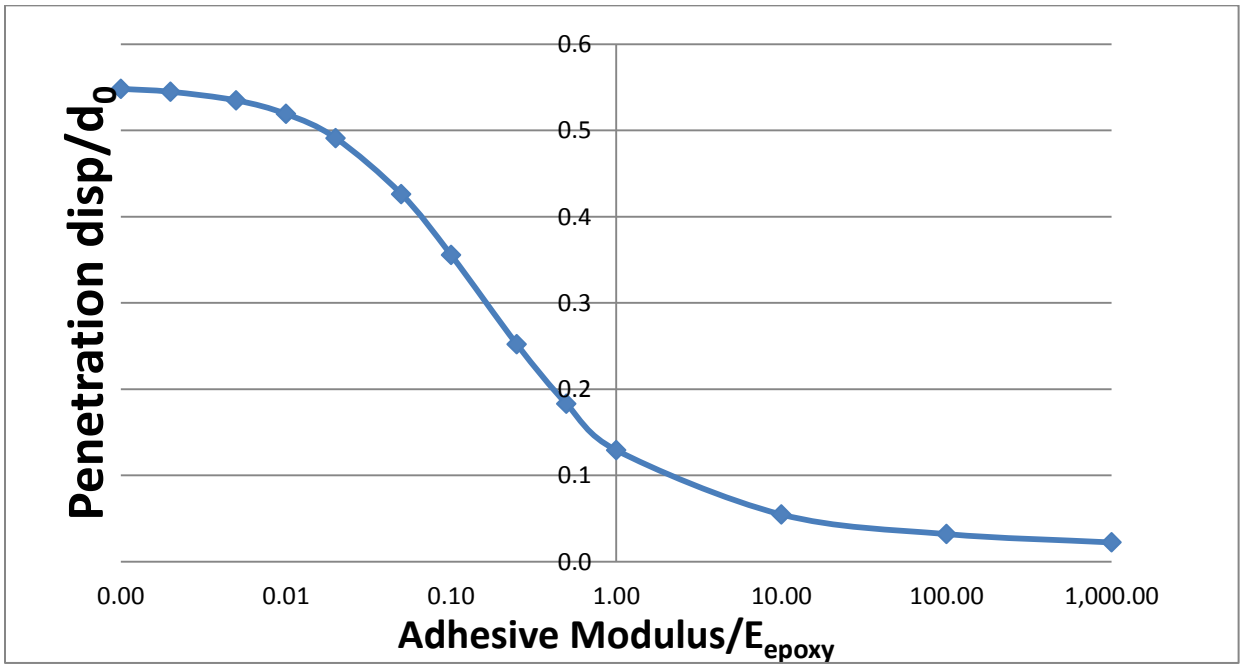

Figure 5.19: Variation of pin penetration displacements with adhesive modulus

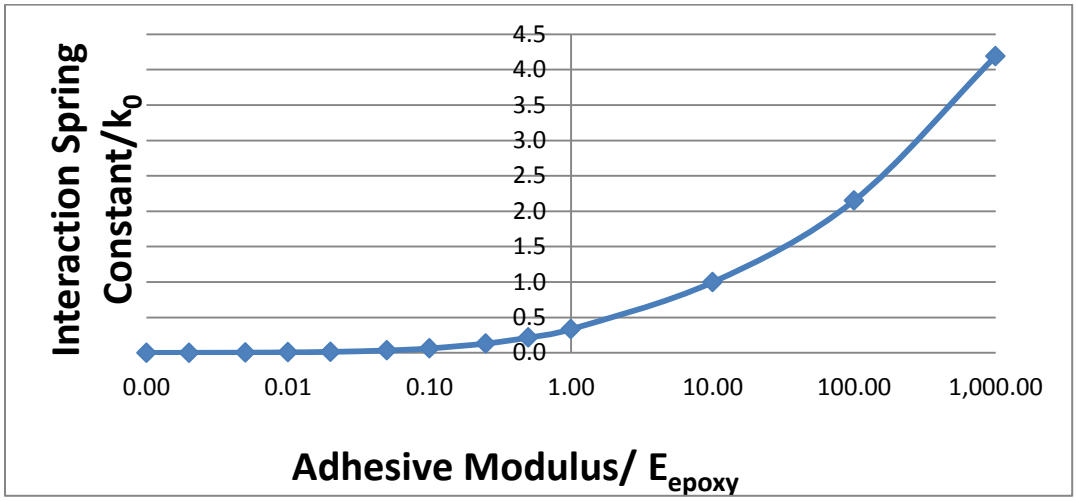

Figure 5.20: Variation of interaction spring constant with adhesive modulus

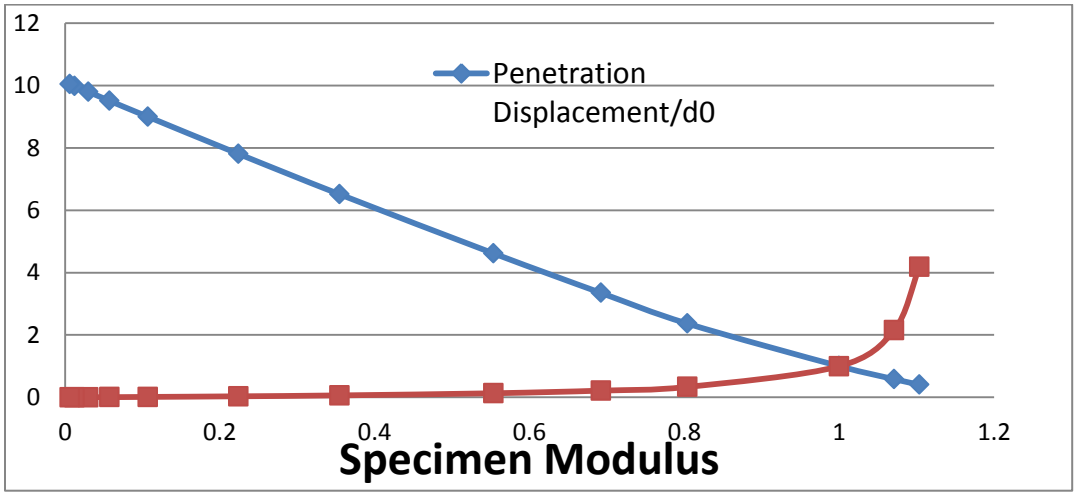

Figure 5.21: Variation of pin penetration displacements and interaction spring constant with specimen modulus

5.4 Significance of loading direction:

Figure 5.22 shows the arrangement of oblique pins in a typical sandwich structure from the top view. The red crosses are the points of intersection of the pins with the bottom facesheet and the brown circles are the points of intersection with the top facesheet. It can be seen that the pattern of the intersecting points have different geometries on different facesheets. This means that the pin tip proximities and arrangement are different on different plates. Figure 5.23 and 5.24 are snapshots of the pin intersections of a typical sandwich structure on the bottom and top facesheets. The patterns and the pin proximities are noticeably different on the top and bottom facesheets.

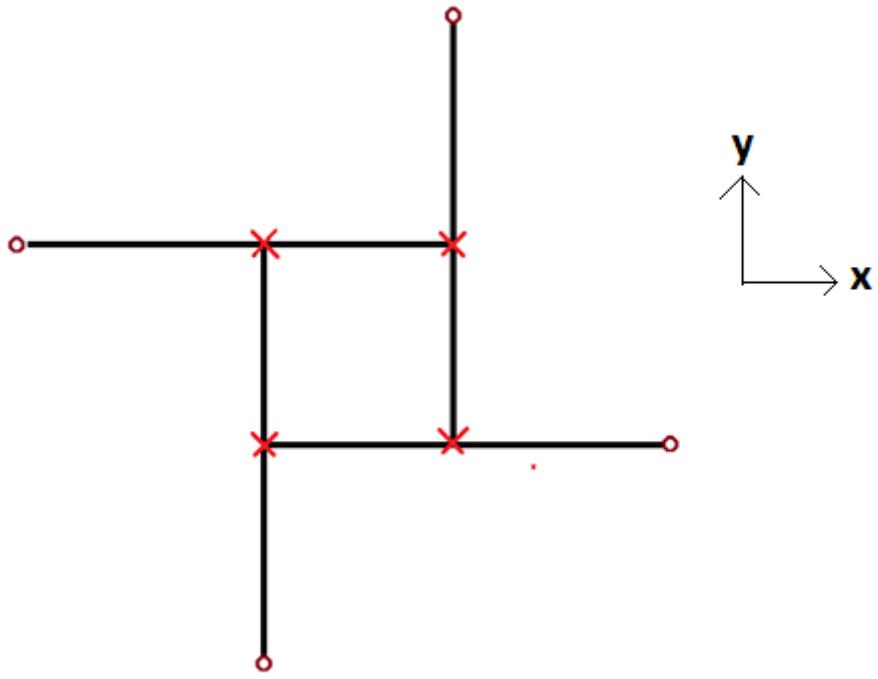

Figure 5.22: Top view of a typical oblique pin arrangement showing the 4 points of intersection with top and bottom plates

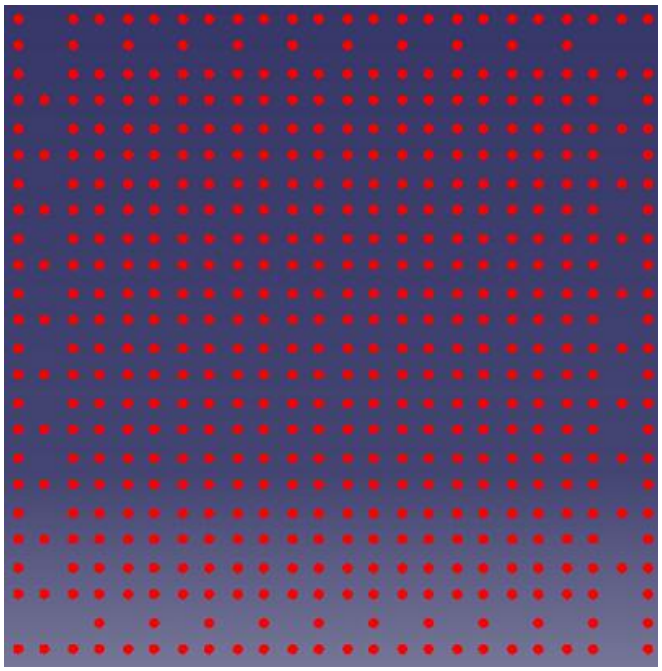

Figure 5.23: Snapshot of the bottom facesheet of a typical sandwich structure showing the pin intersections on the facesheet.

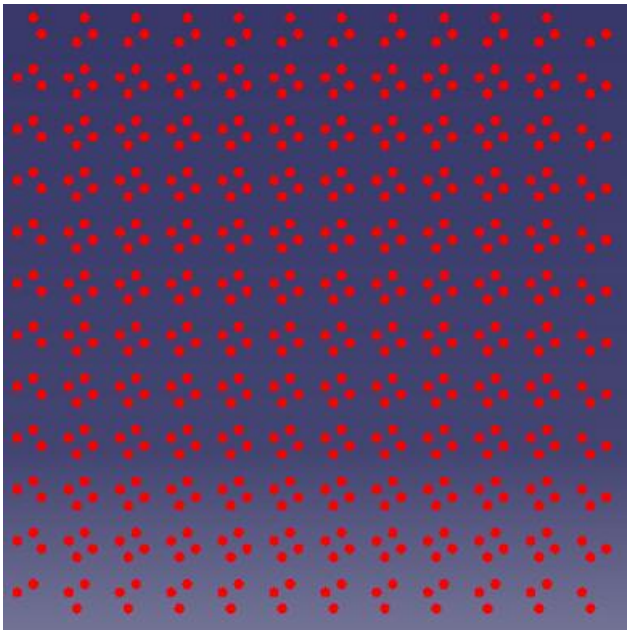

Figure 5.24: Snapshot of the top facesheet of a typical sandwich structure showing the pin intersections on the facesheet.

Since the penetration displacements of the pin tips and the interaction spring constants depend on the pin arrangement and pin proximities, these values will be different on different sides of the facesheets. In certain asymmetric loading scenarios such as bending, the direction of loading will become very significant.

Chapter 6

Conclusions and Recommendations for future work

6.1 Conclusions

The major contributions from the research work presented in this report are:

1. Finite Element models have been developed to estimate the compressive and shear stiffness and strengths of sandwich specimens of different pin densities. The effect of facesheet flexibility (in the thickness direction) on the specimen modulus is shown to be significant. The facesheets have local deformations at the points of contact with the pins, which results in reduction of the compressive stiffness of the sandwich panel.
2. The interaction between the pins and the facesheets have been modeled as interaction springs, whose spring constant depends on a variety of parameters including facesheet thickness, pin angle, core thickness, facesheet modulus, cell spacing etc. The dependence on each of these parameters is studied. The interaction springs models provide a good method to estimate for compressive stiffness of the sandwich specimens.
3. The effect of coupling between axial deformation and bending on the compressive and shear stiffness and the effect of the pin bending stiffness was determined to have a negligible effect on the core stiffness both in compression and shear. Using a pin buckling criteria, the compressive strength strengths based on the pin buckling using the maximum axial compressive force has been determined in different models. While pin buckling can occur in shear, the pin pullout force is also needed to analytically determine the shear strength of the core.

4. An adhesive layer was modeled between the core and the facesheets. It is observed that inclusion of the adhesive layer decreases the compressive modulus of the sandwich specimen. The adhesive layer yields before the pin buckling occurs and the load value at which the adhesive layer yields was estimated. Yielding of the adhesive layer is manifested as a kink in the stress-strain relationship of the specimens. It is observed that the calculated values for compressive modulus before the kink matches reasonably well with experimental values.
5. Geometrically non-linear analysis for estimating large deformations and the stiffness of the pin after first critical load have been performed. This model explains the kinks in the stress-strain curve and the strength of the structure reasonably well, but does not explain the stiffness values of the specimen after the first critical load.
6. Comparison of models with infinite panels and finite panel lengths establishes the size effect on the stiffness and strengths. Finite panels considered exhibit smaller stiffness values than the theoretically predicted values for infinite panels.
7. In addition, application of the FEA models to investigating the effects of pin location on mechanical response has been conducted. These results have indicated that there is a great deal of sensitivity in the mechanical response that depends on the pin locations. This could explain the scatter in experimentally determined values of the core moduli. As the specimen size increases the scatter decreases. These types of analyses described in this report could be used to estimate the

minimum specimen size that can generate stiffness properties within acceptable accuracy.

6.2 Recommendations for future work

Major recommendations for future work in this area of research include:

1. Refined FE models incorporating reveal lengths of the pins will be developed to obtain a better understanding of the pin-facesheet interactions. More detailed studies on the pin-facesheet interactions can be carried out via analyzing local deformation pattern on the facesheets.
2. The effect of the foam core on the compressive modulus and strengths of low density specimens will be studied by incorporating the foam core in the finite element models.
3. A better understanding of the adhesive bonding between the pins and the facesheets will be studied. Adhesive yielding and failure and their effect on the sandwich structures will be analysed in detail.
4. A shear lag model can be constructed for a simplified analysis of the stress state in the adhesive layer. FE models incorporating pin peel strength can be developed to predict shear strength of sandwich panels.
5. Attempts will be made to develop guidelines on how to cut specimens for compression and shear tests to standardize the experiments and reduce scatter.

Bibliography:

[1]. Experimental analysis of the through-thickness compression properties of z-pinned sandwich composites, A. Nanayakkara, S. Feih, A.P. Mouritz, *Composites Part A 42 (2011) 1673–1680*

[2]. Failure analysis of pin-loaded aluminum–glass–epoxy sandwich composite plates, Bulent Murat Icten, Onur Sayman, *Composites Science and Technology 63 (2003) 727–737*

[3]. Flexural properties of z-pinned laminates, P. Chang, A.P. Mouritz, B.N. Cox, *Composites: Part A 38 (2007) 244–251*

[4]. Study on impact properties of through-thickness stitched foam sandwich composites, Xia Fan, Wu Xiao-qing, *Composite Structures 92 (2010) 412–421*

[5]. Indentation study of Z-pin reinforced polymer foam core sandwich structures, Du Long, Jiao Guiqiong, *Composites: Part A 40 (2009) 822–829*

[6]. Mechanical properties balance in novel Z-pinned sandwich panels: Out-of-plane properties, Andrea I. Marasco, Denis D.R. Cartie, Ivana K. Partridge, Amir Reza, *Composites: Part A 37 (2006) 295–302*

[7]. The effect of pin reinforcement upon the through-thickness compressive strength of foam-cored sandwich panels, Denis D. Cartie , Norman A. Fleck, *Composites Science and Technology 63 (2003) 2401–2409*

[8] Pin Reinforcement of Delaminated Sandwich Beams under Axial Compression, Brian. T. Wallace, Bhavani V. Sankar and Peter G. Ifju, *Journal of Sandwich Structures and Materials, Vol. 3—April 2001 117 1530-7972/01/02 0117–13*

[9] Analytical modeling and finite element simulation of the plastic collapse of sandwich beams with pin-reinforced foam cores, Tao Liu a, Zi Chen Deng a,b, Tian Jian Lu c, *International Journal of Solids and Structures 45 (2008) 5127–5151*

[10] A protocol for characterizing the structural performance of metallic sandwich panels: application to pyramidal truss cores, F.W. Zok *, S.A. Waltner, Z. Wei, H.J. Rathbun, R.M. McMeeking, A.G. Evans, *International Journal of Solids and Structures 41 (2004) 6249–6271*

[11] Compression properties of z-pinned sandwich composites A. P. Mouritz, *J Mater Sci (2006) 41:5771–5774*

[12] Buckling Analysis of Debonded Sandwich Panel Under Compression, David W. Sleight and John T. Wang, *NASA Technical Memorandum 4701*

[13] Vaziri, A., Xue, Z., Hutchinson, J.W., 2006. Metal sandwich plates with polymer foam-filled cores. *Journal of Mechanics of Material and Structures 1, 95–125.*